



HAL
open science

Modified functional surfaces for increased biointegration: Surface chemistry, mechanical integrity and long-term stability of zirconia and alumina based ceramics

Carlos Francisco Caravaca

► To cite this version:

Carlos Francisco Caravaca. Modified functional surfaces for increased biointegration: Surface chemistry, mechanical integrity and long-term stability of zirconia and alumina based ceramics. Materials. Université de Lyon, 2016. English. NNT : 2016LYSEI080 . tel-01694086

HAL Id: tel-01694086

<https://theses.hal.science/tel-01694086>

Submitted on 26 Jan 2018

HAL is a multi-disciplinary open access archive for the deposit and dissemination of scientific research documents, whether they are published or not. The documents may come from teaching and research institutions in France or abroad, or from public or private research centers.

L'archive ouverte pluridisciplinaire **HAL**, est destinée au dépôt et à la diffusion de documents scientifiques de niveau recherche, publiés ou non, émanant des établissements d'enseignement et de recherche français ou étrangers, des laboratoires publics ou privés.



NNT : 2016LYSEI080

THESE de DOCTORAT DE L'UNIVERSITE DE LYON
opérée au sein de
INSA Lyon

Ecole Doctorale 34
Matériaux de Lyon

Spécialité de doctorat : Science de Matériaux

Soutenue publiquement le 16/09/2016, par :
Carlos Caravaca

Modified functional surfaces for
increased biointegration: surface
chemistry, mechanical integrity and
long-term stability of zirconia and
alumina based ceramics

Laboratoire de recherche : MATEIS

Devant le jury composé de :

Leriche, Anne	Professeur	UVHC	Président.e
Anglada, Marc	Professeur	UPC Barcelone	Rapporteur
Leriche, Anne	Professeur	UVHC	Rapporteur
Porporati, Alessandro Alan	Docteur	CeramTec GmbH	Examineur
Miranda, Pedro	Professeur	UEx Badajoz	Examineur
Laurenceau, Emmanuelle	M. de Conf.	ECL	Examineur
Chevalier, Jérôme	Professeur	INSA de Lyon	Directeur de thèse
Gremillard, Laurent	DR	INSA de Lyon	Co-directeur
Chevolot, Yann	DR	ECL	Invité

ECOLES DOCTORALES – SPECIALITES
A REMPLIR LORS DE VOTRE INSCRIPTION

A établir obligatoirement avec votre directeur de thèse

Nom : Caravaca

Prénom : Carlos

Signature :

ECOLES DOCTORALES n° code national	SPECIALITES	Cocher la case correspondante
<u>ED CHIMIE DE LYON</u> (Chimie, Procédés, Environnement) EDA206	Chimie Procédés Environnement	<input type="checkbox"/> <input type="checkbox"/> <input type="checkbox"/>
<u>HISTOIRE, GEOGRAPHIE, AMENAGEMENT, URBANISME, ARCHEOLOGIE, SCIENCE POLITIQUE, SOCIOLOGIE, ANTHROPOLOGIE</u> (ScSo) EDA483	Géographie – Aménagement - Urbanisme	<input type="checkbox"/>
<u>ELECTRONIQUE, ELECTROTECHNIQUE, AUTOMATIQUE</u> (E.E.A.) EDA160	Automatique Génie Electrique Electronique, micro et nanoélectronique, optique et laser Ingénierie pour le vivant Traitement du Signal et de l'Image	<input type="checkbox"/> <input type="checkbox"/> <input type="checkbox"/> <input type="checkbox"/> <input type="checkbox"/>
<u>EVOLUTION, ECOSYSTEMES, MICROBIOLOGIE , MODELISATION</u> (E2M2) EDA 341	Paléoenvironnements et évolution Micro-organismes, interactions, infections Biologie Evolutive, Biologie des Populations, écophysiologie Biomath-Bioinfo-Génomique évolutive Ecologie des communautés, fonctionnement des écosystèmes, écotoxicologie	<input type="checkbox"/> <input type="checkbox"/> <input type="checkbox"/> <input type="checkbox"/> <input type="checkbox"/>
<u>INFORMATIQUE ET MATHEMATIQUES DE LYON</u> (InfoMaths) EDA 512	Informatique Informatique et applications Mathématiques et applications	<input type="checkbox"/> <input type="checkbox"/> <input type="checkbox"/>
<u>INTERDISCIPLINAIRE SCIENCES-SANTE</u> (EDISS) EDA205	Biochimie Physiologie Ingénierie biomédicale	<input type="checkbox"/> <input type="checkbox"/> <input type="checkbox"/>
<u>ED MATERIAUX DE LYON</u> EDA 034	Matériaux	<input checked="" type="checkbox"/>
<u>MEGA DE LYON</u> (MECANIQUE, ENERGETIQUE, GENIE CIVIL, ACOUSTIQUE) (MEGA) EDA162	Mécanique des Fluides Génie Mécanique Biomécanique Thermique Energétique Génie Civil Acoustique	<input type="checkbox"/> <input type="checkbox"/> <input type="checkbox"/> <input type="checkbox"/> <input type="checkbox"/> <input type="checkbox"/>

Pour le Directeur de l'INSA Lyon
Et par délégation

Marie-Christine BAIETTO
Directrice du Département FEDORA
Formation par la Recherche Et des Etudes Doctorale

*Cette liste est mise à jour annuellement par le Département FEDORA en collaboration avec les Ecoles
Doctorales.*

Table of contents

Preface	v
Thesis outline and Objectives.....	vii
GENERAL INTRODUCTION	9
1.1 Bioinert ceramics	11
1.1.1 Alumina.....	11
1.1.2 Zirconia.....	12
1.1.3 Zirconia-Toughened Alumina (ZTA)	14
1.2 Orthopaedic implants.....	17
1.2.1 Dental.....	18
1.2.2 Hip joint.....	20
1.3 Cell - Material interactions	28
1.3.1 Fixation of implants.....	28
1.3.2 Importance of roughness	30
1.3.3 Role of surface proteins.....	33
1.3.4 Surface chemistry.....	34
Bibliography.....	37
EFFECT OF ROUGHNESS	43
2.1 Introduction.....	45
2.2 Materials and methods.....	47
2.2.1 Determining the Annealing Temperature to suppress residual stresses.....	48
2.2.2 Surface Characterization	50
2.2.3 Aging assessment.....	51
2.2.4 Mechanical Characterization.....	51
2.2.5 Statistical tests.....	51
2.3 Results.....	52
2.3.1 Determining the Annealing Temperature to suppress residual stresses.....	52
2.3.2 Surface Characterization	54
2.3.3 Aging assessment.....	55
2.3.4 Mechanical Characterization.....	56
2.4 Discussion	59
2.4.1 Surface Characterization	59
2.4.2 Aging assessment.....	60
2.4.3 Mechanical Characterization.....	61
2.4.4 On the different effective residual stresses after sandblasting.....	63
2.5 Conclusions.....	65
Glossary.....	66
Bibliography.....	67

EFFECT OF PROTEINS	71
3.1 Introduction.....	73
3.2 Materials and methods.....	76
3.2.1 Selection of cleaning protocol.....	77
3.2.2 Contact angle on curved surfaces	77
3.2.3 Effect of gamma irradiation.....	77
3.2.4 Organic solvents, NBCS exposure and incubation	78
3.2.5 Statistics	78
3.3 Results.....	79
3.3.1 Cleaning protocol	79
3.3.2 Effect of gamma irradiation.....	80
3.3.3 Organic solvents, NBCS exposure and incubation	80
3.4 Discussion	83
3.4.1 Cleaning protocol	83
3.4.2 Effect of gamma irradiation.....	83
3.4.3 Organic solvents, NBCS exposure and incubation	84
3.5 Conclusions	87
Bibliography	89

EFFECT OF SURFACE CHEMISTRY	91
4.1 Introduction.....	93
4.2 Materials and methods.....	96
4.2.1 Surface characterization.....	97
4.2.2 Mechanical testing	98
4.2.3 Aging kinetics	98
4.2.4 Cellular tests.....	98
4.2.5 Statistical tests.....	99
4.3 Results.....	100
4.3.1 Surface Characterization	100
4.3.2 Mechanical testing	105
4.3.3 Aging kinetics	106
4.3.4 Cellular tests.....	107
4.4 Discussion	109
4.4.1 Surface characterization.....	109
4.4.2 Mechanical testing	112
4.4.3 Aging kinetics	112
4.4.4 Cellular tests.....	112
4.5 Conclusions	115
Bibliography	116

RESUME.....	123
--------------------	------------

Index of Figures	135
-------------------------------	------------

Index of Tables.....	137
-----------------------------	------------

Preface

The work of this thesis was carried out in MATEIS laboratory at INSA de Lyon (Villeurbanne, France), École Centrale de Lyon (Écully, France) and CeramTec GmbH (Plochingen, Germany) in the period October 2012 to May 2016, under the supervision of Jérôme Chevalier and Laurent Gremillard. The funding was provided by the European Commission under the 7th Framework Programme, a Marie Curie Initial Training Networks (ITN) (grant number: 289958) and was encompassed inside the project “BIOBONE: Bioceramics for bone repair”. The final objective of the network was to train young researchers to fill the demand of innovative progress in the strategic area of Bioceramics for bone repair. The approach of the project followed three key principles:

1. A multidisciplinary approach integrating recognized groups and companies working in different areas of R&D.
2. A comprehensive training itinerary, incorporating hands-on training and continuous education in workshops and meetings.
3. A coordinated effort between academic and industrial partners, to allow young researchers to translate their skills into the work market.

BIOBONE partners were spread out over Europe: Spain, United Kingdom, France, Germany, Belgium and Switzerland, and the pool of young researchers comprised twelve PhD positions for the early-stage researchers (ESRs), and three post-doc positions for the experienced researchers (ERs). The total scientific work comprehended three scientific work packages (WP): WP1, processing and new materials, WP2, biodegradation, WP3, cell/material interactions. The present work constitutes a fraction of WP3. Along with the workshops and meetings, six-month secondments on other institutions were planned for each fellow to further complement the formation. My secondment took place at CeramTec GmbH, a company mostly known for manufacturing biomedical ceramic implants for hip arthroplasty.

Without the help and participation of many people, the work of this thesis could not have been accomplished. First, I would like to acknowledge my supervisors Jérôme Chevalier and Laurent Gremillard. They were really helpful when they were available, but even more helpful when they were not. It is true that sometimes I have felt a little bit abandoned, but this deliberated decision of them helped me be more responsible in the decision-making moments and make this work even more personal. Also, even if the topics discussed in this thesis were out of their expertise, they always had interesting remarks and comments. If this work is any good, it will be just a reflection of their excellent guidance.

I would also like to acknowledge Alan Porporati, who kindly welcomed me at CeramTec and who allowed me to work in freedom to fulfill the goals of the secondment. Being a peculiar combination of friend and supervisor, he further helped me integrating the team there, and made the six months I spent there a lot more enjoyable. In the same line, I would like to thank Meinhard Kuntz for his

kindness and consideration whenever he was available (which happened seldom). Finally, all the people at CeramTec, who accepted my limited ability to speak German and still welcomed me and helped me learn it while having a great time.

I would like to express my recognition to all the Biobone people, ESRs, ER and supervisors. This European project has been one of the greatest experiences I have ever had in my life and I will be always grateful. For three years, we have travelled and met all across Europe, we have been trained and formed by great lecturers and we have been given the chance to live in and learn from different cultures and languages. Finally, I cannot but express my gratitude to the European Commission for promoting these kinds of initiatives.

I thank also all my friends at MATEIS because they made the experience of sharing the facilities a lot more interesting and gratifying. Also I would like to include in this list all the people who were once working in MATEIS and moved elsewhere. Thank you very much guys.

Thesis outline and Objectives

This manuscript is structured in three separated chapters preceded by a general introduction that serves as context. Each chapter is organized in the form of a scientific article, which would be submitted contemporaneously to the file of the current document. The three chapters are independent to each other, but cover some of the most important features regarding the interactions between biological environment and implant surfaces. The use of roughness to promote osseointegration of implants is a common practice, especially on dental implants. Roughening is often conducted by mechanical treatments, the most common being sandblasting. Therefore, chapter 2 focus on the implications of roughening by sandblasting on the mechanical behaviour of zirconia, alumina and a zirconia-alumina composite, and the differences between them.

The work brought in chapter 3 was carried out entirely during the six-month secondment at CeramTec GmbH. In a bearing couple, lubrication mechanisms are complex and wettability and proteins play a yet-to understand role. The study compared the wettability of different materials, their ability to welcome protein adsorption and the effect of different cleaning procedures on wettability measurements and protein adsorption.

Finally, the influence of the surface on cell activity is not driven exclusively by roughness: chemical modifications of the surface may enhance the perception of cells for the surface, and by careful tuning of the surface properties one may achieve a better integration without the downsides of roughness. In chapter 4, we explored a novel modification of zirconia, based on known techniques in chemistry, which introduces molecules with special functional groups capable of rendering the surface friendlier for cell adhesion, and opening the window for new exciting developments in the field of bioinert ceramics.

1

GENERAL INTRODUCTION

Contents

1.1. Bioinert ceramics	11
1.1.1. Alumina.....	11
1.1.2. Zirconia	12
1.1.3. Zirconia-Toughened Alumina (ZTA).....	14
1.2. Orthopaedic implants.....	17
1.2.1. Dental	18
1.2.2. Hip joint.....	20
1.3. Cell - Material interactions	28
1.3.1. Fixation of implants.....	28
1.3.2. Importance of roughness	30
1.3.3. Role of surface proteins.....	33
1.3.4. Surface chemistry.....	34
Bibliography.....	37

1.1 Bioinert ceramics

The use of high-performance ceramics for biomedical devices has been documented since the early seventies[1,2]. They were developed as an alternative to surgical metal alloys [3] and as a way of overcoming the risks of periprosthetic osteolysis and intoxication from the debris released due to high levels of wear rates on metal-metal and metal-on-polymer implants for total hip arthroplasty (THA) [4,5], as well as early failure due to scratches and third-body wear[4,6,7]. While several materials have been used throughout the history of arthroplasty, in the following sections, I will be discussing some of the most relevant ceramics: alumina, zirconia and their composites.

1.1.1 Alumina

Alumina is found in nature in abundance. It occurs principally in the form of bauxites and laterites. It is represented as Al_2O_3 and it is available or prepared in several forms. Medical applications use α -alumina (corundum), but there exists other forms of alumina for other applications that may include γ -alumina, η -alumina or ρ -alumina [8].

It is normally colourless or ivory, although jewelry found the use of colored corundum as gemstones: rubies owe their red color to the minimal presence of chromium oxide and sapphires present blue color due to titanium oxide. The crystallographic structure of α -alumina is rhombohedral [9] and is often represented in an hexagonal super-cell as in **Figure 1.1**.

Alumina possesses several advantages including high hardness and scratch resistance, showing a low friction coefficient resulting in excellent wear resistance [2]. This is especially interesting in bearing implants for arthroplasty (e.g. shoulder, hip). In these applications, such properties allow as well a high resistance to third-body wear: when foreign particles are introduced between the two ceramic surfaces, they are broken down with the help of the friction movement and extruded with a lower damage of the bearing surfaces.

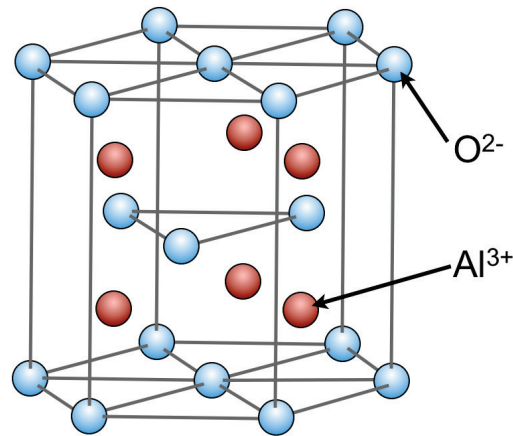


Figure 1.1. Crystallographic structure of α -alumina.

However alumina materials present some limitations in terms of fracture toughness as they lack mechanisms to reduce crack propagation. Although these problems were already addressed by optimizing the microstructure and specially lowering average grain size and size distribution [10], the margin of improvement of toughness is limited, or even irrelevant [11].

1.1.2 Zirconia

Yttria-stabilized zirconia materials emerged as a natural alternative to alumina in the 80's. They were introduced for the first time in 1985, and standardized in 1997 (ISO 13356)[12]. Zirconia presents three allotropes: monoclinic (stable up to 1170 °C), tetragonal (stable between 1170 and 2370 °C) and cubic (stable from 2370 °C). Their crystallographic structures are presented in **Figure 1.2**.

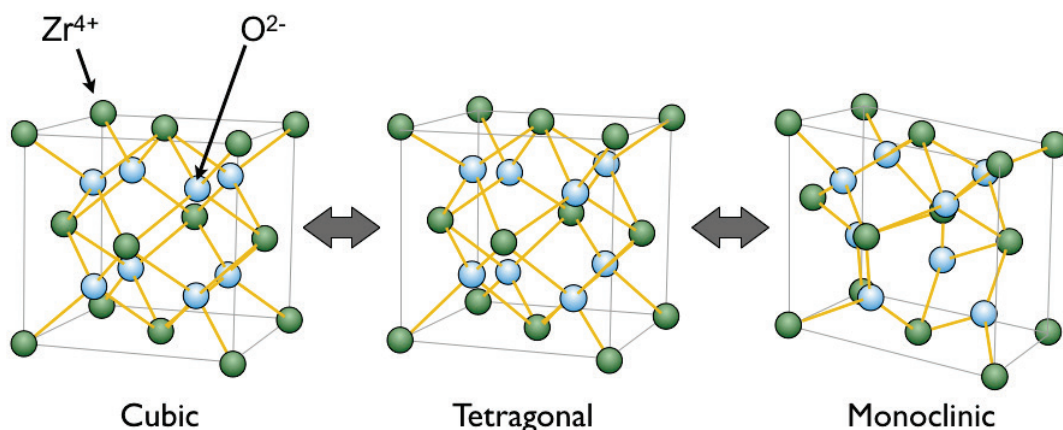


Figure 1.2. Crystallographic structure of the allotropes of zirconia.

A martensitic transformation takes place during sintering, upon heating (monoclinic to tetragonal) and cooling (tetragonal to monoclinic). The tetragonal to monoclinic transformation is accompanied by shear strain and an important volume increase of about 3-5%. This brings important internal stresses that lead

to the disintegration of pure zirconia during cooling and after sintering. Only two solutions can keep the integrity of the pieces: either sinter at a temperature lower than 1170 °C to maintain the monoclinic state during the sintering, or stabilize the tetragonal or cubic phase at room temperature to avoid the transformation during cooling. The materials obtained through the first solution do not present interesting mechanical properties.

The second solution is based on the fundamental approach described by Ruff *et al.* [13] almost a century ago: mixing zirconia and another oxide to partly or completely stabilize the cubic or tetragonal phase. The most common oxides used with zirconia are of Yttrium (Y_2O_3), Cerium (CeO_2), Magnesium (MgO) or Calcium (CaO). Depending on the grade of stabilization, we distinguish three main types of microstructure: Fully-Stabilized Zirconia (FSZ), Partially-Stabilized Zirconia (PSZ) and Tetragonal Zirconia Polycrystal (TZP). In FSZ, there is only cubic phase, and it is generally obtained by adding large quantities of stabilizer (higher than 8% mol of Y_2O_3). In PSZ, the microstructure is composed by a cubic matrix with nanometric precipitates of tetragonal or monoclinic phases, and it is usually obtained by adding CaO or MgO . Finally, TZP is mostly composed of tetragonal phase, although they typically contain some cubic phase in minority. The majority of TZP materials available in the market are obtained by stabilizing the tetragonal phase with CeO_2 or Y_2O_3 [14].

The interest of TZP materials in arthroplasty lays in their unique strengthening mechanism known as transformation toughening, which was first exploited by Garvie *et al.* in 1975 [15]: under stress, the metastable tetragonal grains transform to the monoclinic phase at the crack tip, inducing compressive stresses with the help of the volume expansion due to the structural change and effectively increasing the resistance to crack propagation.

In order to maximize the performance of TZP, there exists a certain preference for using Yttria as stabilizer (3Y-TZP): By using only 3% mol. of Y_2O_3 , the tetragonal phase can be kept at ambient without significant spontaneous transformation during cooling and can transform locally under stresses, for example at the tip of cracks [14]. Unfortunately, the transformation can also be triggered by the presence of water [16]. Later on, through mechanisms of nucleation and propagation [17] the transformed grains generate micro-cracks allowing more water into the cracks and to affect not-yet-transformed zirconia grains, creating more cracks and leading to delayed failure. This mechanism is referred to as hydrothermal aging, low temperature degradation (LTD) or simply "aging".

This process was underestimated at low temperatures, such as ambient or *in vivo*, until 2001, when around 800 zirconia implants from two different lots of Prozyr® ball heads catastrophically failed *in vivo* after less than two years of implantation. By then, different hypotheses were proposed to explain the failure: incompatibilities with the fixation on the stem, insufficient mechanical properties, etc. After a thorough investigation, it was contended that the failure was caused by an accelerated aging inside the neck of the ball head due to an undesired porosity. This triggered the transformation until catastrophic failure

when the transformed, micro-cracked zone reached a critical size [18]. The poor density in the core was attributed to a change in the sintering process, from batch-based to tunnel-based. It is important to note that all implants complied with the relevant ISO Standards and regulations at the time of implantation.

Two main consequences followed: First, this incident gave the aging process a relevant perspective among researchers and manufacturers, and consequently the ISO 13356 was modified in 2008 to include an evaluation of LTD. Second, pure-zirconia components were since then condemned to abandon from arthroplasty applications, except in Japan. At the same period, the use 3Y-TZP was boosted in dentistry, thanks to its excellent aesthetic properties and improved strength compared to other ceramics. At the time of writing, fortunately, there has been no strong warning against zirconia aging in the dental field, but this mechanism remains a point of vigilance.

1.1.3 Zirconia-Toughened Alumina (ZTA)

A possible way to avoiding or reducing aging while keeping sufficiently high mechanical properties is to combine zirconia at different compositions in the form of composites with other oxides, but most commonly with alumina [19,20]: Zirconia-Toughened Alumina (ZTA) and Alumina-Toughened Zirconia (ATZ) (both composites are technically suitable, and are being used for joint replacement implants).

ATZ is typically composed of 80% in volume of TZP and 20% alumina. It is reported to have a superior mechanical and tribological properties compared to alumina [21]. Commercial components made of ATZ include Bio-Hip® by Metoxit AG (Thayngen, Switzerland) and Ceramys® by Mathys Ltd. (Bettlach, Switzerland).

ZTA is a more popular composite, containing up to 30% in volume of Y-TZP (but usually with a lower yttria content than in monolithic zirconia) in an alumina matrix. It combines the advantages of monolithic alumina and zirconia: the addition of zirconia to alumina provides higher strength and fracture toughness with little reduction in hardness and elastic modulus, compared to the monolithic components [21]. Examples of commercial ZTA materials are: BioloX® *delta* by CeramTec Medical Products (Plochingen, Germany), and *Bioceram*® AZ209 by KYOCERA Medical (Osaka, Japan).

ATZ and ZTA materials achieve their higher properties through several mechanisms that will be discussed below. While we focused on ZTA, the main features also apply for ATZ materials.

Phase transformation

Taking advantage of the reinforcing mechanism of TZP, the toughness of ZTA materials gets increased. The enhanced resistance to crack propagation is

achieved through the transformation of tetragonal zirconia grains at the crack tip: Since the transformation is associated with a 3-5% volume expansion, the crack requires extra energy to propagate through the transformed compressive layer, and this either stops the crack or helps to reduce the net crack driving force.

However, compared to monolithic zirconia, ZTA is less prone to LTD, with generally lower kinetics and a lower impact of the transformation on structural integrity [20,22]. The generally higher stability of the composite is attributed to the alumina matrix, which keeps the transformed zone enclosed in a local region and limits the transformation from propagating to neighboring grains. It is to note, however, that several papers have documented time-dependent transformation of ZTA and ATZ under relevant low temperatures [22]. Therefore, the issue of aging cannot be fully discarded.

Platelets to block crack growth

Some manufacturers introduce strontium oxide crystals to create strontium aluminate composites, which form rod structures (platelets) of 3 μm of maximum length and generally account for 3% of the volume [21]. The reinforcing mechanism proposed is presented in **Figure 1.3**. According to Kurtz *et al.* [21], the platelets deflect the crack as it propagates. The use of strontium aluminate platelets is reported in both CeramTec BioloX *delta*, and KYOCERA BiocerAM AZ209. When ZTA materials contain these platelets, they are often referred to as “zirconia toughened platelet-reinforced alumina” (ZTPA).

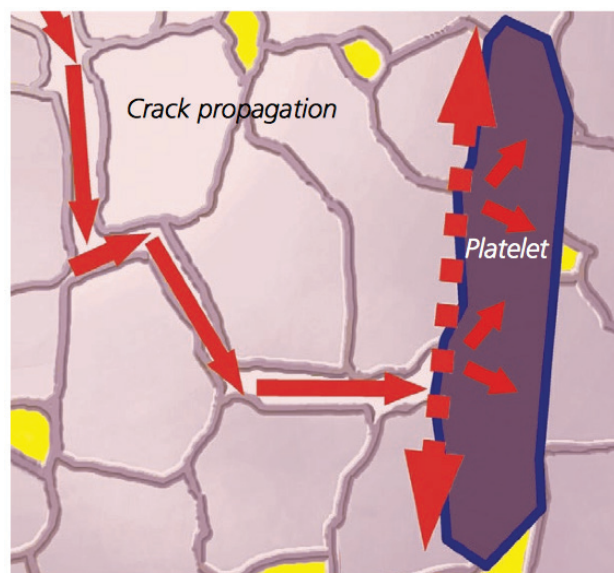


Figure 1.3. Crack deflection on strontium aluminate platelet. (Source: CeramTec GmbH www.ceramtec.com)

Grain size control

As demonstrated by De Aza *et al.* [23], the reduction of grain size and the homogeneity of particle distribution allows to increase the composite's toughness. The microstructure resulted in submicrometer alumina grains and mainly intergranular, nano-sized zirconia particles with a narrow grain size distribution. The small size of zirconia allowed a larger amount of tetragonal zirconia grains in the alumina matrix, and the alumina matrix helped stabilizing the zirconia phase while still allowing the stress-induced toughening mechanism.

Strengthening additives

As explained with TZP, zirconia requires stabilizers to maintain the zirconia grains in the tetragonal phase at ambient temperature. This holds true on ZTA materials as well. However given the stabilizing effect of the alumina matrix, their amount can be reduced, as it happens for instance in Biolox delta [22]: the yttria content (1.3 mol%) is lower than the usual content in monolithic zirconia. Additional evidence is found in KYOCERA AZ209, which does not use any stabilizer.

Other additive found in Biolox delta is chromium oxide. Initially since conception, it was hypothesized that the presence of this oxide increased the hardness and wear characteristics [24], as well as providing its distinctive magenta tone. However, in a recently published statement [25] it was admitted that much higher chromia content is necessary to increase hardness, as independent research already showed in 2005 [26]. In opposition, chromia does seem to have an effect on hydrothermal degradation as reported by Pezzotti *et al.* [27]. According to this article, the zirconia phase is protected from aging at the expense of fast formation of oxygen vacancies in the chromium oxide stabilized alumina matrix.

1.2 Orthopaedic implants

An orthopaedic implant is a medical device that provides fixation of a damaged bone, or replaces articulating surfaces of a joint. The surgical procedures are performed by highly specialized surgeons and typically involve removal of the damaged joint and its substitution by an artificial prosthetic replacement.

There are many kinds of orthopaedic implants, and they use non-living materials to target the specific application: ceramics, metals, polymers and even composites. A great number of these implants deal with healing fractured bones. For these kinds of applications, pins, rods, screws and plates typically made of titanium or stainless steel are used to anchor the bone, and they do not necessarily substitute but support the function of those injured bones either temporarily until healing is complete, or permanently.

In other cases, orthopaedic implants are required to substitute partially or completely the function of a bone, or even the bone itself. This is the case of dental implants and joint substitutions. A very common case with needs for joint arthroplasty is patients with arthritis, which involve inflammation and usually pain in one or more joints. But also joint replacement surgery can follow other clinical pictures: diseases, injuries, etc. And it is in these kinds of applications where bioinert ceramics are considered valuable candidates. **Figure 1.4** represents a good summary of technically available bone substitutions by bioinert implants. In the following lines, the specifics of some of those implants will be discussed.

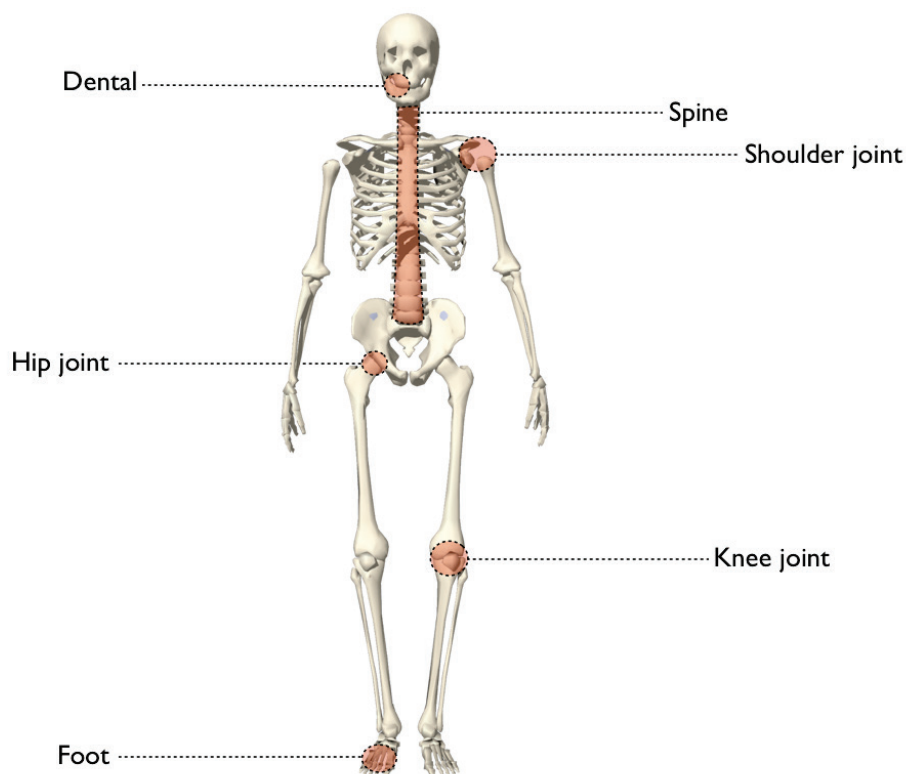


Figure 1.4. Body parts susceptible of being replaced by permanent bioinert implants nowadays.

1.2.1 Dental

The global market of dental implants is estimated to grow at an annual rate of 7.2% from USD 7,336.7 Million in 2015 to USD 10,427.7 Million in 2020 [28]. Europe is estimated to contribute the maximum share to the global dental implants. The high sales numbers in the dental market are attributed to rising incidences of dental caries and other periodontal conditions, increasing incidences of tooth loss and specially the rising aging population. The access to better dental insurance coverage for dental implants and the advantages of dental implants over dental prosthetics due to better aesthetics and hygiene will further help the growth of this market [28]. Some major players in this market include Straumann (Switzerland), Nobel Biocare (Switzerland), Dentsply International (U.S.), Zimmer Holdings (U.S.), Osstem Implant Co. Ltd. (South Korea), Biomet 3i (U.S.), 3M ESPE (U.S.), Danaher Corporation (U.S.), and Avinent Implant System (Spain).

Dental implants are best described as biocompatible anchors that permanently support crowns or dentures. A complete dental set consists of three parts: the implant itself, which is generally screwed to the jaw bone, the crown, which is the visible part that looks like the tooth, and the abutment, which connects the implant to the crown. Implants are preferred over traditional bridges because they do not require altering adjacent teeth, as shown in **Figure 1.5**.

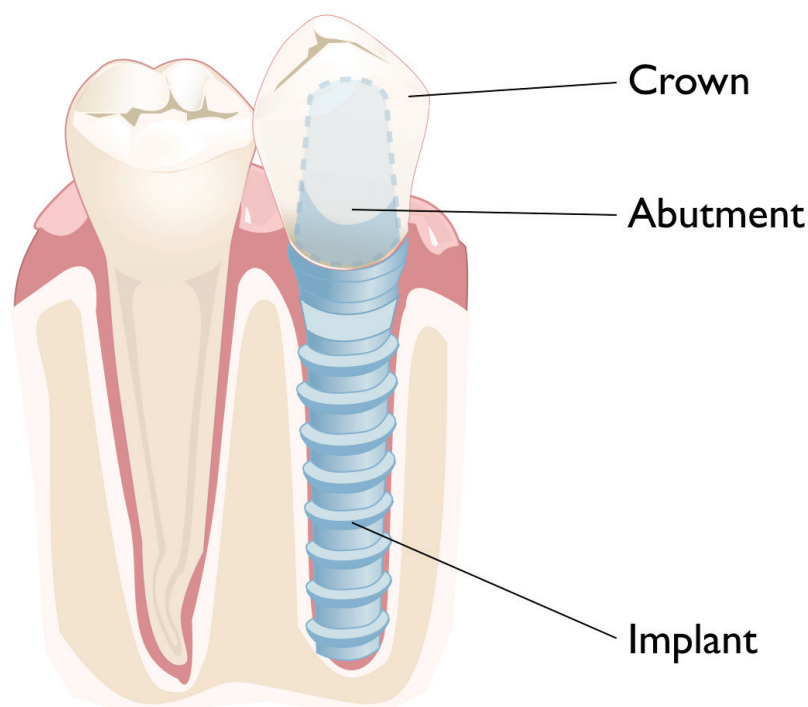


Figure 1.5. Parts on a dental implant.

Up to now, there are three types of dental implants regarding the material they are conformed of: the older all-metal type, the newer ceramic-metallic, and the even newer all-ceramic (**Figure 1.6**). Until recently, practically all dental implants have been of metallic construction, made of commercially pure

titanium or a titanium alloy. The main reason was to give mechanical strength and therefore augment the longevity of the treatment. The improvement of the manufacture techniques and the advancements of material science allowed the conception of ceramic-metal hybrids and all-ceramic implants. Nonetheless, titanium implants still take the biggest share of the dental implant market [29], and this is attributed to their lower costs of manufacture, their sufficiently high mechanical properties, and because they meet the requirements for most applications. In 2015, ceramic (zirconia) implants accounted for less than 2% of the global dental implant market, but it is expected to grow by 6% in 2020 [30].

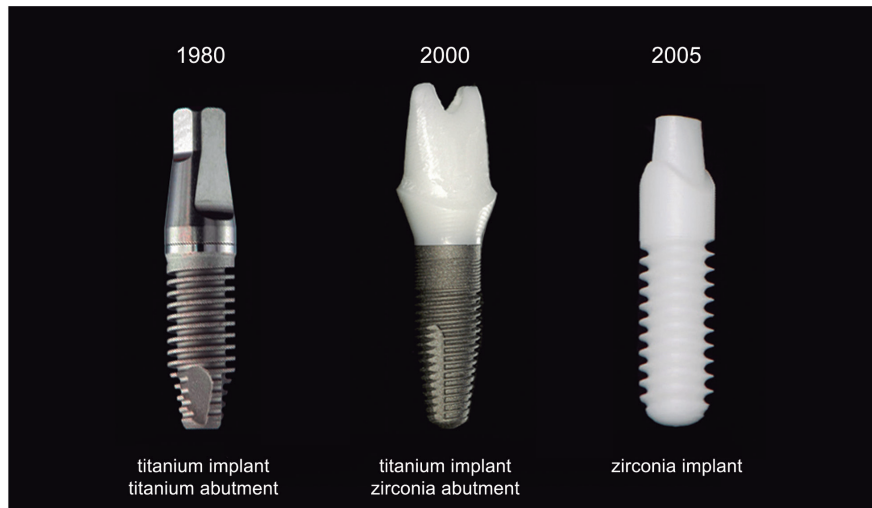


Figure 1.6. Evolution in implant dentistry. (Source: CeraRoot, Oral Iceberg S.L. www.ceraroot.com)

However, in some particular cases, zirconia may be preferred to titanium: metallic implants are dark coloured and they can be visible while implanted through the gingival tissue (gum). This gives an unhealthy look to gums. On the contrary, ceramic implants are white, and when implanted, they are undistinguishable from bone from the outside, even in very thin gums (**Figure 1.7**).

Other cases where zirconia is preferred to titanium include patients with sensibility to metal, or patients willing metal-free devices, given that ceramics are inert, non-corrosive and non-allergic.

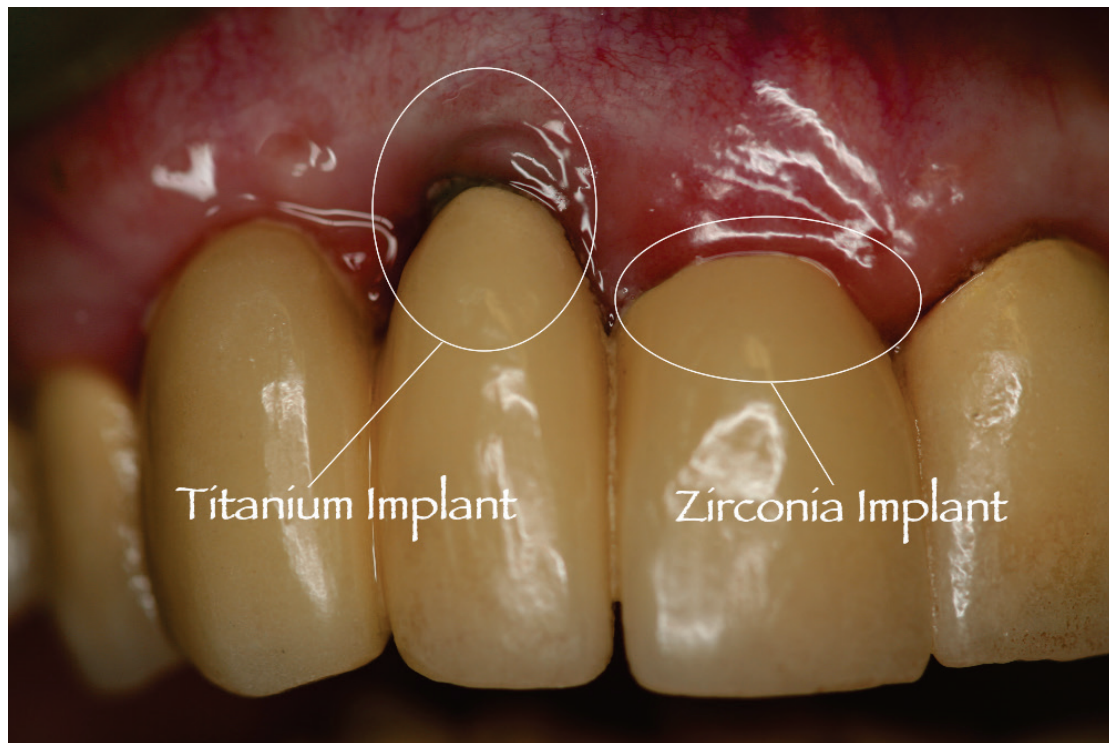


Figure 1.7. Titanium implant (left) and zirconium implant (right). (Source: Miles of Smiles, www.milesosmilesdental.net)

Furthermore, ceramic implants are designed as one single piece, in opposition to the two-piece design on metallic. This supposes an advantage, since the one-piece design reduces bacterial accumulation in the junctions and the risk of infection. Unfortunately, this design is considered a drawback for some dentists, who claim it reduces the degrees of freedom and make the placement more difficult.

1.2.2 Hip joint

The global market of hip reconstruction devices was valued at USD 4800 Million in 2014 and is expected to reach USD 5900 Million by 2020 at an annual growth rate of 3.0% from 2015 to 2020 [31]. The growth of this market is lower than for dental implants, mostly because it is more mature. Favourable to the growth of this market we have available the rising pool of arthritis patients, convenient reimbursements from health insurance policies, and technological advancements that allow higher success rates in ordinary surgeries as well as wider windows for riskier cases, specially among young patients. Additionally, the growing health awareness among masses, along with increasing spending capacity of the population is propelling the market growth. Some major hindering factors such as risks of complications after surgery (either related to the implant, to the patient's health, or to the surgery itself), the waiting list in hospitals and the maximum process fixed by national health authorities could compromise the prospective growth of the otherwise profitable market. Some of the major companies operating in this sector are Zimmer Biomet (USA), DePuy Synthes

(USA), Stryker (UK), and Smith & Nephew (UK), B. Braun Melsungen AG (Germany), Corin (UK), and Waldemar LINK GmbH & Co. KG (Germany).

Hip joint interventions typically consist of the complete replacement of the joint by a multi component system, detailed in **Figure 1.8**: two components go in the acetabular socket, and another two in the femur. The operation requires carving and cutting the original joint to accommodate the implant. As with the stem, the acetabular shell can be either cemented or more commonly forced directly into the bone.

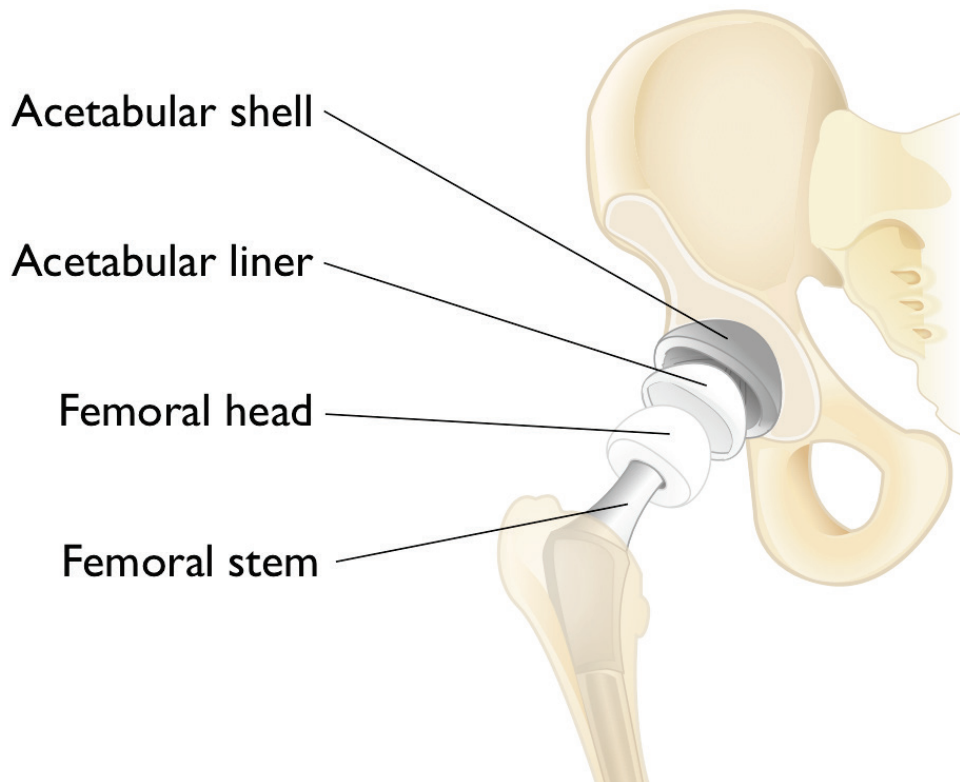


Figure 1.8. Parts on a total hip replacement

When the surgeon evaluates each patient's case, he integrates a great number of details, including (but not limited to) the patient's overall health, the medical prognosis, the quality of bone, his age, and his lifestyle's physical activity. To accommodate the wide range of needs, the surgeon can select the best implant from the multiple solutions offered by the market. One crucial classification of implants describes the way the actual joint is substituted: Hard-on-Hard (HoH) or Hard-on-Soft (HoS) bearings. This nomenclature refers to the nature of the materials used on the liner and the ball head, which are the parts in tribological contact that form the bearing couple. They use metals and ceramics as "Hard" materials, and polymers (polyethylene) as "Soft".

Each configuration has different features but also different associated problems. However, as the competing companies released their products on the market, different preferences and trends have been observed within the market throughout history. Initially, HoH bearings were constituted of metallic components (hence Metal-on-Metal or MoM), such as steel or Cobalt-Chromium-

Molybdenum (CoCrMo) alloy. The high toughness of these materials made them great candidates. However, they are not hard enough and abrasion of the bearing surfaces emitted great quantities of ions and metallic particles that accumulated for years on the surrounding tissue. The process is called metallosis. Pseudotumors, risk of necrosis and generally local pain along with osteolysis are common consequences for affected patients. Loosening or dislocation of the non-cemented implants is as well common. Finally, poisoning from metallosis is rare, but cobaltism is still an established health concern. The use of MoM bearings is currently on very low demand due to the associated problems described above.

HoS bearings represent a very common approach that emerged as an alternative to MoM. They consist on hard (either ceramic or metallic) ball heads and soft (polymeric) liners. The use of polymeric liners has huge industrial advantages such as the lower cost of fabrication and their easier implantation, both helped by the higher tolerances that are imposed in comparison with hard bearings. These two circumstances also allow a greater diffusion of the product among surgeons, including less-experienced ones, as the polymer tends to be a more “forgiving” material.

However, HoS bearings are limited in their performance. While the emission of metallic particles is greatly reduced (specially if the ball head is ceramic), the high wear rates on the polymeric component and consequently important incidence of osteolysis were still limiting factors. Accordingly, HoS bearings are not indicated for patients with active lifestyles (mostly young patients) because the high wear rate increases the risk of component loosening. **Figure 1.9** displays an example of the extreme wear a HoS bearing can go through. Additionally, misalignment of components during surgery can be responsible for accelerated wear. Motivated by the poor wear resistance of polyethylene, liners of highly cross-linked polyethylene (XLPE) began to be manufactured and commercialized instead. XLPE is much more resistant to wear and generates smaller wear particles. However it has reduced mechanical properties, compared to conventional not cross-linked polyethylene. The high cross-linking of the polymer is achieved using high-dose irradiation (50-100 kGy), but it was observed that it also induced the formation of free radicals in the crystalline phase [32], and with time it could cause oxidative degradation of the material. To combat these free radicals, different annealing methods including post-radiation re-melting of the crystals were proposed to allow the recombination of the free radicals [32]. However, this reduced the crystallinity and therefore the fatigue strength. Alternatively, new products of XLPE make use of vitamin E stabilization, which is intended to provide oxidation resistance without sacrificing some of the fatigue strength. Recent results showed promising performance in terms for wear against standard XLPE [33].



Figure 1.9. Ceramic-on-Polymer joint. The ceramic ball head wore the liner and even continued through the metallic shell. (Source: Dr. med. Karl-Heinz Günther, www.doccheck.com)

The use of ceramics in HoH (hence Ceramic-on-Ceramic, written CoC from now) presents several advantages in comparison with HoS bearings: ceramic bearings have the lowest wear rates of any bearing combination, and the higher hardness of ceramics protects them against scratching and third body wear (the bearing breaks the foreign particles down, and extrudes them as shown in **Figure 1.10**). They are however more constrained by the positioning, and while a misalignment in HoS may lead to higher wear, in CoC it can lead to several post-surgery issues such as “chipping” of the implant, “squaking” of the bearing, or even fracture. Hence, CoC bearings require high precision and dexterity during implantation, which less-experienced surgeons may find unsettling.

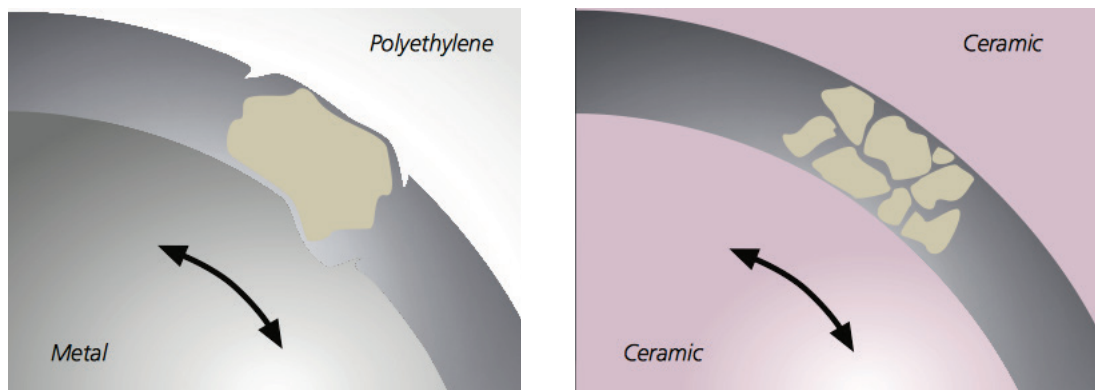


Figure 1.10. Third body wear resistance in CoC. (Source: CeramTec GmbH www.ceramtec.com)

Lubrication in bearings is fundamental, and in hip implants a good lubrication allows to reduce the friction coefficient and hence the exposure to wear. The lowest friction coefficients are displayed by lubricated CoC bearings. However, when they are tested in “dry” conditions, the friction factor increases by 4 or 5 times [34]. Additionally, sometimes audible “squeaking” can be perceived, and is reported both *in vitro* and *in vivo*. It has been related to the loss in the lubrication film (specially after long periods of rest, before the lubrication is restored) and the direct contact of the two bearing surfaces. While a ‘squeaky’ joint may be fully operative in terms of performance and insignificant in patient satisfaction, it is usually considered multifactorial and it is important to identify the source of this squeaking as soon as possible to discard more severe problems [35].

The size of the natural femoral head ranges from 40 to 54 mm (with smaller sizes in women). During the initial development of hip replacement, surgeons tried to make the implants that mimicked the size of the natural femoral head. However, it was soon realized that the higher the contact bearing, the higher the (volumetric) wear. Hence, the ball heads of the first hip implants were designed to be 22 mm. Nonetheless at these sizes the risk of dislocation, shown for example in **Figure 1.11**, is very high. Nowadays implants have sizes starting at 28 mm. After surgery patients are encouraged to resume most of their activities. This strengthens the fixation by stressing the bone and forcing it to adapt to the new implant by means of the natural process governing bone growth. However, patients may still need to change the way they were used to use their joints prior to surgery. For example, they may need to change the way they bend down to prevent the hip from dislocating, *i.e.* the ball head coming out of the socket. In some cases, the doctors are able to perform the necessary movements to put it back, but in others surgery will be the only option.



Figure 1.11. X-ray on hip joint showing dislocation of head (Source: Singh et al. [36])

While re-educating the patient locomotion is crucial, varying the size of the ball head can increase the range of (ROM) of the artificial joint as well as reducing the risk of dislocation. In **Figure 1.12**, we can observe the different ROMs provided by each ball head size. The use of higher size ball heads allows larger ROMs and consequently improving the patient's life after surgery. Because higher size means higher volumetric wear, today they can only be conceived as CoC.

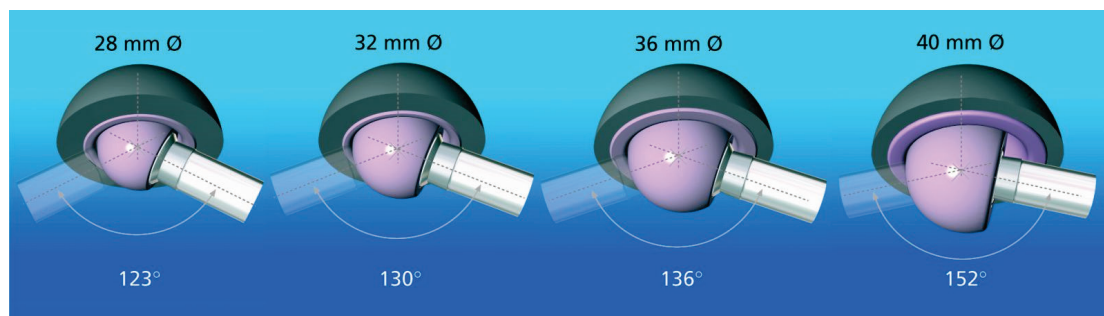


Figure 1.12. Different of ranges of motion (ROM) as a function of the ball head size. (Source: CeramTec GmbH www.ceramtec.com)

There exists another alternative to the conventional system, which is a procedure known as “Birmingham Hip Resurfacing” (BHR). It was pioneered by Derek McMinn and the design presents multiple advantages over the traditional hip replacement. The design of the implant is shown in **Figure 1.13**. The main advantage of this procedure is its minimum invasiveness: to implant joint, the surgeon only needs to remove a few millimetres from the articulating surface. This means the procedure conserves the majority of the bone that in a conventional THA would be otherwise removed, as shown in **Figure 1.14**.

Another great advantage is that as the size of the implant approaches the size of the original joint, larger ROM and lower risk of dislocation are expected.



Figure 1.13. Birmingham Hip Resurfacing implant. (Source: The McMinn Centre www.mcminncentre.co.uk)

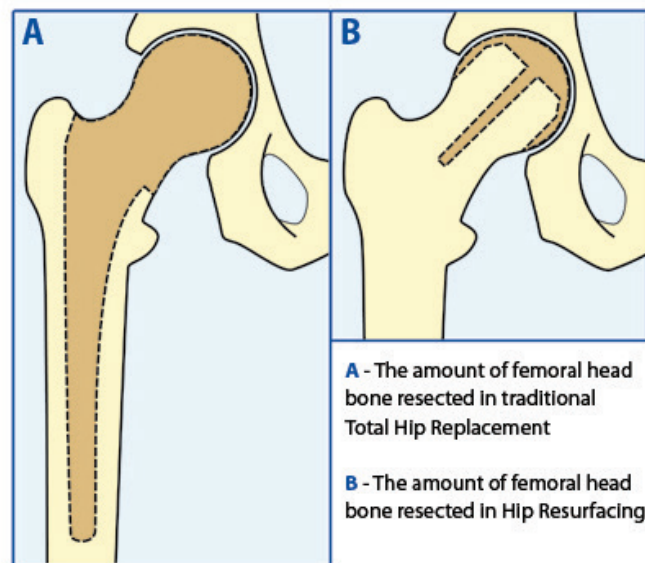


Figure 1.14. Difference between traditional THA and BHR. The coloured zone represents the amount of bone removed. (Source: The McMinn Centre www.mcminncentre.co.uk)

However, since they were conceived in metal as MoM bearings, large volumetric wear (and all the associated problems) is expected on active patients, leading in some cases to revision surgery and associated complications. CoC BHR implants would seem *a priori* the perfect combination. At the moment of writing this thesis, it is an open topic being discussed and researched. Nonetheless, it requires a careful and advanced design and planning for several reasons. One of the reasons may be related to the conformation design of the BHR implant in

conjunction with the brittleness of ceramics: massive ball heads and liners are less prone to break than the thin components of BHR. Another reason is that even if the design is robust, if the implant is ceramic, the surgeon has to be skillful enough to avoid misalignment of the components (which can be an important cause of early failure). Third and equally important, BHR procedures are currently not massively present in the market. Although on paper they would seem very positive for the patients, in reality their success is conditioned to a progressive deployment where only positive results can testify for the success. In order for surgeons to adopt the new system, they need undeniable success stories. Otherwise, the fear of implant failure may doom the technique despite its numerous advantages on paper.

1.3 Cell – Material interactions

1.3.1 Fixation of implants

There are nowadays two ways of fixing implants to bone: through cements, or “cementless”. In general terms, the first uses of cement-based fixation can be tracked down to the end of nineteenth century (1850s and later), first on dental [37], and later on THA in 1891 by Glück [38]. The use of cements in THA was popularized in 1950s by Sir John Charnley (the father of modern THA), who used cement already developed in dentistry. However, in 1980s failures of hip replacements by osteolysis were attributed to an undetermined “cement disease” [39], their use in THA was reduced in favor of cementless techniques. It is now known that such cement disease did not exist and the causes of osteolysis were, among others, the emission of particles from the bearing surfaces (mostly MoM and HoS) [40].

In dental restorations (implants, bridges and crowns), cemented and cementless solutions are applied, depending on the kind of restoration. While dental implants are typically screwed into the bone without using cements, bridges and crowns are cemented either to surrounding teeth or the abutment on the implant, or sometimes screwed to the implant as a temporary solution (**Figure 1.15**). Normally, these temporary restorations are substituted by cemented crowns (or bridges), which offer the elimination of anesthetic screw access holes (as shown in **Figure 1.15**) and greater resistance to porcelain fracture. However, excess of cement left behind inadvertently is considered a major problem and can result in soft tissue damage, bone loss and/or chronic inflammation [41].



Figure 1.15. Detail of screw hole access on a temporary screw-retained restoration
(Source: loveperio.com)

In THA, the application of cementless implants extends from young patients to older patients with good bone stock (including revision THA). In other situations, cemented implants are preferred. The use of screws in THA is controversial [42], and may be indicated in osteoporotic bone and when there is insufficient bony coverage. On the negative side, there is suspicion that in some cases the use of screws may lead to osteolysis [42].

Cementless fixations are generally based on two mechanisms that work simultaneously: mechanical interlocking and biologic fixation. The first mechanism makes use of the bone rigidity to grip the implant under compressive stresses. In most cases, surgeons performing THA carve the acetabular socket a little bit smaller than the acetabular metallic shell, and literally hammer the shell into the pelvis to accommodate it. This design is generally known as “press-fit design” and works right from the moment of insertion, providing a stable fixation and allowing the second mechanism to take place in the next days after surgery. In other cases, the size of the implant is the same as what the surgeon carved, and often screws would be placed to ensure fixation.

In order to promote a simultaneous biologic fixation of the implant, the surface in contact with the bone has been modified in different ways to promote bone growth. Manufacturers propose different strategies of modification but in most cases they involve different scales of roughness, as observed for example in **Figure 1.16**. In general, there are two types of biologic fixations: “ingrowth”, *i.e.* the bone grows into porous structure of implant, and “ongrowth”, *i.e.* bone grows onto the micro-divots in a grit blasted surface. Bone ingrowth enhances mechanical fixation, but requires more growth time than ongrowth fixation. Both strategies can be pursued either with the use of coatings (this is specially true for ingrowth), or direct roughening of the surface by sandblasting or acid etching in the case of ongrowth. In some cases, hydroxyapatite coatings had been used as osteoconductive agent in combination with any of the two mentioned strategies. It is often claimed that it may allow a more rapid closure of gaps between bone and prosthesis. However, while it has shown a shorter time to biologic fixation in animal models, there are doubts on the clinical advantage in humans [43–45].

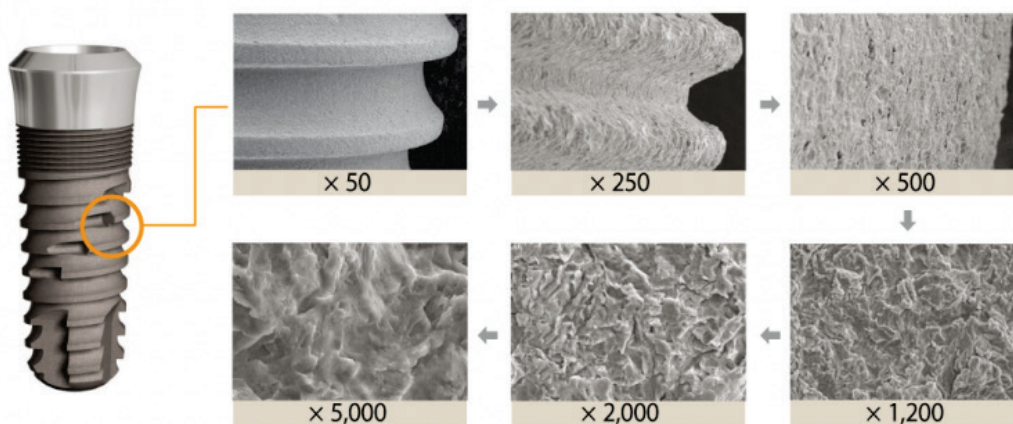


Figure 1.16. Example of dental implant with roughness at different scales. (Source: dentis-implant.com)

A known issue associated to an imperfect fixation is the encapsulation of the implant by a fibrous tissue. It is usually consequence of micro-motions and the usual consequence is revision surgery. Additionally, some studies suggest that rougher surfaces elicit a prolonged inflammatory response than smooth surfaces. This inflammation would be detrimental to bone ingrowth and could lead to fibrous encapsulation as well [46].

1.3.2 Importance of roughness

Compared to smooth surfaces, textured implants exhibit more surface area for integrating with bone via osseointegration process. A high number of *in vivo* studies have demonstrated that an increased surface area on the implant improves bone-to-implant contact after surgery [47], by enhancing cellular activity and improving bone apposition on the surface. A good example taken from the work of Gahlert *et al.* [48] is reproduced in **Figure 1.17**: the implant on top has been sandblasted and presents a much higher bone-to-implant than the implant on bottom, which presents a smoother machined surface. The reason of this better interaction is multi factorial and not fully understood. In many cases, cell adhesion and bone formation are more efficient for certain types of roughness, in particular those displaying nano-scale roughness [49].

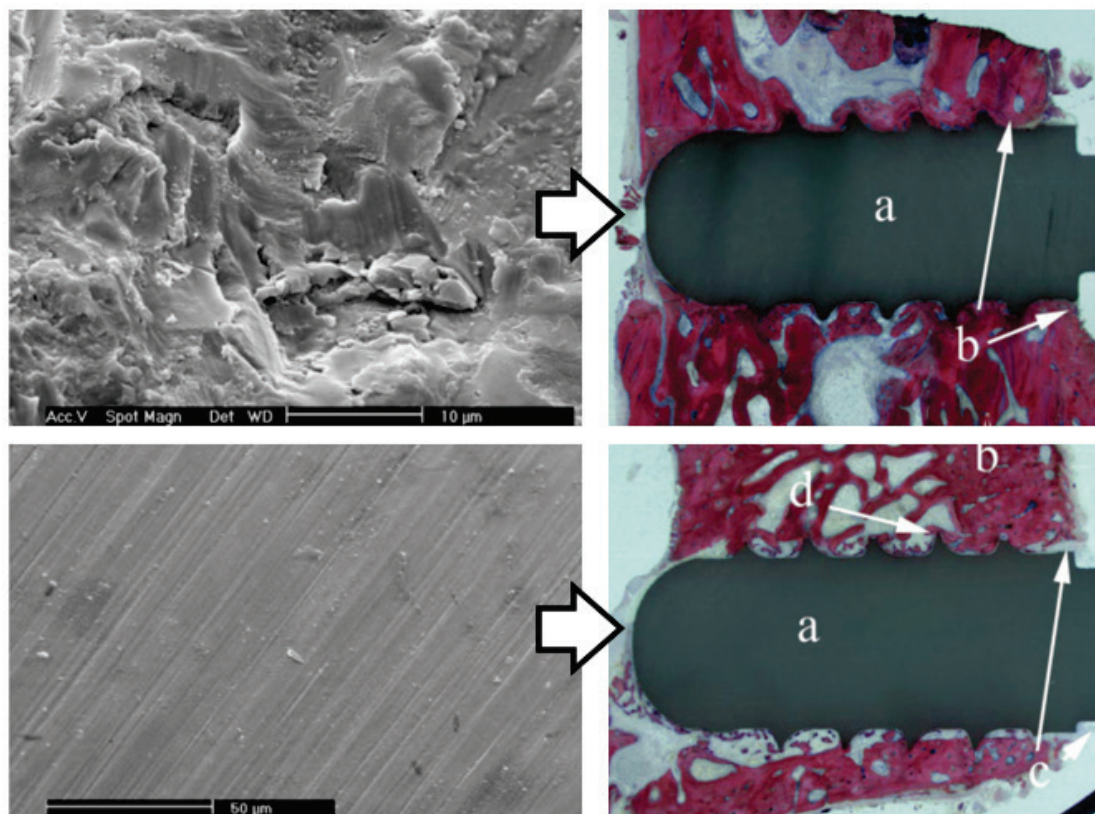


Figure 1.17. Zirconia dental implants *in vivo*. The images on top correspond to a sandblasted surface, while the images at the bottom correspond to a machined surface. (a) Implant, (b) bone, (c) tissue at the neck of the implant, (d) peaked threads. (Source: Gahlert *et al.* [48])

In general terms, the increase of roughness can be achieved in any surface through either adding material (*e.g.* coatings, plasma spray, ion deposition) or removing it (*e.g.* grit-blasting, acid-etching, plasma-etching), and each different technique will provide a different surface texture, which is normally analysed using statistical parameters. These parameters are used to describe numerically the appearance of the surface topography. There exist three major groups: height, space and hybrid parameters. Height refers to the relative height of the features; spatial or texture parameters describe the horizontal distance between irregularities; hybrid include both spatial and height parameters to describe the developed area, the slope or the curvature of the irregularities [50]. In practice, there are many different surface roughness parameters (more than 150 can be found in literature according to Wennerberg *et al.* [50]), and it becomes a problem of comparability between works of different authors if they do not use the same parameters to describe their surfaces. However, there is still doubt about which set of parameters is the most suitable for implants. Typically, manufacturers and some researchers solely use the average peak height, either in the bidimensional (R_a) or tridimensional form (S_a), to describe an implant's roughness. However, the average roughness parameter is known to be quite stable and not very sensitive to occasional high peaks or deep valleys, and it is incapable *per se* of differentiating profiles such as the ones shown in **Figure 1.18**.

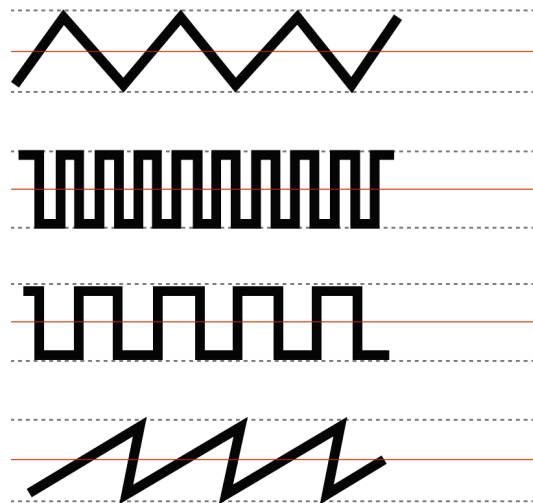


Figure 1.18. Four different profiles with the same average height parameter (R_a).

The techniques used to roughen a surface, in the majority of cases do not merely 'add' roughness, but they modify the material in more ways. From a theoretical point of view, a rough surface is plane surface with a distribution of surface defects. These defects may play different roles on the properties of the new surface, for example they may modify the mechanical properties of the material and its mechanical performance in long term. No matter how advanced the manufacture process is, all materials will present intrinsic flaws in their structure. When a material fails, the starting point of the cracks that lead to the failure is usually located in the best orientated and normally the biggest defect. This defect is known as the critical defect. If the surface treatment generates

bigger defects than the intrinsic ones, then the treatment will be contributing to weakening the material. This is especially evident in the case of roughening by subtraction of surface material using blasting or grinding techniques. However, in those cases the treatment also exerts stresses to the surface, generating a distribution of residual (tensile and compressive) ones after it. Compressive residual stresses oppose to crack propagation, whilst tensile residual stresses facilitate it. It is obvious that if a surface treatment creates both surface defects and residual stresses, the interplay between both will define their impact on the mechanical properties of the material.

Many authors have studied the consequences of roughening techniques such as sandblasting or grinding on zirconia-based ceramics, and in the majority of cases reviewed sandblasting increased the overall strength of the material while grinding (either dry or wet) reduced it [51–56]. Other papers report increase in strength after grinding as well [57,58], and even some others describe loss of strength after sandblasting [56,59,60]. Additionally, when some of these blasted surfaces were annealed, they exhibited lower strengths [54,57], evidencing the role of compressive stresses on the higher values of strength. But as Chintapalli *et al.* showed, not all configurations of sandblasting treatments lead to better mechanical performance of zirconia [56].

Most of the literature found on the topic of mechanical effects of roughening ceramics focused on zirconia materials for dental applications, where roughness is in principle necessary to promote adhesion to cements and resins used to fix crowns and bridges. Surprisingly, little number of them [59,60] studied the same effects on alumina-based materials, despite the fact that they are still considered suitable candidates for crowns [61]. In fact, most of the literature found on sandblasted alumina studied the ability of rough ceramic surfaces to bond using different dental resin-cement systems, focusing in the short and the long term [62–66]. Being alumina materials much harder than zirconia but also less tough, risks of a higher damage on alumina may endanger its performance when only their bond to cements is studied. Moreover, it is of interest to study the differences between alumina and zirconia materials when they are exposed to the same sandblasting treatment, and this is the focus of chapter 2 of this manuscript.

Sandblasting and grinding are also known to alter the aging performance of zirconia-based materials [55,67,68]. On the one hand, open surface defects become entry points for water and nucleation points for the propagation of LTD, as explained by Deville *et al.* [18]. On the other hand, compressive residual stresses hinder the tetragonal-to-monoclinic transformation, stalling the propagation of LTD [55,67–71]. These two effects counteract each other, and we have investigated them in chapter 2.

Additionally, another very important aspect affected by roughness is the amount and nature of proteins that adhere on the surface, which will define the interaction between biological environment and implant's material. The effect is dependent on the interplay between the difference in scale of the roughness and the adsorbing molecule. Generally speaking, there are two main factors affecting

protein adsorption to consider: the increase in surface area, and the change of interaction potentials. The first implies that the higher the surface area, the larger the potential amount of adsorbed proteins, and this is especially true for small sized proteins. The second relates to the chemical interaction between substrate and protein: for example, the van der Waals interaction is very dependent on the geometry of the interacting entities [72]. This is only one aspect governing osseointegration. The ability of the surface to recruit the right molecules (proteins or others) to help cell adhesion is fundamental for an optimal integration.

1.3.3 Role of surface proteins

Throughout their lifetime, cells interact between each other, their environment and their substrate. They do it through complex cellular structures involving many proteins. There are significant differences between the complexes used by cells adhere to each other and those used to adhere to substrate, although the fundamental idea behind adhesion remains the same: to enable cellular communication through the generation and transduction of mechanical signals (*i.e.* forces produced by and exerted on the cell) [73].

Cell adhesions are mediated by either transmembrane cell-adhesion molecules (CAMs), which bind similar partner proteins, or adhesion receptors, which bind various ligands [74]. Some of these proteins include selectins, integrins, syndecans and cadherins. These proteins are used to essentially link the intracellular to the extracellular space to help relay information to the cell interior about the surroundings.

The extracellular matrix (ECM) is a collection of biomolecules secreted by cells that provide biochemical and structural support, and a medium for communication assisted by CAMs. In fact, recent research shows that the functioning of cells is very influenced by ECM [75], for example it is known that osteoblast cells secrete bone-forming ECM. The secreted molecules adsorb on the substrate following their own dynamics. Among all, glycoproteins such as fibronectin or vitronectin play a fundamental role in the adhesion and spreading of cells by allowing CAMs to bind to them [76]. However, as others have suggested [77] the actual substrate chemistry plays a very important role on the formation and degradation of ECM, and it is also correlated to as important other features as fibronectin adsorption or cell adhesion and signaling.

The nature of the interactions describing cell adhesion is far too complex [78] to be synthesized in a few lines, and exceeds the scope of this document. Therefore, we can just summarize it by saying that the ability of a substrate to allow the deployment of anchor points for cells increases the chances of a better integrated implant.

There are other facets of implant surface where proteins and other biological molecules are known to play some important role: in joint replacements,

biological molecules may influence and even define lubrication in the bearing couple. While it is true that the lubrication mechanisms of joint replacements are not fully understood yet [79], it has been discovered that proteins (especially those with the highest molecular weight) help lubrication by avoiding surface-to-surface direct contact [80–82]. For example, Liao *et al.* [80] observed that using as lubricant a modified serum lacking high-molecular-weight proteins produced a much higher wear rate than control serum. A similar result was reported by Myant *et al.* on MoM [82]: for globulin-based lubricant wear was negligible, whereas for bovine serum and albumin-based lubricant important wear damage was found (globulin presents a much higher molecular weight than albumin).

The exact role of proteins in lubrication is still in question. However, it is possible that protein adsorption could also alter the surface properties of the material, modifying the wettability of the surface and affecting lubrication [81]. In general terms, a higher wettability has always been associated to a better lubrication. This conception comes from the idea that a hydrophilic surface should recruit a higher quantity of (water-based) lubrication. But a literature survey shows that the situation is much more complicated than that: Borruto *et al.* [83], and 12 years later Pawlak *et al.* [84], studied different combinations of hydrophobic and hydrophilic bearing couplings through pin-on-disc tests and reported that the lowest wear was achieved when pairing a hydrophilic pin against a hydrophobic disc. Additionally, as indicated by Wang *et al.* [85], protein adsorption may be influenced by the actual wettability of the surface. Moreover, it is not hard to find in literature contradictory reports on the wettability of typical bearing materials used for joint replacement (alumina, zirconia, CoCrMo) given the sensibility of these materials to organic contamination [86]. All these points of interest were addressed in chapter 3 of this manuscript, where we used wettability measurements to study protein adsorption and the effect of different surface cleaning methods on both wettability and protein adsorption.

1.3.4 Surface chemistry

It was hinted in the previous section that surface chemistry has an important role on the development of ECM and the perception of the substrate by cells. When we talk about surface chemistry, we are talking about the chemical properties that define the way a surface interacts with its environment. In crystallography, a surface is observed as a disruption of periodicity, where the crystallographic structure found in the bulk no longer applies. At the very surface, not all chemical bonds are satisfied (because the structure is discontinued) and this generates an instability that can only be reduced by either reacting with surrounding external molecules, recruiting adsorbents, rearranging bonds or a little bit of everything. The chemical properties of a surface derive from its urge for stability, which is given by the kind of bulk crystallographic structure and the different elements that compose it. This means that at a molecular level, the local chemical properties will also affect the way proteins adsorb, the way ECM forms and hence the way cells interact with the substrate.

This opens the possibility of a new way of modifying a surface to promote more osseointegration: tuning the surface chemical properties will allow us to achieve a higher level of affinity and a richer interaction inside the body. A great deal of surface treatments has been used for years in chemistry to induce new chemical properties on surfaces. The simplest approach is to coat the surface. For example, the use of hydroxyapatite coatings of titanium implants has been around for more than two decades [87], with high success rate for some authors and mixed results for others [88]. One of the known problems of this technology comes from the risk of early resorption or even detachment and delamination of the coating from the implant [89], especially if the coating exceeds certain thickness.

Another more advanced approach would be the adsorption of chemical compounds on the surface. These can be either physisorbed (with the evident risk of desorption) or chemisorbed (which requires chemical interactions with the surface for the more stable adsorption). In the majority of cases, the physisorption is impractical for improving the integration of implants and it is only used as a way of studying the effect of different surface properties on cells and other biological agents, such as proteins [90]. If the adsorption is performed involving a chemical reaction of the adsorbents, it is rather called chemisorption and in this context it is frequently referred to as “surface functionalization”.

The functionalization of a surface is normally carried out using linear molecules with the target functional group in one of the extremes, and another group capable of binding to the surface on the other. Typically, the adsorption of these molecules forms self-assembled monolayers (SAMs). The molecules involved normally present a “head-group” that reacts with the surface, and a “tail” that contains the functional group. Once the head is bonded, the self-assembly is achieved by the reciprocal repulsion of the tails, which end up all oriented to the same direction and pointing the functional group opposing to the surface. This technique encompasses a large family of modifications, and one of the most common ones is silanization.

Silanization is the modification of a silicon oxide surface by the introduction of an alkoxy silane to form a SAM. This modification is based on the formation of the siloxane bond (Si-O-Si), which uses one oxygen atom to bind a silicon atom of the surface and another silicon atom present in the alkoxy silane molecule. There exists extensive literature demonstrating the practical applicability of this technique, both in the semiconductor industry and biomaterials research [91,92]. Multiple studies on cells used different functional groups on the modified surfaces and they observed a correlation between the functional group and the cellular activity. In general, researchers have identified amine (-NH₂) and carboxyl (-COOH) terminated as better promoters of cell adhesion than hydroxyl (-OH) or methyl (-CH₃) terminated SAMs [93–99].

However, the use of silanization is not necessary the endpoint. Once a surface has been stably functionalized through SAMs, more layers could be added to increase the complexity of the framework. Given the high-level specificity of

human cell interactions, last trends in biomaterial research focus on mimicking cellular environments to control cellular responses. It is clear that once a surface can be functionalized using whichever technique, the focus of research moves to the functional group on the external side of the SAM. In the case of ceramics, the great majority of research on this field was performed on silicon oxide (silica). This is because the surface of silica is naturally hydroxylated [100], which allows high densities of adsorbed molecules, and the formation of the siloxane bond ensures a stable functionalization. The technique is commonly used on gold, but it is available as well on other metals and semiconductors [101]. However the formation of SAM on these surfaces requires organosulfur compounds to bind with the surface.

The use of SAMs to promote osseointegration is not a novel idea. The limitations of this are given by the difficulty associated to establishing stable bindings and dense SAMs on the surface of an implant, which will rarely be conceived in silica or gold. The interest of adapting this technique to bioinert ceramics such as alumina or zirconia is evident: it opens the possibility of new ways of interaction by mimicking the surface of natural bone and allowing bone apposition. In chapter 4 of this manuscript, we explore a new paradigm of surface modification for zirconia by direct silanization of its surface. We strongly believe this kind of research will drive the next generation of implants to higher levels of integration while reducing the disadvantages associated to classical surface modifications (*e.g.* roughening).

Bibliography

- [1] P. Boutin, Alumina and its use in surgery of the hip. (Experimental study), *Presse Med.* 79 (1971) 639–40.
- [2] P. Boutin, D. Blanquaert, A study of the mechanical properties of alumina-on-alumina total hip prosthesis., *Rev. Chir. Orthop. Reparatrice Appar. Mot.* 67 (1981) 279–87.
- [3] G. Cordingley, R., Kohan, L., Ben-Nissan, B., Pezzotti, Alumina as an Orthopaedic Biomaterial - Characteristics, Properties, Performance and Applications, *J. Aust. Ceram. Soc.* 39 (2007) 20–28.
- [4] C. Klapperich, J. Graham, L. Pruitt, M.D. Ries, Failure of a metal-on-metal total hip arthroplasty from progressive osteolysis, *J. Arthroplasty.* 14 (1999) 877–881.
- [5] S.J. MacDonald, Can a safe level for metal ions in patients with metal-on-metal total hip arthroplasties be determined?, *J. Arthroplasty.* 19 (2004) 71–77.
- [6] A.J. Altenburg, J.J. Callaghan, T.M. Yehyaw, D.R. Pedersen, S.S. Liu, J.A. Leinen, et al., Cemented total hip replacement cable debris and acetabular construct durability., *J. Bone Joint Surg. Am.* 91 (2009) 1664–70.
- [7] P. Campbell, H. McKellop, R. Alim, J. Mirra, S. Nutt, L. Dorr, et al., Cobalt-Base Alloys for Biomedical Applications, ASTM International, 100 Barr Harbor Drive, PO Box C700, West Conshohocken, PA 19428-2959, 1999.
- [8] P. Patnaik, *Handbook of Inorganic Chemicals*, McGraw-Hill, 2003.
- [9] C. Barth, M. Reichling, Imaging the atomic arrangements on the high-temperature reconstructed $[\alpha]$ -Al₂O₃(0001) surface, *Nature.* 414 (2001) 54–57.
- [10] B.J. McEntire, B.S. Bal, M.N. Rahaman, J. Chevalier, G. Pezzotti, Ceramics and ceramic coatings in orthopaedics, *J. Eur. Ceram. Soc.* 35 (2015) 4327–4369.
- [11] N. Miyahara, Y. Mutoh, K. Yamaishi, K. Uematsu, M. Inoue, Grain Boundary Controlled Properties of Fine Ceramics: JFCC Workshop Series: Materials Processing and Design, in: K. Ishizaki, K. Niihara, M. Isotani, R.G. Ford (Eds.), Springer Netherlands, Dordrecht, 1992: pp. 125–136.
- [12] D. Hannouche, M. Hamadouche, R. Nizard, P. Bizot, A. Meunier, L. Sedel, Ceramics in total hip replacement., *Clin. Orthop. Relat. Res.* (2005) 62–71.
- [13] O. Ruff, F. Ebert, Contributions on the ceramics of highly fireproof material I: The forms of zirconium dioxide, *Zeitschrift Fur Anorg. Und Allg. Chemie.* 180 (1929) 19–41.
- [14] J. Chevalier, L. Gremillard, A. V. Virkar, D.R. Clarke, The tetragonal-monoclinic transformation in zirconia: lessons learned and future trends, *J. Am. Ceram. Soc.* 92 (2009) 1901–1920.
- [15] R.C. Garvie, R.H. Hannink, R.T. Pascoe, Ceramic steel?, *Nature.* 258 (1975) 703–704.
- [16] J. Chevalier, L. Gremillard, S. Deville, Low-Temperature Degradation of Zirconia and Implications for Biomedical Implants, *Annu. Rev. Mater. Res.* 37 (2007) 1–32.
- [17] J. Chevalier, B. Cales, J.M. Drouin, Low-temperature aging of Y-TZP ceramics, *J. Am. Ceram. Soc.* 82 (1999) 2150–2154.
- [18] S. Deville, L. Gremillard, J. Chevalier, G. Fantozzi, A critical comparison of methods for the determination of the aging sensitivity in biomedical grade yttria-stabilized zirconia., *J. Biomed. Mater. Res. B. Appl. Biomater.* 72 (2005) 239–245.

- [19] J. Schneider, S. Begand, R. Kriegel, C. Kaps, W. Glien, T. Oberbach, Low-Temperature Aging Behavior of Alumina-Toughened Zirconia, *J. Am. Ceram. Soc.* 91 (2008) 3613–3618.
- [20] S. Deville, J. Chevalier, G. Fantozzi, J.F. Bartolomé, J. Requena, J.S. Moya, et al., Low-temperature ageing of zirconia-toughened alumina ceramics and its implication in biomedical implants, *J. Eur. Ceram. Soc.* 23 (2003) 2975–2982.
- [21] S.M. Kurtz, S. Kocagöz, C. Arnholt, R. Huet, M. Ueno, W.L. Walter, Advances in zirconia toughened alumina biomaterials for total joint replacement., *J. Mech. Behav. Biomed. Mater.* 31 (2014) 107–16.
- [22] J. Chevalier, S. Grandjean, M. Kuntz, G. Pezzotti, On the kinetics and impact of tetragonal to monoclinic transformation in an alumina/zirconia composite for arthroplasty applications., *Biomaterials.* 30 (2009) 5279–5282.
- [23] A.H.H. De Aza, J. Chevalier, G. Fantozzi, M. Schehl, R. Torrecillas, Crack growth resistance of alumina, zirconia and zirconia toughened alumina ceramics for joint prostheses, *Biomaterials.* 23 (2002) 937–945.
- [24] W.G. Hamilton, J.P. McAuley, D.A. Dennis, J.A. Murphy, T.J. Blumenfeld, J. Politi, THA With Delta Ceramic on Ceramic: Results of a Multicenter Investigational Device Exemption Trial, *Clin. Orthop. Relat. Res.* 468 (2009) 358–366.
- [25] M. Kuntz, The effect of chromia content on hardness of zirconia platelet toughened alumina composites, Plochingen, Germany, 2014.
- [26] G. Magnani, A. Brillante, Effect of the composition and sintering process on mechanical properties and residual stresses in zirconia–alumina composites, *J. Eur. Ceram. Soc.* 25 (2005) 3383–3392.
- [27] G. Pezzotti, M.C. Munisso, A.A. Porporati, K. Lessnau, On the role of oxygen vacancies and lattice strain in the tetragonal to monoclinic transformation in alumina/zirconia composites and improved environmental stability, *Biomaterials.* 31 (2010) 6901–6908.
- [28] Marketsandmarkets.com, Dental Implants and Prosthetics Market by Material (Titanium, Zirconium, PFM, All Ceramics), Stage (Two Stage, Single Stage), Connectors (External hexagonal) & Product Type (Crowns, Bridges, Dentures, Abutments) - Global Forecast to 2020, 2015.
- [29] Marketsandmarkets.com, Dental Implants & Prosthetics Market worth \$10,427.7 Million by 2020, (n.d.). <http://www.marketsandmarkets.com/PressReleases/dental-implants-market.asp> (accessed May 24, 2016).
- [30] Persistence Market Research, Dental Implants Market - Global Study on Dental Implants - Asia Pacific to Witness Fastest Growth by 2020, 2014.
- [31] Marketsandmarkets.com, HIP Reconstruction Devices Market by Product (Primary, Partial, Revision, Hip Resurfacing), and Geography (U.S., Canada, EU-5, Japan, BRIC, Turkey, Indonesia) - Global Forecast to 2020, 2016.
- [32] E. Oral, O.K. Muratoglu, Vitamin E diffused, highly crosslinked UHMWPE: a review, *Int. Orthop.* 35 (2011) 215–223.
- [33] C. Scemama, Le polyéthylène hautement réticulé de deuxième génération dopé à la vitamine E versus conventionnel dans l'arthroplastie totale de hanche : étude prospective randomisée à 3 ans minimum de recul, 2014.
- [34] N.E. Bishop, A. Hothan, M.M. Morlock, High friction moments in large hard-on-hard hip replacement bearings in conditions of poor lubrication, *J. Orthop. Res.* 31 (2013) 807–813.

- [35] A.M. Imbuldeniya, S.J. Pearce, W.L. Walter, B.A. Zicat, W.K. Walter, Squeaking: Current knowledge and how to avoid it, *Curr. Rev. Musculoskelet. Med.* 6 (2013) 342–349.
- [36] S. Singh, H. Bhalodiya, Head size and dislocation rate in primary total hip arthroplasty, *Indian J. Orthop.* 47 (2013) 443–448.
- [37] H. Yu, M. Zheng, R. Chen, H. Cheng, Proper selection of contemporary dental cements., *Oral Health Dent. Manag.* 13 (2014) 54–9.
- [38] P.F. Gomez, J.A. Morcuende, Early attempts at hip arthroplasty--1700s to 1950s., *Iowa Orthop. J.* 25 (2005) 25–9.
- [39] L.C. Jones, D.S. Hungerford, Cement disease., *Clin. Orthop. Relat. Res.* (1987) 192–206.
- [40] W.H. Harris, Osteolysis and particle disease in hip replacement. A review., *Acta Orthop. Scand.* 65 (1994) 113–23.
- [41] W.F. Campbell, M.W. Herman, Choosing Between Screw-Retained and Cement-Retained Implant Crowns, Inclusive. *Restor. Driven Implant Solut.* 2 (2011) 20–26.
- [42] C.R. Wheelless, *Wheeles' Texbook of Orthopaedics, Screw Fixat. Acetabular Components.* (2015).
http://www.wheelesonline.com/ortho/screw_fixation_of_acetabular_components (accessed April 8, 2016).
- [43] A.J. Yee, H.K. Kreder, I. Bookman, J.R. Davey, A randomized trial of hydroxyapatite coated prostheses in total hip arthroplasty., *Clin. Orthop. Relat. Res.* (1999) 120–32.
- [44] L. Sun, C.C. Berndt, K.A. Gross, A. Kucuk, Material fundamentals and clinical performance of plasma-sprayed hydroxyapatite coatings: a review., *J. Biomed. Mater. Res.* 58 (2001) 570–92.
- [45] E.J. McPherson, L.D. Dorr, T.A. Gruen, M.T. Saberi, Hydroxyapatite-coated proximal ingrowth femoral stems. A matched pair control study., *Clin. Orthop. Relat. Res.* (1995) 223–30.
- [46] R.K. Sinha, *Hip Replacement: Current Trends and Controversies*, CRC Press, 2002.
- [47] R.K. Alla, K. Ginjupalli, N. Upadhya, M. Shamma, S.R. Ravi, Rama Krishna, Surface Roughness of Implants: A Review, *Trends Biomater. Artif. Organs.* 25 (2011) 112–118.
- [48] M. Gahlert, T. Gudehus, S. Eichhorn, E. Steinhauser, H. Kniha, W. Erhardt, Biomechanical and histomorphometric comparison between zirconia implants with varying surface textures and a titanium implant in the maxilla of miniature pigs., *Clin. Oral Implants Res.* 18 (2007) 662–8.
- [49] A. Wennerberg, T. Albrektsson, On implant surfaces: a review of current knowledge and opinions., *Int. J. Oral Maxillofac. Implants.* 25 (2009) 63–74.
- [50] A. Wennerberg, T. Albrektsson, Suggested guidelines for the topographic evaluation of implant surfaces., *Int. J. Oral Maxillofac. Implants.* 15 (2000) 331–344.
- [51] T. Kosmač, C. Oblak, P. Jevnikar, N. Funduk, L. Marion, The effect of surface grinding and sandblasting on flexural strength and reliability of Y-TZP zirconia ceramic, *Dent. Mater.* 15 (1999) 426–433.
- [52] T. Kosmač, C. Oblak, P. Jevnikar, N. Funduk, L. Marion, Strength and reliability of surface treated Y-TZP dental ceramics., *J. Biomed. Mater. Res.* 53 (2000) 304–313.

- [53] H.P. Papanagiotou, S.M. Morgano, R. a Giordano, R. Pober, In vitro evaluation of low-temperature aging effects and finishing procedures on the flexural strength and structural stability of Y-TZP dental ceramics., *J. Prosthet. Dent.* 96 (2006) 154–164.
- [54] H. Sato, K. Yamada, G. Pezzotti, M. Nawa, S. Ban, Mechanical Properties of Dental Zirconia Ceramics Changed with Sandblasting and Heat Treatment, *Dent. Mater. J.* 27 (2008) 408–414.
- [55] T. Kosmač, Č. Oblak, L. Marion, The effects of dental grinding and sandblasting on ageing and fatigue behavior of dental zirconia (Y-TZP) ceramics, *J. Eur. Ceram. Soc.* 28 (2008) 1085–1090.
- [56] R.K. Chintapalli, A. Mestra Rodriguez, F. Garcia Marro, M. Anglada, Effect of sandblasting and residual stress on strength of zirconia for restorative dentistry applications., *J. Mech. Behav. Biomed. Mater.* 29 (2014) 126–37.
- [57] M. Guazzato, L. Quach, M. Albakry, M. V Swain, Influence of surface and heat treatments on the flexural strength of Y-TZP dental ceramic., *J. Dent.* 33 (2005) 9–18.
- [58] D.M. Qeblawi, C.A. Muñoz, J.D. Brewer, E.A. Monaco Jr, The effect of zirconia surface treatment on flexural strength and shear bond strength to a resin cement, *J. Prosthet. Dent.* 103 (2010) 210–220.
- [59] Y. Zhang, B.R. Lawn, E.D. Rekow, V.P. Thompson, Effect of sandblasting on the long-term performance of dental ceramics., *J. Biomed. Mater. Res. B. Appl. Biomater.* 71 (2004) 381–386.
- [60] Y. Zhang, B. Lawn, K. Malament, V.T. P, E. Rekow, Damage accumulation and fatigue life of particle-abraded ceramics, *Int. J. Prosthodont.* 19 (2006) 442–448.
- [61] A. Shenoy, N. Shenoy, Dental ceramics: An update., *J. Conserv. Dent.* 13 (2010) 195–203.
- [62] A. Sadan, M.B. Blatz, D. Soignet, Influence of silanization on early bond strength to sandblasted densely sintered alumina, *Quintessence Int. (Berl).* 34 (2003) 172–176.
- [63] E. Papia, P.V. von Steyern, Bond strength between different bonding systems and densely sintered alumina with sandblasted surfaces or as produced, *Swed. Dent. J.* 32 (2008) 35–45.
- [64] B. Ersu, B. Yuzugullu, A. Ruya Yazici, S. Canay, Surface roughness and bond strengths of glass-infiltrated alumina-ceramics prepared using various surface treatments., *J. Dent.* 37 (2009) 848–856.
- [65] L.F. Valandro, M. Ozcan, M.A.C. Bottino, R. Scotti, A. Della Bona, Bond strength of a resin cement to high-alumina and zirconia-reinforced ceramics: the effect of surface conditioning., *J. Adhes. Dent.* 8 (2006) 175–81.
- [66] S.P. Passos, L.F. Valandro, M.A. Bottino, M.J. Santos, G.C. Santos Jr., Shear bond strength of resin cement bonded to alumina ceramic after treatment by aluminum oxide sandblasting or silica coating, *J Prosthodont.* 20 (2010) 561–565.
- [67] J.-W. Kim, N.S. Coval, P.C. Guess, E.D. Rekow, Y. Zhang, Concerns of hydrothermal degradation in CAD/CAM zirconia., *J. Dent. Res.* 89 (2010) 91–5.
- [68] E. Camposilvan, Q. Flamant, M. Anglada, Surface roughened zirconia: towards hydrothermal stability., *J. Mech. Behav. Biomed. Mater.* 47 (2015) 95–106.

- [69] F.G. Marro, R. Chintapalli, P. Hvizdoš, F. Soldera, F. Mücklich, M.J. Anglada, Study of near surface changes in yttria-doped tetragonal zirconia after low temperature degradation, *Int. J. Mat. Res.* 100 (2009) 0–4.
- [70] S. Lawson, Environmental degradation of zirconia ceramics, *J. Eur. Ceram. Soc.* 15 (1995) 485–502.
- [71] R.C. Garvie, P.S. Nicholson, Phase Analysis in Zirconia Systems, *J. Am. Ceram. Soc.* 55 (1972) 303–305.
- [72] K. Rechendorff, The influence of surface roughness on protein adsorption, University of Aarhus, Denmark, 2006.
- [73] C.J. Miller, L.A. Davidson, The interplay between cell signalling and mechanics in developmental processes, *Nat Rev Genet.* 14 (2013) 733–744.
- [74] H. Lodish, A. Berk, S.L. Zipursky, P. Matsudaira, D. Baltimore, J. Darnell, *Molecular Cell Biology*, (2000).
- [75] Extracellular Matrix and Cell Adhesion Molecules, *Br. Soc. Cell Biol.* (n.d.). <http://bscb.org/learning-resources/softcell-e-learning/extracellular-matrix-and-cell-adhesion-molecules/> (accessed April 25, 2016).
- [76] W.S. To, K.S. Midwood, Plasma and cellular fibronectin: distinct and independent functions during tissue repair, *Fibrogenesis Tissue Repair.* 4 (2011) 1–17.
- [77] V. Llopis-Hernández, P. Rico, J. Ballester-Beltrán, D. Moratal, M. Salmerón-Sánchez, Role of Surface Chemistry in Protein Remodeling at the Cell-Material Interface, *PLoS One.* 6 (2011) e19610.
- [78] S. Schlie-Wolter, A. Ngezhayo, B.N. Chichkov, The selective role of ECM components on cell adhesion, morphology, proliferation and communication in vitro., *Exp. Cell Res.* 319 (2013) 1553–61.
- [79] C. Myant, P. Cann, On the matter of synovial fluid lubrication: Implications for Metal-on-Metal hip tribology, *J. Mech. Behav. Biomed. Mater.* 34 (2014) 338–348.
- [80] Y.S. Liao, P.D. Benya, H.A. McKellop, Effect of protein lubrication on the wear properties of materials for prosthetic joints., *J. Biomed. Mater. Res.* 48 (1999) 465–73.
- [81] S.C. Scholes, A. Unsworth, The effects of proteins on the friction and lubrication of artificial joints., *Proc. Inst. Mech. Eng. H.* 220 (2006) 687–93.
- [82] C. Myant, R. Underwood, J. Fan, P.M. Cann, Lubrication of metal-on-metal hip joints: The effect of protein content and load on film formation and wear, *J. Mech. Behav. Biomed. Mater.* 6 (2012) 30–40.
- [83] A. Borruto, G. Crivellone, F. Marani, Influence of surface wettability on friction and wear tests, *Wear.* 222 (1998) 57–65.
- [84] Z. Pawlak, W. Urbaniak, A. Oloyede, The relationship between friction and wettability in aqueous environment, *Wear.* 271 (2011) 1745–1749.
- [85] K. Wang, C. Zhou, Y. Hong, X. Zhang, A review of protein adsorption on bioceramics, *Interface Focus.* 2 (2012) 259–277.
- [86] D.J. Preston, N. Miljkovic, J. Sack, R. Enright, J. Queeney, E.N. Wang, Effect of hydrocarbon adsorption on the wettability of rare earth oxide ceramics, *Appl. Phys. Lett.* 105 (2014).
- [87] W.R. Lacefield, Hydroxyapatite coatings., *Ann. N. Y. Acad. Sci.* 523 (1988) 72–80.

- [88] D. Alfaiate, T. Escobar, P. Oliveira, I. Almeida, D. Rosas, B. Borges, Hydroxyapatite-coated implants: clinical advantages – a review of the literature, *Clin. Oral Implants Res.* 25 (2014).
- [89] K. Mediaswanti, C. Wen, E.P. Ivanova, C.C. Berndt, J. Wang, Sputtered Hydroxyapatite Nanocoatings on Novel Titanium Alloys for Biomedical Applications, in: *Titan. Alloy. - Adv. Prop. Control*, 2013.
- [90] Y. Tamada, Y. Ikada, Effect of Preadsorbed Proteins on Cell Adhesion to Polymer Surfaces, *J. Colloid Interface Sci.* 155 (1993) 334–339.
- [91] A.P. Alekhin, G.M. Boleiko, S.A. Gudkova, A.M. Markeev, A.A. Sigarev, V.F. Toknova, et al., Synthesis of biocompatible surfaces by nanotechnology methods, *Nanotechnologies Russ.* 5 (2010) 696–708.
- [92] W. Lu, A.M. Sastry, Self-Assembly for Semiconductor Industry, *IEEE Trans. Semicond. Manuf.* 20 (2007) 421–431. doi:10.1109/TSM.2007.907622.
- [93] N. Faucheux, R. Schweiss, K. Lützow, C. Werner, T. Groth, Self-assembled monolayers with different terminating groups as model substrates for cell adhesion studies., *Biomaterials.* 25 (2004) 2721–30.
- [94] J. Li, T. Guan, C. Hao, L. Li, Y. Zhang, Effects of Self-Assembled Monolayers with Different Chemical Groups on Ovarian Cancer Cell Line Behavior In Vitro, *J. Chem.* 2015 (2015) 1–10.
- [95] Y. Arima, H. Iwata, Preferential adsorption of cell adhesive proteins from complex media on self-assembled monolayers and its effect on subsequent cell adhesion., *Acta Biomater.* 26 (2015) 72–81.
- [96] A. Oliveros, C.L. Frewin, S.J. Schoell, M. Hoeb, M. Stutzmann, I.D. Sharp, et al., Assessment of cell proliferation on 6H-SiC biofunctionalized with self-assembled monolayers, *J. Mater. Res.* 28 (2012) 78–86.
- [97] H. Schweikl, R. Müller, C. Englert, K.-A. Hiller, R. Kujat, M. Nerlich, et al., Proliferation of osteoblasts and fibroblasts on model surfaces of varying roughness and surface chemistry., *J. Mater. Sci. Mater. Med.* 18 (2007) 1895–905.
- [98] Y. Arima, H. Iwata, Effects of surface functional groups on protein adsorption and subsequent cell adhesion using self-assembled monolayers, *J. Mater. Chem.* 17 (2007) 4079.
- [99] B.G. Keselowsky, D.M. Collard, A.J. García, Surface chemistry modulates fibronectin conformation and directs integrin binding and specificity to control cell adhesion, *J. Biomed. Mater. Res. Part A.* 66A (2003) 247–259.
- [100] L.T. Zhuravlev, Concentration of hydroxyl groups on the surface of amorphous silicas, *Langmuir.* 3 (1987) 316–318.
- [101] A. Ulman, Formation and Structure of Self-Assembled Monolayers, *Chem. Rev.* 96 (1996) 1533–1554.

2

EFFECT OF ROUGHNESS

Impact of sandblasting on the mechanical properties and aging resistance of alumina and zirconia based ceramics

Contents

2.1 Introduction.....	45
2.2 Materials and methods.....	47
2.2.1 Determining the Annealing Temperature to suppress residual stresses	48
2.2.2 Surface Characterization	50
2.2.3 Aging assessment	51
2.2.4 Mechanical Characterization.....	51
2.2.5 Statistical tests.....	51
2.3 Results.....	52
2.3.1 Determining the Annealing Temperature to suppress residual stresses	52
2.3.2 Surface Characterization	54
2.3.3 Aging assessment	55
2.3.4 Mechanical Characterization.....	56
2.4 Discussion	59
2.4.1 Surface Characterization	59
2.4.2 Aging assessment	60
2.4.3 Mechanical Characterization.....	61
2.4.4 On the different effective residual stresses after sandblasting.....	63
2.5 Conclusions	65
Glossary	66
Bibliography.....	67

2.1 Introduction

The use of high-performance ceramics, such as alumina or zirconia, for biomedical devices has been documented since the early seventies [1,2]. They were developed as an alternative to surgical metal alloys [3] and as a way of overcoming the risks of periprosthetic osteolysis and intoxication by wear debris from metal-on-polyethylene or metal-on-metal implants for total hip arthroplasty [4,5], as well as early failure due to scratches and third-body wear [4,6,7]. The use of ceramic materials as femoral heads and/or acetabular cups reduces wear rate of bearing components and produces negligible amount of ion release. The clinical success associated to the use of ceramics led to the implantation of more than 12 million ceramic components over the last four decades [8]. High performance ceramics are also gaining popularity in dentistry [9]. This is in particular the case of zirconia, which is now widely used for dental restorations and under strong development for endosseous implants.

Nonetheless, both alumina and zirconia can be labeled as “bioinert” materials, since they do not cause adverse immunological reaction but neither positive cellular activity: indeed upon implantation, a fibrous non-adherent membrane shields the surface of the implant impeding a direct integration to bone [10,11]. The causes of this shielding are not yet fully clear, but they have been often correlated to micro-motion and migration of the prosthetic component, and lead to clinical loosening [12,13]. This is why, when implanted, the ceramic parts are usually coupled with a metallic structure (so called ‘metal-back’) in total hip arthroplasty (THA). The metal-back shell is usually made of titanium and entrusted with the task of attaching the acetabular cup to bone [14]. Its surface is usually treated to improve its attachment to bone and when necessary the fixation is improved with the use of screws. In some other cases the cup is cemented to the bone. In the case of dental implants, which by default involve a bone-implant interface, several strategies are currently explored to improve bone osseointegration by chemical or mechanical modification of the surfaces.

Therefore, there is great interest in endowing osteoconductive and osseointegration capabilities to current bioinert ceramics: on one hand, it could permit the elimination of the metal-backing as it would be no longer needed, making the implant less invasive and hence conserving more bone stock. On the other hand, the growth of new bone over the implant surface could help fixing it, avoiding micro-movements or migrations. All this could mean reducing the incidence of revision surgeries and improving the patient’s life. In the case of dental implants, only surfaces with a chemical and/or topographic modification are currently able to answer the need of sufficient osseointegration, warrant of a long lifetime.

Techniques such as sandblasting and chemical etching have been used with metals for long in order to increase their roughness and resulting in clinical success [15–17], especially in dentistry [18]. The same techniques have been used as well on ceramics [19]. However, sandblasting involves the creation of defects at the surface and of residual stresses under it. Since ceramics have

limited fracture toughness in comparison to metals, a modification in the distribution of Surface Defects (SD) and Residual Stresses (RS) will affect the final strength of the piece.

In the present work, two zirconia-based materials were studied, in addition to alumina. Zirconia materials are typically designed to exploit a specific reinforcing mechanism known as “transformation toughening”, in which crack propagation is hindered through the transformation of the tetragonal grains into the more stable monoclinic ones. Unfortunately, this transformation can also be triggered by the presence of water, which may progressively lead to surface roughening and micro-cracking, compromising the integrity of the material [20]. This mechanism is referred to as “hydrothermal aging”, “Low Temperature Degradation (LTD)” or simply “aging”. In the case of composites containing zirconia, aging is generally less rapid than in pure zirconia, in some cases practically inexistent, and its effects are more limited [21–23]. However, any process modification, including surface treatments, must be carefully assessed.

In literature, there are several examples of surface modifications that influenced LTD kinetics in zirconia-based ceramics: in some the outcome was positive due to compressive RS [24,25], and in others negative due to cracks on the surface [26]. Therefore, the combined effect of SD and RS would impact differently the behaviour of these materials against LTD and this needs to be evaluated. In addition to this, Whalen *et al.* [27] reported in 1989 a surface recrystallization after annealing a heavily damaged ground zirconia. According to them, the recrystallization process during annealing transformed the twinned monoclinic grains into more stable tetragonal nano-grains, and this impacted the aging behaviour: the recrystallization layer helped retarding the nucleation process of the LTD. Surprisingly, this study has not received the merited echo despite its fundamental and practical interest: recrystallization is possible for metals, but the amount of plastic deformation at the surface has to be important enough before annealing for short time treatments. This phenomenon could be exploited in zirconia for creating a surface with a lower sensitivity to aging without compromising its mechanical strength.

There is a great deal of works already studying the effects of blasting treatments on strength and fatigue on different zirconia-based materials [24,28–35]. It was found as well a great number of works dealing with LTD [25,26,36,37]. However, none of the reviewed literature presented a comparison between different materials, their performance and behaviour after a roughening treatment, and the implications of such modification on their long-term stability.

Therefore the aim of this paper was to assess the effect of sandblasting on strength and aging kinetics (when relevant, i.e. in zirconia containing ceramics) and to understand the respective roles of SD and RS (possibly created by plastic deformation and/or tetragonal to monoclinic transformation). To study the individual contribution of each one, polishing (to remove SD) and annealing steps (to remove RS) were included in the sample preparation process. The effect of annealing treatments after sandblasting on surface microstructure and by consequence on strength and LTD were also explored.

2.2 Materials and methods

The materials studied in this work were Alumina, 3Y-TZP (Zirconia) and a Zirconia Toughened Alumina (ZTA), provided by CeramTec GmbH (Plochingen, Germany) in the form of sintered bending bars ($3 \times 4 \times 60$ mm³). All materials studied were biomedical grade and their properties are condensed in **Table 2.1**. The specimens of each material were divided into six groups and were treated as shown in **Table 2.2**. All samples were ground by the supplier, using a proprietary standard procedure, on which and we had no information. Hence, we labelled this initial state as “As-Received”.

Table 2.1. Properties of studied materials

Composition (wt%)	Standard	Alumina		ZTA		Zirconia	
		Al ₂ O ₃	99.8 Rest	Al ₂ O ₃	74	ZrO ₂	93
	---	Other oxides		ZrO ₂	24	Y ₂ O ₃	4.9
				Other oxides	2	Other oxides	2.1
Grain size (μm)	---	1.8		Al ₂ O ₃	0.87	0.15 – 0.20	
				ZrO ₂	0.36		
Bulk Density (g/cm ³)	DIN EN 623-2	3.96		4.37		6.08	
Fracture toughness, K_{Ic} (MPa·m ^{1/2})	SEVNB DIN CEN/TS 14425-1	4.3		6.4		6.7	
Young's Modulus (GPa)	DINV ENV 843-2	406		357		210	
Poisson's ratio	DINV ENV 843-2	0.23		0.24		0.3	
Vickers Hardness HV1	DINV ENV 843-4	2000		1760		1350	

Table 2.2. Group names, treatments followed and expected presence of SD and RS. Single plus (+) represents low, double plus (++) high, and null () absence.

Series	Treatments	Expected qualitative content	
		SD	RS
AR	As-Received	+	++
PA	Polished + Annealed		
PAS	Polished + Annealed + Sandblasted	+	+
PASA	Polished + Annealed + Sandblasted + Annealed	+	
S	Sandblasted	++	++
SW	Sandblasted + aging 50h in water at 134° C	++	++

The polishing step was performed in an automatic polishing machine up to 1 μm of diamond suspension. The sandblasting treatment was performed using 110 μm diameter alumina powder as blasting medium, at a pressure of 2 bar in a 90° angle, a distance of 25 mm and during 10 seconds. We chose these conditions because Chintapalli *et al.* [37] found they increased the strength of zirconia. The annealing step was performed for 10 min in air, using heating and cooling rates of 5° C/min. A preliminary study was necessary to obtain the final annealing temperature, as we were aiming for the minimum temperature capable of removing the majority of residual stresses without modifying the microstructure and grain size.

2.2.1 Determining the Annealing Temperature to suppress residual stresses

The presence of RS due to polishing or sandblasting is imputable to a localized plasticity below the grinding particles by dislocation motion and t-m transformation in the case of zirconia. This creates an elastic-plastic mismatch when the particles are removed from the surface. Indentation is therefore an excellent tool to investigate localized plasticity and RS, as it induces the same type of RS, although different in magnitude. Indentations were therefore chosen as a model to obtain the annealing temperature capable of suppressing the majority of RS without substantially changing the microstructure.

The method followed is described in detail by Chevalier *et al.* [38]. Upon indenting a polished surface, a RS field is created around the indentation up to a certain distance. When indenting with secondary Vickers diamond pyramid with lower loads around the initial one at different distances making sure the cracks are aligned in the radial and tangential directions with the macro flaw as the center (**Figure 2.1**), we will observe that the closer in distance, the shorter the radial cracks and the longer the tangential ones are. This is because the radial cracks are affected by the residual tangential tensile stresses that promote the propagation, while the tangential cracks are closed by the radial compressive stresses. By carefully studying the RS distribution around the initial indentation after different thermal treatments, we can select the temperature that best suits our purposes (i.e. for which the tangential and radial stresses become null).

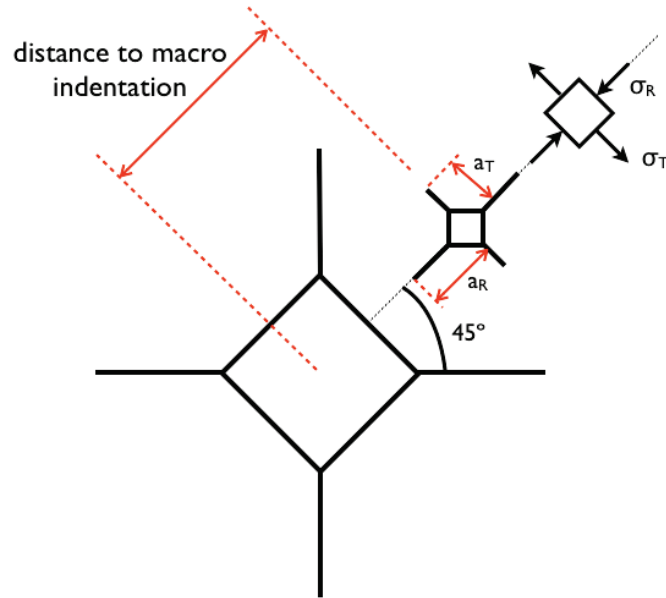


Figure 2.1 Representation of a macro indentation and its effect on the crack lengths of the smaller indentation through the residual stress field.

As described by Chevalier *et al.*, one can calculate both the tangential (σ_T) and radial (σ_R) RS by measuring the crack lengths in the radial (a_R) and tangential directions (a_T) of the small indent localized at a certain distance of the macro-indentation, and making use of:

$$\sigma_{res} = K_{Ic} \frac{1 - (a/a_0)^{-3/2}}{Y a^{1/2}} \quad (1)$$

where a_0 represents the crack length at “infinite” distance from the macro indentation (i.e. out of the RS field generated by the indentation), and Y is a parameter that depends on the type of the crack and loading. In this particular case, we are only interested in the evolution of the variable part, as expressed in:

$$\frac{\sigma_{res} Y}{K_{Ic}} = \frac{1 - (a/a_0)^{-3/2}}{a^{1/2}} \quad (2)$$

Hence, we can plot instead $\sigma_{res} Y / K_{Ic}$ versus distance to the macro indentation. Four samples for each material were polished up to 1 μm of diamond suspension, and indented with loads of 196 N (20 kgf) in the case of Alumina, and 294 N (30 kgf) in the case of ZTA and Zirconia. After the macro-indentations, three samples were annealed following the procedure presented above and at the temperatures of 600, 900 and 1200° C, for Alumina and ZTA samples. Since Chevalier *et al.* [38] already proposed the temperature of 1200° C for the 3Y-TZP, in the present work only this temperature was studied for Zirconia.

After the thermal treatment, the samples were indented at different distances of the macro-indentation with micro-indentations of 4.9 N (0.5 kgf) in the case of Alumina and 9.8 N (1 kgf) in the case of ZTA and Zirconia. Before measuring the cracks, the samples were left five days in air at room temperature in a protective box to allow the stable crack propagation to stop.

For the measurement of the crack lengths, an optical microscope (Carl Zeiss AxioPhot) was used with a precision of up to 1 μm .

2.2.2 Surface Characterization

Surface roughness is generally reported using only the Arithmetical mean height of the Surface, S_a . For example, it is often argued that S_a of 1-2 μm is optimal for titanium implants in terms of bone integration. However, as pointed by Wennerberg *et al.* [39], this sole value is by far insufficient to describe the surface features. Following then the remarks made by Wennerberg *et al.*, the sample surfaces studied in this work were extensively characterized by optical interferometry (OI, Veeco Wyko 9300NT, Bruker, Germany). We focused on four different 3D parameters of diverse nature, as done by Svanborg *et al.* [40]: one for amplitude (S_a), a spatial one (S_{ds}), a hybrid one (S_{dr}) and finally a functional one (S_{ci}). **Table 2.3** summarizes their definitions. The measurement area was of 150 μm x 150 μm (resolution of 758 x 758 pixels).

Table 2.3. Statistical parameters studied and their definitions

Parameter	Description
S_a	Arithmetical mean height of the surface (arithmetic average of the absolute values of vertical deviation from the mean surface).
S_{ds}	Summit density, i.e. number of summits per unit area. Summits are constrained to be separated 1% of the minimum X or Y dimension, and found above a threshold of 5% of S_z (maximum height of the surface) above the mean plane.
S_{dr}	Developed Interfacial Area Ratio represents the ratio of increment of specific surface over the sampling area.
S_{ci}	Core Fluid Retention Index, represent a measure of the volume (for example, of a fluid filling the core surface) that the surface would support from 5% - 80% of the bearing ratio. For a Gaussian height distribution, S_{ci} approaches 1.56

The roughness parameters were calculated after applying a robust high-frequency-pass Gaussian filter, with a cut-off wavelength of 10 μm . This numerical filtering allows studying the roughness at different length scales of roughness. A 10 μm filter was selected to approach the typical scale of a cell. For each group, three specimens were studied.

In order to evaluate the presence of surface recrystallization on PASA Zirconia, we performed focused-ion beam (FIB, Nvision 40, Zeiss, Germany) nanotomography analysis (custom hardware and software developed by FIBICS Inc., Ottawa, Canada), combining FIB and in-situ Scanning Electron Microscope (SEM) imaging with a voxel size target of 3 nm^3 . The analysis allowed us then to reconstruct 2D orthogonal views of the cross-sections.

2.2.3 Aging assessment

Aging was performed in autoclave at 134° C and under 2 bars steam pressure. The relative amount of monoclinic and tetragonal phase was evaluated through X-Ray Diffraction (Rigaku D/Max-B, Cu KL_{2,3} radiations) by comparing the areas of the corresponding peaks for the tetragonal (t₁₀₁) and monoclinic phase (m₁₁₁ and -₁₁₁) of Zirconia and calculating the volume content by making use of Garvie-Nicholson equation [41], modified by Toraya [42].

2.2.4 Mechanical Characterization

For the evaluation of the mechanical behaviour, 4-point bending tests (inner and outer spans of 10 and 21 mm respectively) were performed in a universal testing machine (Model 8502, Instron Corp., Canton, USA) in air up to fracture of the specimen, using a constant test speed of 0.5 mm/min. The load at failure was recorded and the fracture strength was obtained through:

$$\sigma = \frac{3F(L-L_i)}{2bd^2} \quad (3)$$

where F is the load at failure, L is the length of the support span, L_i is the length of the loading span, b is the width of the specimen and d its thickness.

2.2.5 Statistical tests

The mechanical results were statistically analyzed by means of Weibull distribution, expressed in:

$$P(\sigma) = 1 - \exp\left(-\left(\frac{\sigma}{\sigma_0}\right)^m\right) \quad (4)$$

where P is the probability of failure, σ and σ_0 are the applied stress and the distribution central value and m is the Weibull modulus. The sample population was adjusted to ten samples per condition and material. The probability of failure is evaluated by a ranking approach given by:

$$P = \frac{i-0,5}{N} \quad (5)$$

where N is the number of specimens, and i is the ranking from 1 to N . P is then associated to the corresponding σ by ordering the failure data from the smallest to the largest.

When necessary, data was statistically compared through either t-test or one-way ANOVA, using both a confidence interval of 5% ($\alpha=0.05$).

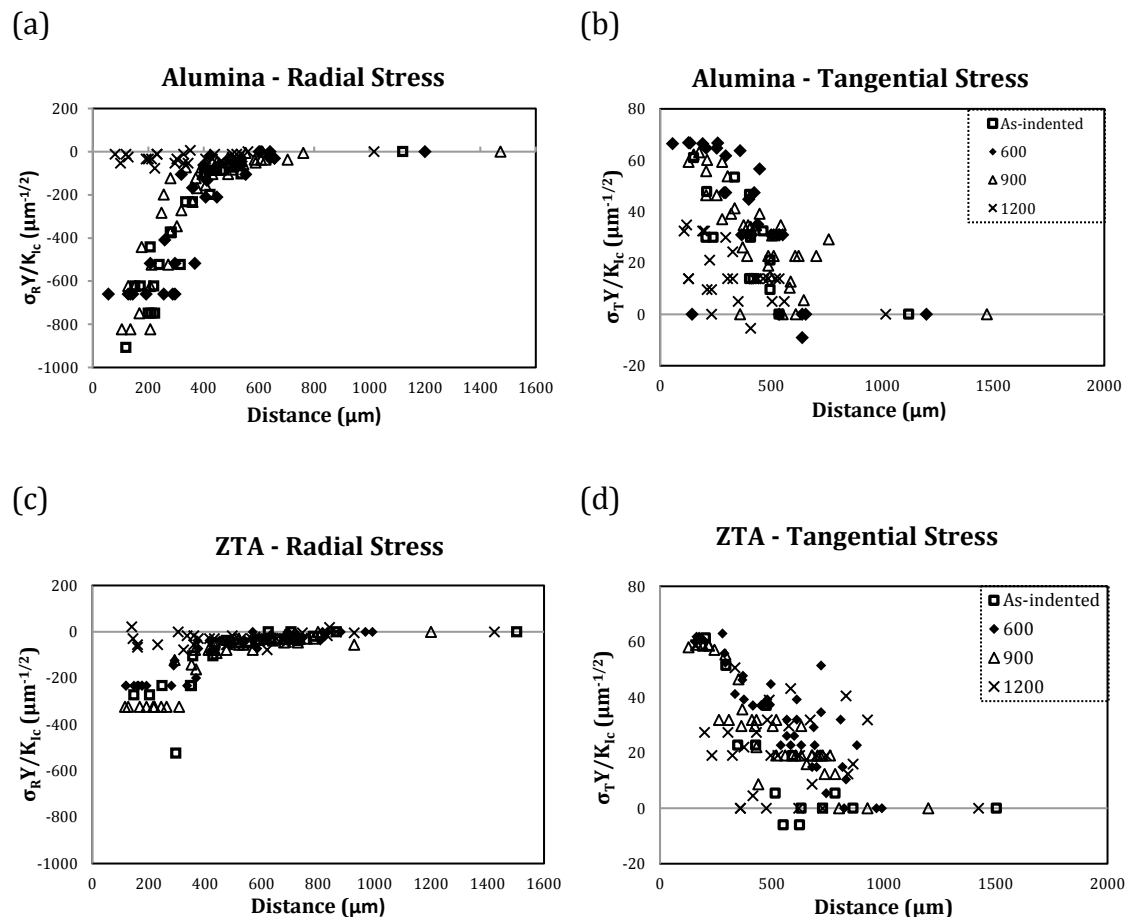
2.3 Results

2.3.1 Determining the Annealing Temperature to suppress residual stresses

The results from the indentation study are shown in **Figure 2.2**. In the horizontal axis is represented the distance to the center of the macro-indentation, and in the vertical axis the function $\sigma_{res}Y/K_{Ic}$ expressed in equation (2). To simplify, the values reported by the function are proportional to the residual stresses.

In general terms, tangential stress distributions seemed very scattered and unclear in all three materials. On the contrary, radial stress plots allow discerning the effect of temperature. The higher the temperature, the more the residual radial stresses approaches to zero, even close to the big indentation, as shown by the bottom image of **Figure 2.3**.

Looking at results, the annealing temperature was fixed at 1200° C for the three materials, as it was the minimum temperature capable of eliminating the majority of RS. This temperature was already proposed by Chevalier *et al.* [38] for 3Y-TZP, and our results extended it for our Alumina and ZTA samples as well.



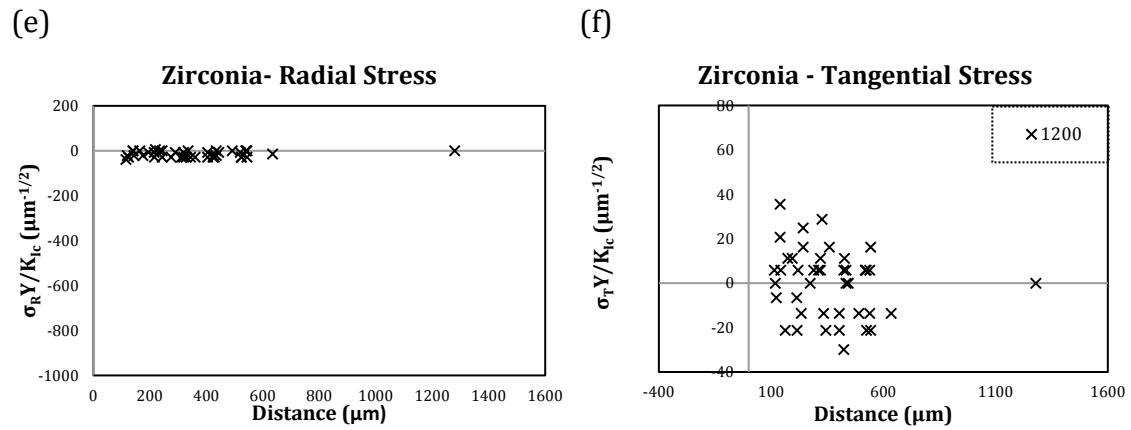


Figure 2.2. Residual stresses around the macro indentation on each material

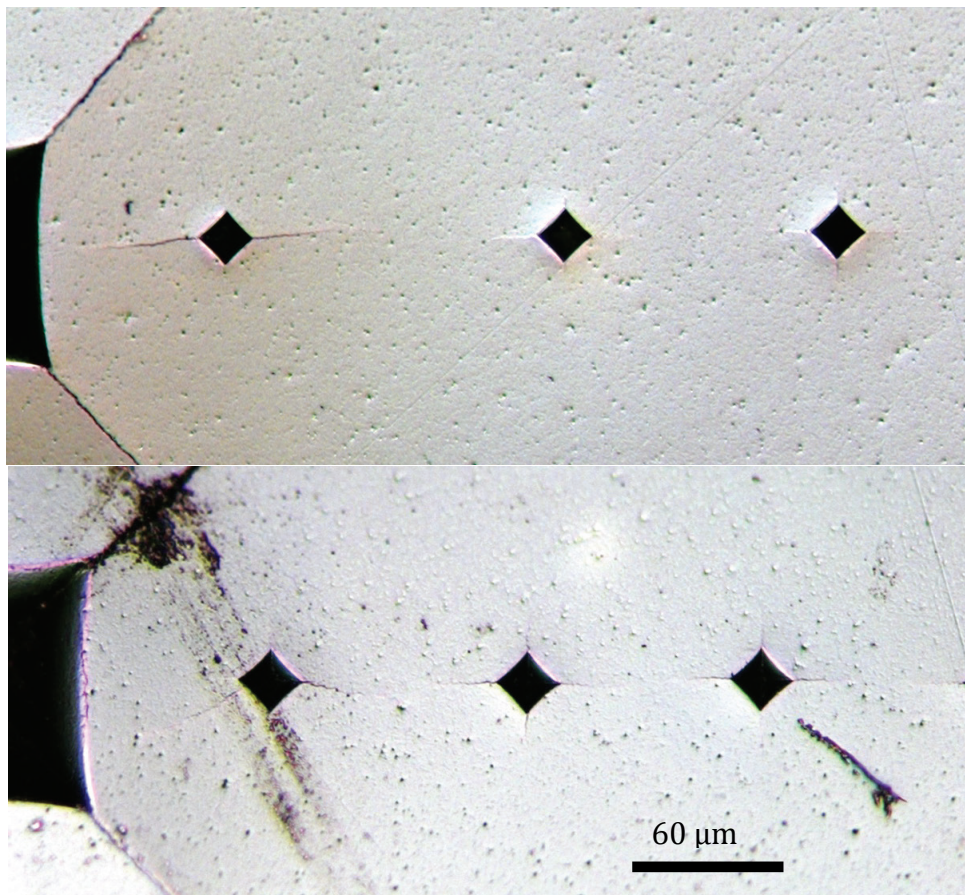


Figure 2.3. Indentations on the surface of ZTA. (a) Annealed at 900° C, and (b) completely annealed at 1200° C.

2.3.2 Surface Characterization

Table 2.4 summarizes the values obtained for each series. PASA and PAS roughness were never significantly different, and therefore are shown in the same line. PA Alumina exhibited a higher Sa and Sdr, and a lower Sds and Sci than ZTA or Zirconia due to the presence of grain pullouts in an otherwise flat surface. This also explains why Sci is particularly low in Alumina: its roughness is far from following a Gaussian distribution and the present voids in the surface belong to the lower heights (i.e. out from the 5 to 80% bearing area).

On all three materials, PAS and S series presented equivalent roughness. However, differences were found between materials. On the one hand, ZTA exhibited the lowest Sa, Sdr and Sds of the three materials in both series, providing a smoother surface compared to Zirconia and especially to Alumina. The fact that Alumina presented the roughest surface may be explained by its lower toughness, which allowed a higher damage of the surface. Alumina presented as well twice as much specific surface as Zirconia and three times as much as ZTA.

Table 2.4. Results of surface roughness for each material and series, obtained through OI.

	Material	Sa (nm)	Sdr	Sds ($\times 10^3$ mm ⁻²)	Sci
AR	Alumina	253 (33)	58.0 (5.7)	58 (7)	1.12 (0.03)
	ZTA	126 (6)	26.0 (2.6)	46 (8)	1.14 (0.05)
	Zirconia	93 (16)	7.6 (1.8)	31 (7)	1.18 (0.18)
PA	Alumina	82 (45)	9.19 (6.9)	17 (17)	0.36 (0.15)
	ZTA	12 (4)	0.19 (0.1)	50 (22)	1.21 (0.30)
	Zirconia	5 (≈ 0)	0.04 (≈ 0)	83 (3)	1.49 (0.02)
PAS/PASA	Alumina	243 (28)	75.2 (14.9)	46 (6)	1.21 (0.04)
	ZTA	134 (22)	23.5 (7.3)	39 (2)	1.36 (0.04)
	Zirconia	236 (25)	43.3 (0.7)	50 (2)	1.28 (0.11)
S	Alumina	277 (3)	82.9 (3.8)	55 (3)	1.12 (0.02)
	ZTA	138 (6)	27.1 (1.5)	43 (1)	1.37 (0.03)
	Zirconia	233 (23)	43.1 (2.9)	49 (1)	1.31 (0.09)

Standard deviation is presented in parentheses. High-frequency-pass Gaussian filter $10 \times 10 \mu\text{m}$

The FIB nano-tomography analysis performed on PASA Zirconia showed the presence of a very thin nano-grain layer at the surface up to 150 nm, as presented in **Figure 2.4**. The recrystallized zone in the surface can be distinguished from the bulk by looking at the difference in grain size: in the bulk, grain size is in the range of 500 nm while at the surface it goes below 100 nm.

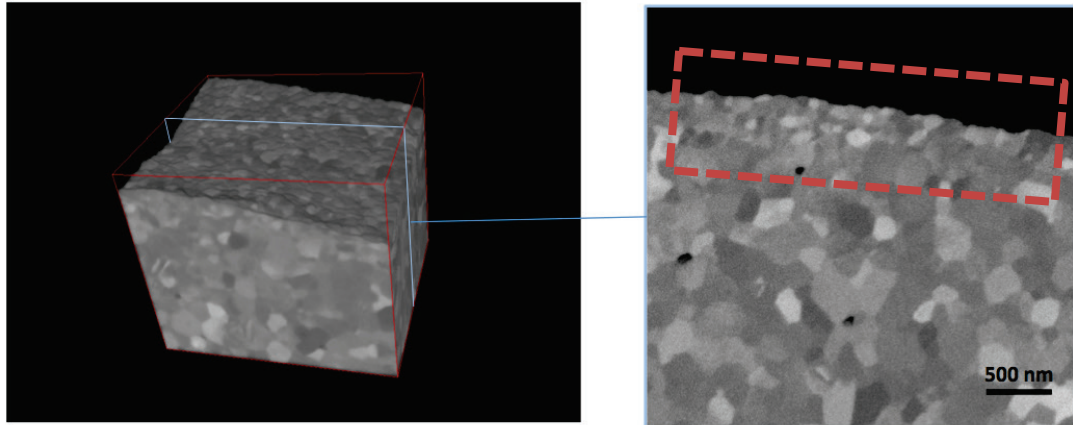


Figure 2.4. On the left the analyzed volume ($3.2 \times 3.1 \times 2.9 \mu\text{m}$) and on the right, the cross-section showing the profile in depth. The recrystallized zone is highlighted by the dashed red rectangle.

2.3.3 Aging assessment

The accelerated aging kinetic results are condensed in **Figure 2.5**. The aging evolution in all series of ZTA appears undistinguishable (ANOVA, $p \gg 0.05$). In Zirconia, significant differences (ANOVA, $p < 0.05$) were found in all curves, except in PAS and S, which followed the exact same path (t-test, $p \gg 0.05$). Interestingly, in PASA Zirconia the increase of monoclinic phase for the first 10 hours of aging was zero, and it seemed to reach saturation at a lower content than 70%, unlike the other series.

Additionally, ZTA and Zirconia presented different monoclinic content from the beginning: while in ZTA monoclinic zirconia phase content departed from around 25%, in Zirconia, the monoclinic content was distributed from 0 to 10%. Moreover, sandblasting increased the monoclinic content on Zirconia, but it did not increase it on ZTA.

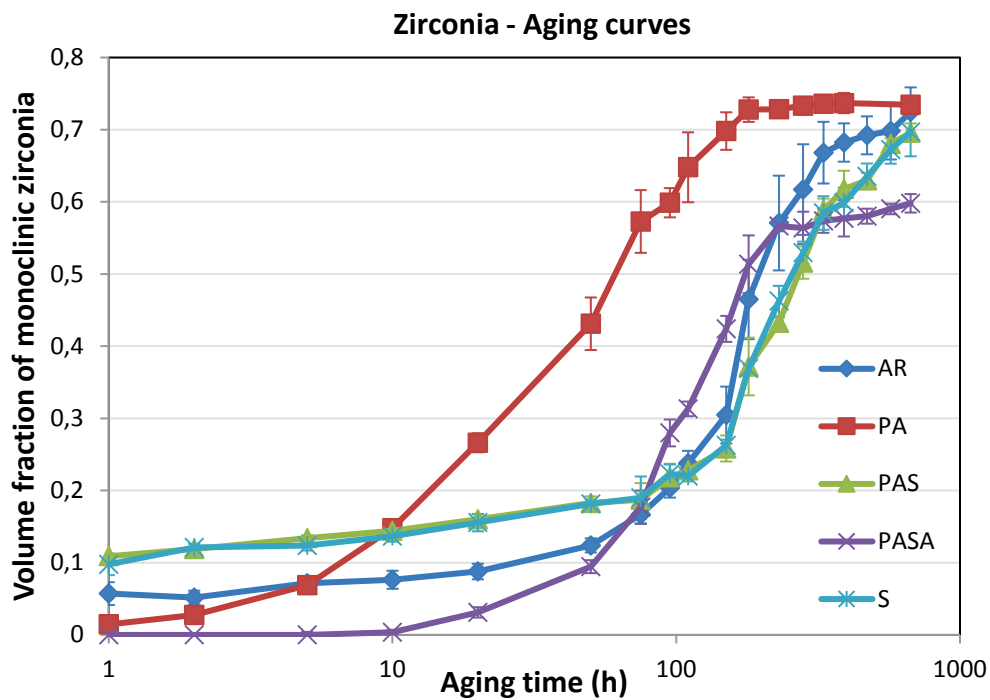
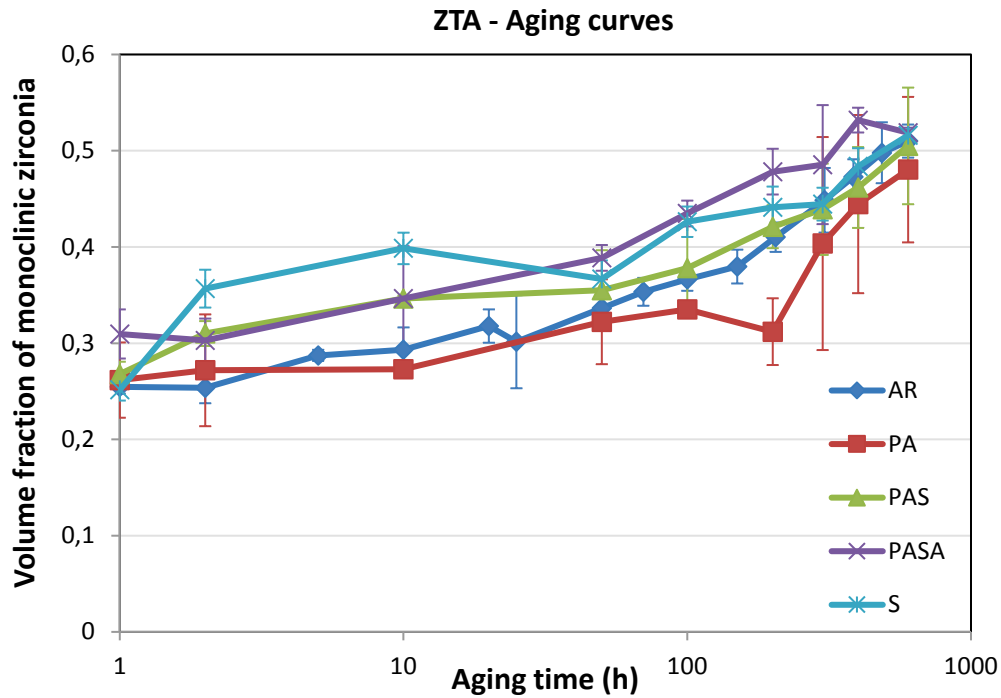


Figure 2.5. Evolution of monoclinic zirconia content after accelerated aging in autoclave in ZTA (a) and Zirconia (b).

2.3.4 Mechanical Characterization

Figure 2.6 and Table 2.5 summarize the results obtained for each series and material. The data is presented by means of Weibull statistic.

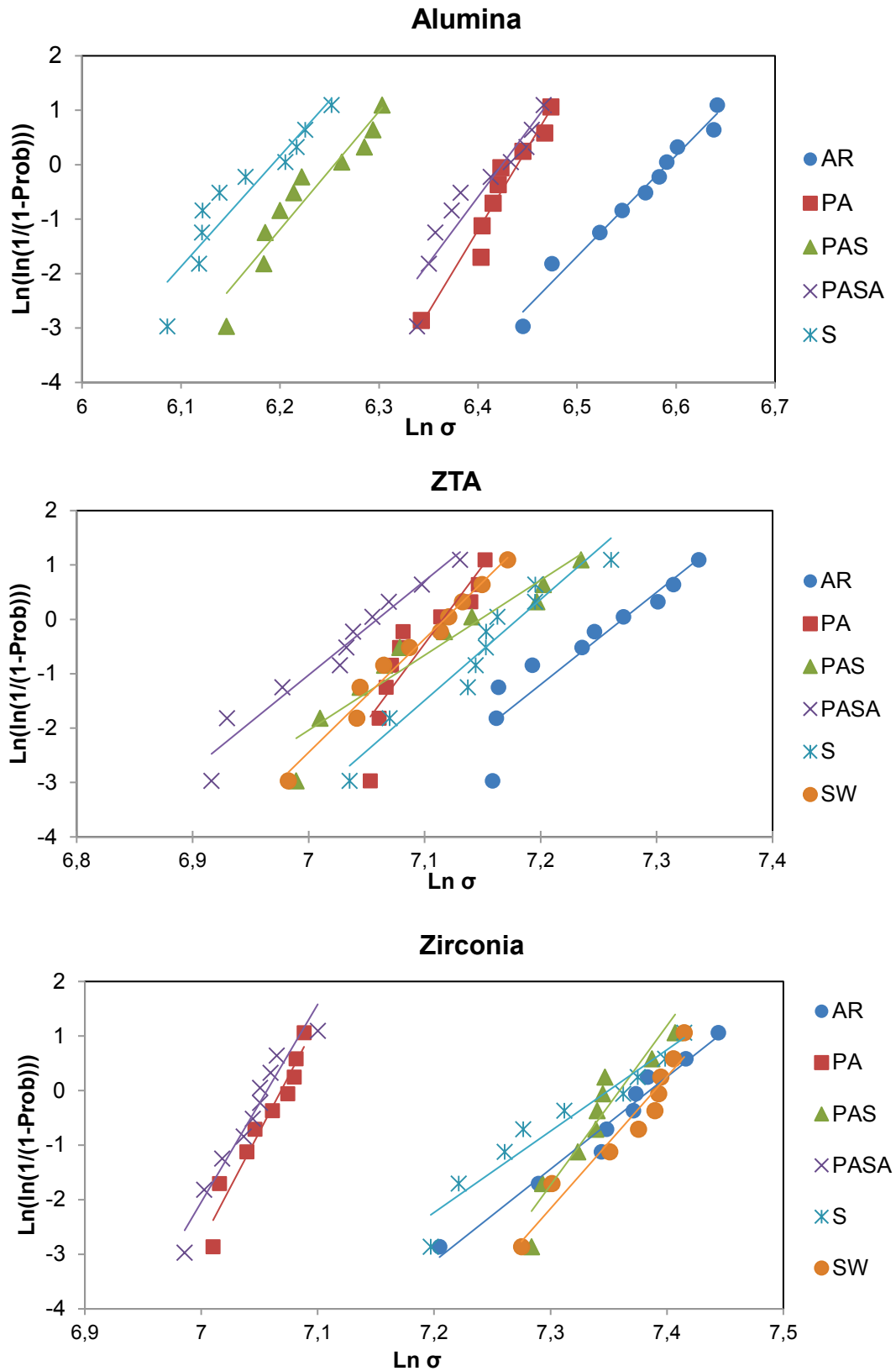


Figure 2.6. Weibull distributions of 4-point bending test results

As shown, each material reacts differently to sandblasting. For the comparisons between series, we focused on the central value of each Weibull distribution, σ_0 , which corresponds to a value of σ with a 63.2% of probability of failure (Table

2.5). In general terms, ZTA is the material whose Weibull distributions present the least differences. The plots of Alumina and specially Zirconia appear much separated. Indeed, among Zirconia series we can distinguish two separate groups: those samples containing RS (AR, PAS, S, SW) and those not (PA, PASA). No significant difference was found among the samples of the first group (ANOVA, $p > 0.05$), or the ones of the second group (t-test, $p > 0.05$), pointing to the idea that RS are dominant. The thin recrystallization layer in PASA Zirconia did not affect its mechanical resistance.

Regarding the values of strength, the difference between Alumina and TZP-containing materials is manifest. Zirconia samples almost double and in some series triple the strength of Alumina. ZTA presented values close to those of Zirconia, despite their low content of Y-TZP (around 17% in volume [43]).

Additionally, we observed a decrease in strength in Alumina after sandblasting, both from PA to PAS and from AR to S. In ZTA, sandblasting has not much effect on the strength from PA to PAS, and very limited in the case of AR to S. Zirconia exhibited a large increase in strength from PA to PAS, and a moderated decrease from AR to S. Interestingly, while annealing PAS (to obtain PASA) reduced the strength on ZTA and Zirconia, on Alumina it increased. Finally, 50h aged (SW) ZTA presented a similar strength to as-sandblasted (S), and in Zirconia we observed a slight increase of strength after aging.

Table 2.5. Central value of Weibull distributions corresponding to a probability of failure of 63,2% (MPa) (left) and Weibull modulus (right).

	Alumina		ZTA		Zirconia	
PA	623	17	1230	29	1174	41
PAS	520	22	1271	14	1560	23
PASA	616	24	1163	17	1155	42
AR	744	19	1480	17	1612	17
S	488	20	1313	19	1556	15
SW	---	---	1232	21	1618	24

2.4 Discussion

2.4.1 Surface Characterization

Roughness results on AR samples will not be discussed. The supplier machined the samples before we could get our hands on, and therefore we cannot know whether the differences observed are linked to different treatment conditions, or different material response. For this reason we decided to take the PA surfaces as “fresh” reference for the comparisons.

The relationship between roughness and in-vivo behaviour (i.e. biointegration) and especially the role of each surface feature is still a subject not fully understood. It is generally accepted that surfaces with Ra or Sa between 0.2 and 1 μm [44,45] promote cell attachment. In addition, Arvidsson *et al.* [18] concluded that lower Sci values promoted bone-anchoring *in vivo*.

As a way of giving context to these results, they were compared to the typical values found in commercial dental products: Nanotite[®] (Biomet 3i, USA), Tioblast[®] and Osseospeed[®] (Astra Tech AB, Sweden)[40], WhiteSky[®] (Brendent Medical GmbH, Germany) and Zit-Z[®] (Ziterion, Germany)[46]. They are condensed in **Table 2.6**.

Table 2.6. Surface roughness of commercial dental implants (Source: Svanborg *et al.* [40] (Titanium); Zinelis *et al.* [46] (Zit-Z and WhiteSky))

	Name	Sa (nm)	Sdr	Sds ($\times 10^3 \text{ mm}^{-2}$)	Sci
Titanium	Nanotite*	280 (6)	17,04 (5.46)	224 (60)	1,49 (0.03)
	Tioblast*	640 (3)	17,82 (1.51)	125 (9)	1,46 (0.07)
	Osseospeed*	1320 (21)	32,8 (7.30)	102 (6)	1,44 (0.07)
Zirconia	Zit-Z	660 (50)	-	-	-
	WhiteSky	1310 (60)	-	-	-
	PAS**	236 (25)	43.3 (0.7)	50 (2)	1.28 (0.11)
	PAS (no filter)	607 (45)	44.6 (0.5)	43 (1)	1.43 (0.04)

Standard deviation is presented in parentheses

* The data presented were measured after application of high-frequency-pass Gaussian filter of size $50 \times 50 \mu\text{m}$

** *Idem* after high-frequency-pass Gaussian filter of size $10 \times 10 \mu\text{m}$

The comparison puts in perspective the studied materials against commercial surfaces. Apart from Sa, authors and vendors do not usually provide more parameters. This circumstance leads to a poor understanding of surface topography and leaves us only in speculation of how close we are from real products. Besides, the values reported for Zit-Z and WhiteSky are not filtered, and hence they present a higher apparent roughness than filtered PAS Zirconia. This is why we have decided to include the non-filtered PAS roughness results.

This shows that at least, the values of each parameter are comparable to those of commercial products.

Titanium exhibits an overall rougher surface than our ceramic materials, which is comprehensible given the higher plasticity of metals. However, their Sdr appears lower than on PAS, even after having filtered them. This could reflect the more brittle nature of zirconia materials. In order to reach the roughness levels of titanium we should have had to increase the intensity of sandblasting, which might had been acceptable for zirconia and ZTA (in view of the fracture properties shown on **Figure 2.6**), but would have clearly compromised the integrity of Alumina.

2.4.2 Aging assessment

The fact that all series of ZTA appeared undistinguishable could be related to the higher stability of ZTA against LTD in comparison with pure 3Y-TZP [47]. Surprisingly, all type of samples started with the same amount of monoclinic phase, even PA and PASA. The reason could probably be that in ZTA, after the thermal treatment and during cooling, internal stresses arise from the difference of thermal expansion coefficients between zirconia and alumina phases, and this mismatch could be triggering the tetragonal to monoclinic transformation, even if at high temperature during annealing there is no monoclinic phase.

The absence of phase transformation after sandblasting was not expected either. Assuming the alumina phase is under compressive RS while zirconia is under tensile ones, this result may be explained by RS related to thermal expansion coefficients mismatch being much higher than the stresses brought by sandblasting.

In Zirconia, the aging kinetics were more dependent on the treatments. AR, PAS and S series all present a significant initial monoclinic phase, due to the machining and sandblasting mechanical treatments. This initial monoclinic content is removed by the annealing treatment (PA and PASA).

Aging resistance can be influenced by two microstructural parameters: grain size and RS. Lower grain size is generally associated to higher resistance to ageing [48,49]; internal compressive RS may oppose to the grain volume increase during the t-m transformation, and thus delay or suppress ageing [23–25,41,50,51]. Our results were perfectly coherent with the known literature on the subject.

In PA Zirconia, the annealing step removed all the internal compressive RS, and as shown in **Figure 2.5**, the monoclinic content in PA Zirconia immediately rose within the first 5-10 hours of aging, being largely the first to reach saturation. This shows that having compressive RS (such as the ones deriving from sandblasting) helps retarding LTD.

PASA Zirconia had no more compressive RS, so according what it was exposed previously it should display behaviour similar to PA. However, its resistance to aging was much higher. The reason for this higher resistance to aging was associated to the layer of recrystallized tetragonal nano-grains, formed during the second annealing, as shown in **Figure 2.4** and as reported by Whalen *et al.* [26]. Since the LTD process follows a cascade of propagating events since the first nucleation [52], retarding the apparition of the first monoclinic grains enhances the material resistance to aging. Kosmač *et al.* [23] also observed partitioned tetragonal grains that provided some resistance to LTD on ground and annealed Zirconia. However, once the degradation reached normal-sized deeper grains, at about 20 to 50 hours, it went as fast as PA Zirconia, because neither of them presented internal RS.

Additionally, the reason of PAS Zirconia for not reaching saturation at the same level as the others could be attributed to the fact that the XRD technique is more sensitive to the surface than the bulk. Degradation happened not because all the tetragonal nano-grains transformed on the surface, but because some did and allowed water through the cracks [35]. This means that even in saturation, some tetragonal nano-grains remain on the surface thus decreasing the measured monoclinic content.

AR, S and PAS series presented delayed ageing kinetics as compared to PASA and PA series, due to the presence of important compressive RS. S and PAS series exhibited identical behaviour probably because the selected sandblasting treatment was sufficient to remove and 'rewrite' the previous surface states. AR series aged a bit faster, probably because of less intensive compressive RS.

2.4.3 Mechanical Characterization

We can safely assume that PA contained no RS after annealing, and at least for ZTA and Zirconia, that the critical defects are intrinsic (*i.e.* not caused by the surface treatment). In the case of Alumina, the grain pullouts caused by polishing across its surface represent important extrinsic defects (*i.e.* induced by the surface treatment). However, it presented no statistical difference with PASA (t-test, $p \gg 0.05$). This means that both have statistically equal critical-defect sizes without the influence of any RS, which implies that these defects are intrinsic.

Following the same argumentation with ZTA and Zirconia, we can assume that PASA contained no RS but they did present SD resulting from sandblasting. In comparison with PA, only ZTA presents statistical differences (t-test, $p < 0.05$), which points to extrinsic defects as the ones responsible for the failure of the samples.

PAS presented the same kind of SD as PASA, but it also contained RS. It is arguable that the critical defects in PAS would be of the same kind as in PASA, given that now we have to consider the effect of RS. And there certainly seems to be differences between Alumina and TZP-containing materials: despite the

unknown nature of defects, we could estimate an effective value of RS on each material by simply subtracting central values of PAS and PASA, yielding an effective tensile stress of 96 MPa for Alumina, and compressive effective stress of -108 and -405 MPa for ZTA and Zirconia respectively. The fact of having a weakening effect of RS on Alumina while strengthening on ZTA/Zirconia requires a more dedicated discussion that we will address in a separate section.

S series of Zirconia and ZTA presented no statistical difference (t-test, $p > 0.05$) with their respective PAS series. Therefore, we shall conclude that their critical defects must be of the same type. While ideally the role of RS in S samples should have been compared to a hypothetical sandblasted-annealed surface (following the same terminology "SA"), our limited resources encouraged us to rather focus on PA, PAS and PASA. However, if we accept S and PAS are not significantly different from each other, for the comparisons with S we could use PASA instead. If we did so, we would find that albeit the calculated RS in Zirconia for S and PAS were equal, in S ZTA they were significantly higher (t-test, $p < 0.05$) than the ones in PAS (-150 vs. -108 MPa). This could be interpreted as a consequence of the different origins of S and PAS: S was obtained from AR, which contained RS; PAS was obtained from PA, which did not. This could mean either that we have smaller SD in S (due to the pre-existent compressive RS, which minimized the damage), that the sandblasting increased the compressive RS by merging with the pre-existent RS, or both.

Alumina presented a very small but statistically significant difference between S and PAS (t-test, $p < 0.05$). This could be understood in the same way as in ZTA. Sandblasting increased the RS in S, but as we have seen before, the higher fragility of Alumina did not allow it to accommodate RS as well as on TZP-containing materials, eventually weakening Alumina. The difference between S and PAS also meant that it was not possible to conclude with certainty whether or not that the intrinsic defects are the ones responsible for failure, which prevents us from estimating RS in S in comparison with PASA.

AR samples contained SD and RS strictly related to the grinding performed by the supplier. Their comparison to PA reveals that grinding induces a higher bending strength through compressive RS, and despite the creation of SD. Although we lack information of their performance after annealing, we can safely assume intrinsic critical defects, since the AR surfaces are not rougher than S. The presence of highly compressive RS in all three materials is the reason why AR samples were the strongest among all series studied.

Finally, the effect of LTD on the flexural strength was investigated on Zirconia and ZTA by comparing S and SW. In both ZTA and Zirconia, differences between the two conditions were very small, pointing to the fact that even long times of accelerated aging were not sufficient to compromise the mechanical properties. In both cases, the increment of monoclinic content was around 10% in volume. ZTA presented a statistically significant (t-test, $p < 0.05$) loss of strength of 7%. The explanation to this is probably multifactorial, but the exposition to LTD could have forced the t-m transformation on the SD crack tip, inducing more RS

and possibly extending the existing crack. In fact, we calculated the critical defect size (a_c) as:

$$a_c = \frac{1}{\pi} \left(\frac{K_{Ic}}{\sigma_0} \right)^2 \quad (6)$$

and we obtained 7.6 and 8.6 μm for ZTA S and SW respectively. Hypothetically just two or three transforming zirconia grains would be enough to account for the 1- μm difference. However, given the speculative nature of these arguments no conclusions can be sustained beyond reasonable doubt.

In **Table 2.7**, we present a summary of the conclusions extracted from the comparisons between series.

Table 2.7. Summary of results obtained for each series and material of estimated RS and defect types responsible of failure. Positive RS (>0) mean tensile, and negative (<0) compressive. Defects are either intrinsic (i.e. already present in the material, and related to fabrication) or extrinsic (i.e. created during surface modification). A question mark (?) expresses uncertainty due to lack of explicit evidence.

Series	Alumina		ZTA		Zirconia	
	RS (MPa)	Defect type	RS (MPa)	Defect type	RS (MPa)	Defect type
PA	0	Intrinsic	0	Intrinsic	0	Intrinsic
PAS	96	Intrinsic	-108	Extrinsic	-405	Intrinsic
PASA	0	Intrinsic	0	Extrinsic	0	Intrinsic
AR	-121	Intrinsic	-250	Intrinsic	-438	Intrinsic
S	?	?	-150	Extrinsic	-401	Intrinsic
SW			-69	Extrinsic?	-468	Intrinsic

2.4.4 On the different effective residual stresses after sandblasting

Let us assume that the distribution of intrinsic defects present in all three materials is equivalent, and we accept that the critical defect responsible for the failure of Alumina and Zirconia is intrinsic, and for ZTA extrinsic. Given the different bulk properties of each material, their response to sandblasting and the distribution of RS that is generated due to the treatment is hence difference. Our hypothesis is that in PAS Alumina, there is a bigger volume of material under tensile RS, in comparison with Zirconia, where the RS distribution may be more localized and smaller volume under tensile solicitations. The bigger the tensile-stressed volume, the higher the probability of having a big defect with potential of becoming critical, and hence the lower the fracture strength. A graphical representation of this idea is shown in **Figure 2.7**.

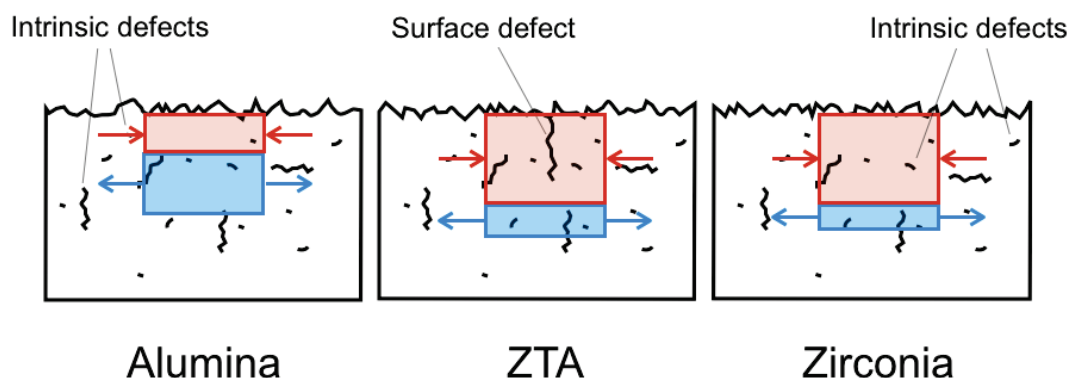


Figure 2.7. Graphical representation of the hypothesized residual-stress distribution for each material

If this hypothesis was proven correct, it would open the way to optimizing the sandblasting treatment to improving the mechanical resistance of alumina while presenting surface roughness. Perhaps a more aggressive treatment, with a thicker compressive layer, might be relevant, provided that it would not increase too much the density of SD.

A future work will aim at quantifying the RS versus depth, to understand the mechanisms governing this phenomenon in each material and confirm the hypothesis schematized in **Figure 2.7**.

2.5 Conclusions

The results obtained can be summarized as follows:

1. The materials reacted differently against the same sandblasting treatment. The higher fragility of Alumina led to grain pullout and thus a rougher surface in contrast to the tougher ZTA and Zirconia, which presented a generally smoother surface.
2. Residual stresses are dominant in comparison with surface defects regarding their effect on mechanical properties and aging behaviour. Surface defects were of less importance than intrinsic ones except in ZTA, where they did show a significant influence reducing its flexural strength.
3. In Alumina, residual stresses associated to sandblasting weaken the material, while in Zirconia and ZTA they significantly reinforce it. Effective tensile stresses are calculated in Alumina, while they are compressive for ZTA and zirconia. The actual mechanisms governing this phenomenon are still hypothetical and should be studied to optimize residual surface stresses.
4. Annealing sandblasted Zirconia generates a layer of recrystallized nano-grains of tetragonal phase, which constitutes an effective shielding against LTD. Such recrystallization was not observed in ZTA, whose aging performance seems not to be affected neither by surface roughness nor the presence of treatment-induced RS.

Glossary

ZTA:	Zirconia-toughened alumina
TZP:	Tetragonal zirconia polycrystal
AR:	As-received
PA:	Polished, Annealed
PAS:	Polished, Annealed, Sandblasted
PASA:	Polished, Annealed, Sandblasted, Annealed
S:	As-received, Sandblasted
SW:	As-received, Sandblasted, Aged for 50h in autoclave at 134° C
FIB:	Focus-ion beam
SD:	Surface defects
RS:	Residual stresses
LTD:	Low thermal degradation

Bibliography

- [1] Boutin P. Alumina and its use in surgery of the hip. (Experimental study). *Presse Med* 1971;79:639-40.
- [2] Boutin P, Blanquaert D. A study of the mechanical properties of alumina-on-alumina total hip prosthesis. *Rev Chir Orthop Reparatrice Appar Mot* 1981;67:279-87.
- [3] Cordingley, R., Kohan, L., Ben-Nissan, B., Pezzotti G. Alumina as an Orthopaedic Biomaterial - Characteristics, Properties, Performance and Applications. *J Aust Ceram Soc* 2007;39:20-8.
- [4] Klapperich C, Graham J, Pruitt L, Ries MD. Failure of a metal-on-metal total hip arthroplasty from progressive osteolysis. *J Arthroplasty* 1999;14:877-81.
- [5] MacDonald SJ. Can a safe level for metal ions in patients with metal-on-metal total hip arthroplasties be determined? *J Arthroplasty* 2004;19:71-7.
- [6] Altenburg AJ, Callaghan JJ, Yehyawli TM, Pedersen DR, Liu SS, Leinen JA, et al. Cemented total hip replacement cable debris and acetabular construct durability. *J Bone Joint Surg Am* 2009;91:1664-70.
- [7] Campbell P, McKellop H, Alim R, Mirra J, Nutt S, Dorr L, et al. *Cobalt-Base Alloys for Biomedical Applications*. vol. 1365. 100 Barr Harbor Drive, PO Box C700, West Conshohocken, PA 19428-2959: ASTM International; 1999.
- [8] CeramTec GmbH. BioloX Ceramic materials n.d.
- [9] Marketsandmarkets.com. *Dental Implants and Prosthetics Market by Material (Titanium, Zirconium, PFM, All Ceramics), Stage (Two Stage, Single Stage), Connectors (External hexagonal) & Product Type (Crowns, Bridges, Dentures, Abutments) - Global Forecast to 2020*. 2015.
- [10] Ichikawa Y, Akagawa Y, Nikai H, Tsuru H. Tissue compatibility and stability of a new zirconia ceramic in vivo. *J Prosthet Dent* 1992;68:322-6.
- [11] Hayashi K, Matsuguchi N, Uenoyama K, Sugioka Y. Re-evaluation of the biocompatibility of bioinert ceramics in vivo. *Biomaterials* 1992;13:195-200.
- [12] Sundfeldt M, Carlsson L V, Johansson CB, Thomsen P, Gretzer C. Aseptic loosening, not only a question of wear: a review of different theories. *Acta Orthop* 2006;77:177-97.
- [13] De Man FHR, Tigchelaar W, Marti RK, Van Noorden CJF, Van der Vis HM. Effects of mechanical compression of a fibrous tissue interface on bone with or without high-density polyethylene particles in a rabbit model of prosthetic loosening. *J Bone Joint Surg Am* 2005;87:1522-33.
- [14] Wroblewsky BM. *Revision Surgery in Total Hip Arthroplasty*. Springer-Verlag London Limited; 1990.
- [15] Lincks J, Boyan BD, Blanchard CR, Lohmann CH, Liu Y, Cochran DL, et al. Response of MG63 osteoblast-like cells to titanium and titanium alloy is dependent on surface roughness and composition. *Biomaterials* 1998;19:2219-32.
- [16] Wennerberg A. The importance of surface roughness for implant incorporation. *Int J Mach Tools Manuf* 1998;38:657-62.
- [17] Nishimoto SK, Nishimoto M, Park S-W, Lee K-M, Kim H-S, Koh J-T, et al.

- The effect of titanium surface roughening on protein absorption, cell attachment, and cell spreading. *Int J Oral Maxillofac Implants* 2008;23:675–80.
- [18] Arvidsson A, Sater BA, Wennerberg A. The Role of Functional Parameters for Topographical Characterization of Bone-Anchored Implants. *Clin Implant Dent Relat Res* 2006;8:70–6.
- [19] Gahlert M, Gudehus T, Eichhorn S, Steinhauser E, Kniha H, Erhardt W. Biomechanical and histomorphometric comparison between zirconia implants with varying surface textures and a titanium implant in the maxilla of miniature pigs. *Clin Oral Implants Res* 2007;18:662–8.
- [20] Chevalier J, Grandjean S, Kuntz M, Pezzotti G. On the kinetics and impact of tetragonal to monoclinic transformation in an alumina/zirconia composite for arthroplasty applications. *Biomaterials* 2009;30:5279–82.
- [21] Kuntz M. Validation of a New High Performance Alumina Matrix Composite for use in Total Joint Replacement. *Semin Arthroplasty* 2006;17:141–5.
- [22] Deville S, Chevalier J, Fantozzi G, Bartolomé JF, Requena J, Moya JS, et al. Low-temperature ageing of zirconia-toughened alumina ceramics and its implication in biomedical implants. *J Eur Ceram Soc* 2003;23:2975–82.
- [23] Kosmač T, Oblak Č, Marion L. The effects of dental grinding and sandblasting on ageing and fatigue behavior of dental zirconia (Y-TZP) ceramics. *J Eur Ceram Soc* 2008;28:1085–90.
- [24] Camposilvan E, Flamant Q, Anglada M. Surface roughened zirconia: towards hydrothermal stability. *J Mech Behav Biomed Mater* 2015;47:95–106.
- [25] Kim J-W, Covell NS, Guess PC, Rekow ED, Zhang Y. Concerns of hydrothermal degradation in CAD/CAM zirconia. *J Dent Res* 2010;89:91–5.
- [26] Whalen PJ, Reidinger F, Antrim RF. Prevention of Low-Temperature Surface Transformation by Surface Recrystallization in Ytria-Doped Tetragonal Zirconia. *J Am Ceram Soc* 1989;72:319–21.
- [27] Chintapalli RK, Mestra Rodriguez A, Garcia Marro F, Anglada M. Effect of sandblasting and residual stress on strength of zirconia for restorative dentistry applications. *J Mech Behav Biomed Mater* 2014;29:126–37.
- [28] Guazzato M, Quach L, Albakry M, Swain M V. Influence of surface and heat treatments on the flexural strength of Y-TZP dental ceramic. *J Dent* 2005;33:9–18.
- [29] Kosmač T, Oblak C, Jevnikar P, Funduk N, Marion L. Strength and reliability of surface treated Y-TZP dental ceramics. *J Biomed Mater Res* 2000;53:304–13.
- [30] Kosmač T, Oblak C, Jevnikar P, Funduk N, Marion L. The effect of surface grinding and sandblasting on flexural strength and reliability of Y-TZP zirconia ceramic. *Dent Mater* 1999;15:426–33.
- [31] Qeblawi DM, Muñoz CA, Brewer JD, Monaco Jr EA. The effect of zirconia surface treatment on flexural strength and shear bond strength to a resin cement. *J Prosthet Dent* 2010;103:210–20.
- [32] Sato H, Yamada K, Pezzotti G, Nawa M, Ban S. Mechanical Properties of Dental Zirconia Ceramics Changed with Sandblasting and Heat Treatment. *Dent Mater J* 2008;27:408–14.
- [33] Zhang Y, Lawn B, Malament K, P VT, Rekow E. Damage accumulation and

- fatigue life of particle-abraded ceramics. *Int J Prosthodont* 2006;19:442–8.
- [34] Zhang Y, Lawn BR, Rekow ED, Thompson VP. Effect of sandblasting on the long-term performance of dental ceramics. *J Biomed Mater Res B Appl Biomater* 2004;71:381–6.
- [35] Deville S, Gremillard L, Chevalier J, Fantozzi G. A critical comparison of methods for the determination of the aging sensitivity in biomedical grade yttria-stabilized zirconia. *J Biomed Mater Res B Appl Biomater* 2005;72:239–45.
- [36] Gaillard Y, Jiménez-Piqué E, Soldera F, Mücklich F, Anglada MJ. Quantification of hydrothermal degradation in zirconia by nanoindentation. *Acta Mater* 2008;56:4206–16.
- [37] Chintapalli RK, Marro FG, Jimenez-Pique E, Anglada M. Phase transformation and subsurface damage in 3Y-TZP after sandblasting. *Dent Mater* 2013;29:566–72.
- [38] Chevalier J, Olagnon C, Fantozzi G. Study of the residual stress field around Vickers indentations in a 3Y-TZP. *J Mater Sci* 1996;31:2711–7.
- [39] Wennerberg A, Albrektsson T. Suggested guidelines for the topographic evaluation of implant surfaces. *Int J Oral Maxillofac Implants* 2000;15:331–44.
- [40] Svanborg LM, Andersson M, Wennerberg A. Surface characterization of commercial oral implants on the nanometer level. *J Biomed Mater Res B Appl Biomater* 2010;92:462–9.
- [41] Garvie RC, Nicholson PS. Phase Analysis in Zirconia Systems. *J Am Ceram Soc* 1972;55:303–5.
- [42] Toraya H, Yoshimura M, Somiya S. Calibration Curve for Quantitative Analysis of the Monoclinic-Tetragonal ZrO₂ System by X-Ray Diffraction. *J Am Ceram Soc* 1984;67:C-119-C-121.
- [43] Clarke IC. Clinical and Tribological Perspectives of Wear in Alumina-Alumina THR. *Key Eng Mater* 2002;240–242:755–64.
- [44] Yamashita D, Machigashira M, Miyamoto M, Takeuchi H, Noguchi K, Izumi Y, et al. Effect of surface roughness on initial responses of osteoblast-like cells on two types of zirconia. *Dent Mater J* 2009;28:461–70.
- [45] Yang Y, Zhou J, Liu X, Zheng M, Yang J, Tan J. Ultraviolet light-treated zirconia with different roughness affects function of human gingival fibroblasts in vitro: The potential surface modification developed from implant to abutment. *J Biomed Mater Res B Appl Biomater* 2014.
- [46] Zinelis S, Thomas A, Syres K, Silikas N, Eliades G. Surface characterization of zirconia dental implants. *Dent Mater* 2010;26:295–305.
- [47] Kurtz SM, Kocagöz S, Arnholt C, Huet R, Ueno M, Walter WL. Advances in zirconia toughened alumina biomaterials for total joint replacement. *J Mech Behav Biomed Mater* 2014;31:107–16.
- [48] Sato T, Shimada M. Transformation of Yttria-Doped Tetragonal ZrO₂ Polycrystals by Annealing in Water. *J Am Ceram Soc* 1985;68:356–9.
- [49] Ohmichi N, Kamioka K, Ueda K, Marsui K, Ohgai M. Phase Transformation of Zirconia Ceramics by Annealing in Hot water. *J Ceram Soc Japan* 1999;107:128–33.
- [50] Marro FG, Chintapalli R, Hvizdoš P, Soldera F, Mücklich F, Anglada MJ. Study of near surface changes in yttria-doped tetragonal zirconia after low temperature degradation. *Int J Mat Res* 2009;100:0–4.

- [51] Lawson S. Environmental degradation of zirconia ceramics. J Eur Ceram Soc 1995;15:485-502.
- [52] Chevalier J. What future for zirconia as a biomaterial? Biomaterials 2006;27:535-43.

3

EFFECT OF PROTEINS

Wettability of bearing surfaces in arthroplasty: Influence of cleaning method and protein adsorption

Contents

3.1 Introduction.....	73
3.2 Materials and methods.....	76
3.2.1 Selection of cleaning protocol.....	77
3.2.2 Contact angle on curved surfaces	77
3.2.3 Effect of gamma irradiation.....	77
3.2.4 Organic solvents, NBCS exposure and incubation	78
3.2.5 Statistics	78
3.3 Results.....	79
3.3.1 Cleaning protocol	79
3.3.2 Effect of gamma irradiation.....	80
3.3.3 Organic solvents, NBCS exposure and incubation	80
3.4 Discussion	83
3.4.1 Cleaning protocol	83
3.4.2 Effect of gamma irradiation.....	83
3.4.3 Organic solvents, NBCS exposure and incubation	84
3.5 Conclusions	87
Bibliography.....	89

3.1 Introduction

In orthopedics, wettability has always been associated to tribology and the ability of the bearing to remain lubricated. However, the lubrication process in a bearing implant (such as in total hip or knee arthroplasty) is a complex phenomenon. Two model regimes of lubrication in artificial joints have been proposed for hard-on-hard bearing couples, as described by Myant *et al.* [1]: elastohydrodynamic film lubrication and boundary lubrication, depending on the formation or not of a fluid film in-between the two surfaces of friction. Additionally to these accepted regimes, proteins and other species present in the synovial fluid are involved in lubrication, becoming especially important in the boundary regime as potential lubricants [1]. In particular, it has been discovered that proteins (especially those with the highest molecular weight) help lubrication by avoiding surface-to-surface direct contact [2–4]. For example, Liao *et al.* [2] observed that using a modified serum lacking high-molecular-weight proteins as lubricant in a hip-joint simulator, it produced a much higher wear rate than control serum. A similar result was reported by Myant *et al.* on metal-on-metal joints [4]: for globulin-based lubricant wear was negligible, whereas for bovine serum and albumin-based lubricant important wear damage was found (globulin presents a much higher molecular weight than albumin).

Unfortunately, wettability plays a yet-to-understand role in lubrication [5,6]. For instance, it may affect the available content of lubricant in the contact zone. In 1998, Borruto *et al.* [5] studied the effect of wettability on lubrication by pairing different materials with different wettability in a pin-on-disc tribometer, under dry conditions and using oil and water as lubricants. Inspired by this work, in 2011 Pawlak *et al.* [6] repeated the same kind of experiment on different materials, arriving to the same conclusions: best tribological performance (lowest friction coefficient) was obtained when pairing a hydrophobic disc against a hydrophilic pin. The accumulation of the lubricant under the hydrophilic pin, and the repulsion of it by the hydrophobic sliding disc were responsible for the enhanced lubrication. However, these results can hardly apply to ball bearings without further research given the complexity of lubrication in the typical hip simulator or the natural gait cycles *in-vivo*.

Regarding the proteins, according to Wang *et al.* [7] many factors can affect the adsorption of proteins on a surface, including wettability. The adsorption is primarily determined by the properties of proteins, the properties of substrate and media, and the protein-substrate interaction. For instance, hydrophobic surfaces show better bovine serum albumin (BSA) adsorption affinity [8,9]. According to Jachimska *et al.* [8], contact angle is very sensitive to the degree of protein adsorption on a solid surface. The cause of all these phenomena is given by the heterogeneous surface of proteins [7] and substrate: they will present different regions (polar, unipolar, positively charged, negatively charged, etc), and this will allow them to interact differently. The result of this interaction is that proteins may assemble differently on each surface depending on the favorable orientations, and that resulting wettability may as well be affected [8].

However *in-vivo* bearing surfaces will rarely be exposed to just proteins. Typical composition of synovial fluids include hyaluronic acid, lubricin, proteins and an assortment of other substances, which keep its viscosity high to reduce friction between the articular cartilage of synovial joints during movement [10]. Additionally, *in-vitro* simulations often use serum as lubrication medium [3,11]. This all means that lubrication is studied with a multi-component medium, where some of its components will adsorb on the bearing surface, and this circumstance will inevitably change the original wettability of the surface.

In general terms, contact angle represents the macro-scale effect of interactions that take place at the atomic level between the molecules of the surface, the liquid and the environment. Any other species on the surface will change the surface energy and affect the interaction. Hence, the preparation of the surface has a critical impact on the measurement and it is impossible for the operator to distinguish “bad” results from “good” results without previous experience and without valid values of reference. A good example is found in literature [12] when in 1964 it was attempted to obtain the wettability of pristine gold surfaces. The impossibility to distinguish between pristine and contaminated measurements derived in accusations and counter-accusations of hydrophobic/hydrophilic contamination between two research groups. The confrontation remained until 1970 with a new work that found a contact angle of zero under conditions designed to eliminate all sources of contamination.

In the absence of any contamination, the great majority of scientific evidence [12–16] points to the superhydrophilicity of metallic oxides (i.e. complete wetting, contact angle zero). But due to the omnipresence of hydrocarbon contamination, this clean state is metastable. To illustrate this, Preston *et al.* [14] plotted the wettability of water on different oxides versus the content of carbon on the surface, obtained by XPS. The plot is reproduced in **Figure 3.1**. The trend shows that the less carbon content (related to hydrocarbon contamination), the lower the contact angle in the equilibrium, being the limit at zero. In other words: in metallic oxides, carbon contamination raises the water contact angle from the initial superhydrophilic state.

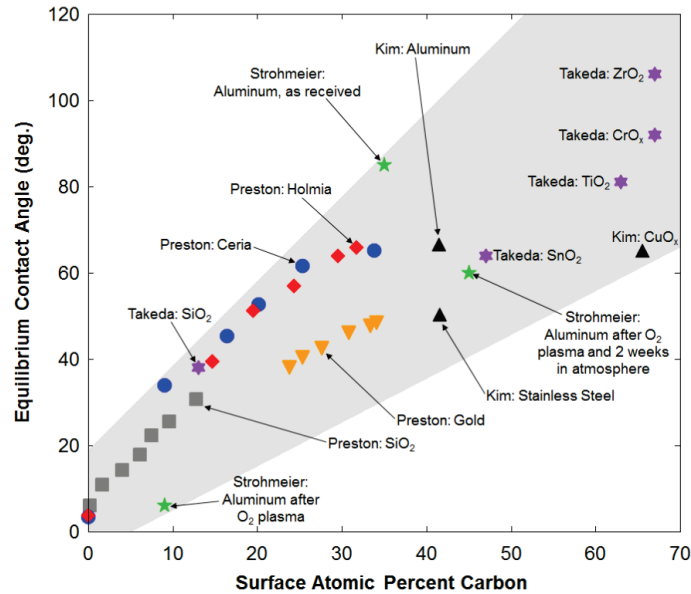


Figure 3.1. Comparison of experimental data from Preston[14] to previously results for equilibrium contact angle as a function of surface atomic percent carbon (Source: Preston et al., 2014).

Among all the papers reviewed for this study, many different techniques have been reported to have an effect on such hydrocarbon layer at the surface. One of the most interesting mentions was the use of gamma irradiation [17], where researchers studied the effect of the treatment on the wettability of a fresh oxidized surface of Zircaloy (*i.e.* the surface is pure zirconium oxide). They observed an important decrease of the contact angle after the irradiation, especially when it was performed with the surface immersed in deionized water. The reason for this cleaning effect was attributed to the production of radicals and highly reactive species through radiolysis of water [17–19]. Although gamma irradiation as sterilization step is performed in vacuum, there are chances of radiolysis of the trapped air, which could potentially neutralize organic contamination present in the surface [17], and this needs to be evaluated.

In summary, wettability measurements are dramatically affected by surface contamination. In some occasions researchers use different cleaning methods regardless of their ability to remove such contamination [11,20–22], underestimating or even ignoring its possible influence. With the objective to investigate the scope of this perturbation, in this work we first evaluated the ability of each presented cleaning protocol to remove contamination, and its effects on contact angle wettability on flat samples. Once selected the best cleaning protocol, we studied the wettability on curved surfaces (hip ball heads), and the effect of gamma irradiation as a post packaging procedure. Finally, we exposed the samples to solutions of serum and investigated the effect of the adsorption of proteins and other substances on wettability.

3.2 Materials and methods

The studied samples were provided by CeramTec GmbH (Plochingen, Germany), and consisted of cylinder-shaped pellets of Ø18 mm and ball heads of Ø28 mm, Ø32 mm and Ø36 mm of BIOLOX® *delta* (Delta), BIOLOX® *forte* (Forte) and Cobalt Chromium Molybdenum (CoCr) (ISO 5832-12). All samples (both pellets and ball heads) were polished to comply with ISO 7206-2:2011, which stipulates that ceramic ball heads must present an average roughness (Ra) of no more than 20 nm. Static and dynamic contact angle measurements were performed in a goniometer (DSA25, Krüss, Germany) equipped with an automatic drop dispenser using de-ionized water, and the images were analyzed using Krüss DSA4 proprietary software. All measurements were performed using 1 µL as the drop volume, and in a closed room where temperature and relative humidity was kept reasonably constant at 23 °C (±3) and 39 % (±7) of relative humidity. The cleaning procedures used in this work are summarized in **Table 3.1**.

Table 3.1. Description of the cleaning procedures.

Treatment label	Description
NoC	No Cleaning – Samples were tested as-polished, without further cleaning.
EthUS	Ethanol in UltraSonic bath – The samples were immersed in ethanol inside an ultrasonic bath for 5 min, and dried with a stream of pure N ₂ gas.
EthUS+W	Ethanol in Ultrasonic bath and Wipers – The samples were cleaned as EthUS, and cleaned again with clean-room wipers soaked in ethanol.
PC	Production Cleaning – Samples were cleaned by CeramTec GmbH using a proprietary procedure consisting of subsequent ultrasonic baths at different pH, and a final step of rinsing in deionized water to neutralize. After this, the samples were dried under a stream of hot air and packed in sealed plastic bags under vacuum.
PC+Al	Production Cleaning Al Foil – Samples were equally cleaned as PC, but the samples were wrapped in aluminum foil before being packed in sealed plastic bags under vacuum.
PC+EthW	Production Cleaning and Ethanol Wipers – The samples were cleaned as PC, and cleaned again right before the measurements with clean-room wipers soaked in ethanol.
PC+AcetW	Production Cleaning and Acetone Wipers – The samples were cleaned as PC, and cleaned again right before the measurements with clean-room wipers soaked in acetone.
PC+IsopropW	Production Cleaning and Isopropanol Wipers – The samples were cleaned as PC, and cleaned again right before the measurements with clean-room wipers soaked in isopropanol.
GS	The samples were cleaned as PC, kept in sealed plastic bags for 5 days and sterilized under gamma irradiation with a dosage of 27-28 kGy.

GS+Al	The samples were cleaned as PC+Al, kept in sealed plastic bags for 5 days and sterilized under gamma irradiation with a dosage of 27-28 kGy.
-------	--

3.2.1 Selection of cleaning protocol

The presence of surface contamination is a source of surface heterogeneities, and contact angle hysteresis increases with amount of surface heterogeneities [23]. Hence, on equally mirror-finish polished surfaces, the cleaning method providing the lowest hysteresis is the one capable of removing the highest amount of contamination [24].

The evaluation focused on cleaning protocols typically used in laboratory (NoC, EthUS and EthUS+W) and compared them with typical cleaning protocols used at industrial scale (PC, PC+Al, PC+EthW). To avoid any effect of shape, only flat pellets were used.

We used one sample per condition, and each surface was tested at least at five different locations amid its area, making sure not to test the same spot twice.

3.2.2 Contact angle on curved surfaces

Wettability of ball heads was assessed by placing the water drop in the apex of the sphere and manually fitting the baseline to the curvature of the surface. In this part, we performed only quasistatic analysis due to the difficulties of measuring the receding angle, which in some cases coincided with the curvature of the test surface. Through image analysis, the software automatically calculated the angles assuming the deposited drop was perfect sphere [25]. Each surface was statically tested at least at eight different locations amid its area.

3.2.3 Effect of gamma irradiation

Ball heads cleaned as GS and GS+Al were sterilized in their sealed plastic bags according to current standards (DIN EN ISO 11137, as of March 2015) by an external service, which followed all safety standards and measures. All samples were kept in the same sealed bags until the moment of testing. The results of contact angle made on GS and GS+Al were compared to the ones obtained for PC and PC+Al to investigate the effect of gamma irradiation on the wettability of packed products.

3.2.4 Organic solvents, NBCS exposure and incubation

In order to study the effect on wettability of the serum adsorption films, some ball heads were incubated at 36° C for 30 min in diluted solutions containing Newborn Calf Serum (ISO 9001:2008, Biochrom AG, Germany). The concentration of the incubation environment was estimated in the range of 0.30 – 0.35 g/L. After the incubation time, the surfaces were rinsed with deionized water and dried with a stream of N₂ gas prior to the measurement. To verify the effect of the presence of adsorbents, “blank” incubations were performed and taken as reference. They consist of the same procedure at 36° C for 30 min, but only using deionized water as liquid medium. We studied as well the effect of the use of different cleaning procedures (PC, PC+Al, PC+AcetW, PC+IsopropW) prior to incubation on the contact angle of samples. Differences in results would be related to a different adhesion distribution, affected by the different surface preparation treatment.

For this, three different series were prepared: “Pristine” (i.e. as cleaned and no incubation), “Without Serum” (i.e. after incubation without serum) and “With Serum “ (i.e. after incubation with serum). For each series, four groups were distinguished regarding the way they were cleaned. We used five ball heads per cleaning condition and each surface was tested at least at eight different locations amid its area, making sure not to test the same point more than once (a total of 40 drops per material and condition).

3.2.5 Statistics

Statistical analysis was performed using StatPlus (AnalystSoft Inc., Alexandria, USA). When necessary, data was statistically compared through either t-test or one-way ANOVA, using both a confidence interval of 5% ($\alpha=0.05$). The results in this work are presented in the form of column plots where the value being plot is the arithmetic mean of a data population and the error bars represents two times the standard deviation of that population.

3.3 Results

3.3.1 Cleaning protocol

Quasistatic and hysteresis results of contact angle measurements performed on flat surfaces cleaned through different methods are presented in **Figure 3.2**.

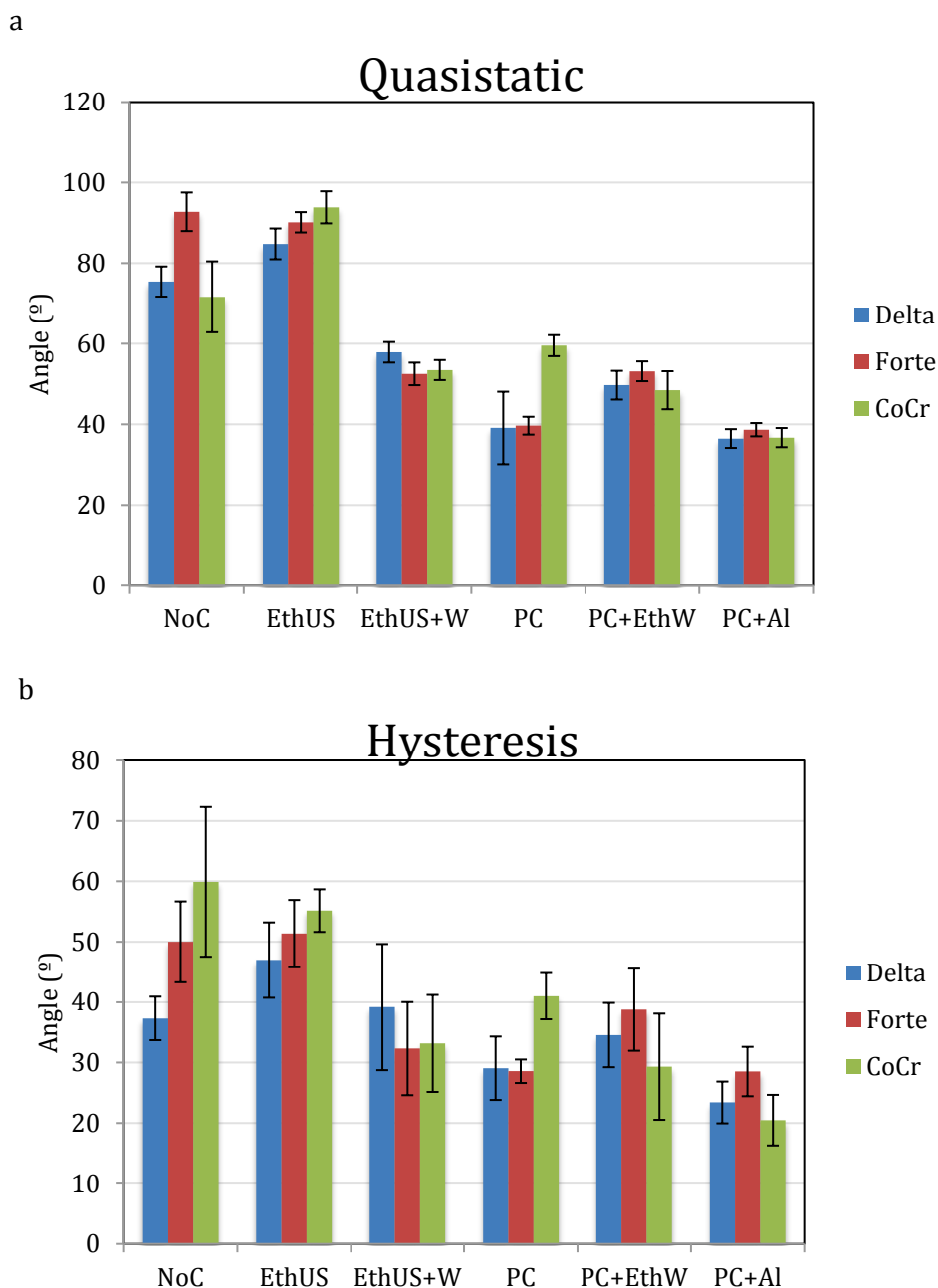


Figure 3.2. (a) Results of quasistatic contact angle, and (b) hysteresis after dynamic measurements. All these results were obtained on flat surfaces

Despite the higher variability in the measurements of contact angle hysteresis, the three materials exhibit a very similar wettability after each cleaning treatment, especially between Delta and Forte. The plots show a similar tendency in both parameters, presenting an overall decrease in the quasistatic value as the hysteresis lowers.

3.3.2 Effect of gamma irradiation

Results of the effect of gamma irradiation are summarized in **Figure 3.3**, where we compared the wettability of samples before and after storage and exposition to radiation. An overall increase in the contact angle is perceived on all surfaces after gamma exposition, except on CoCr under aluminum foil, which decreased. The effect is much more intense from PC to GS, than from PC+Al to GS+Al.

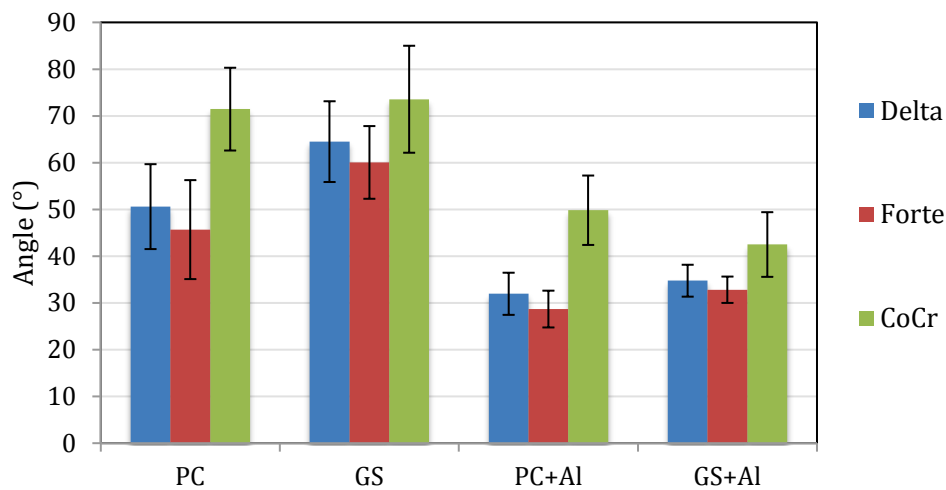


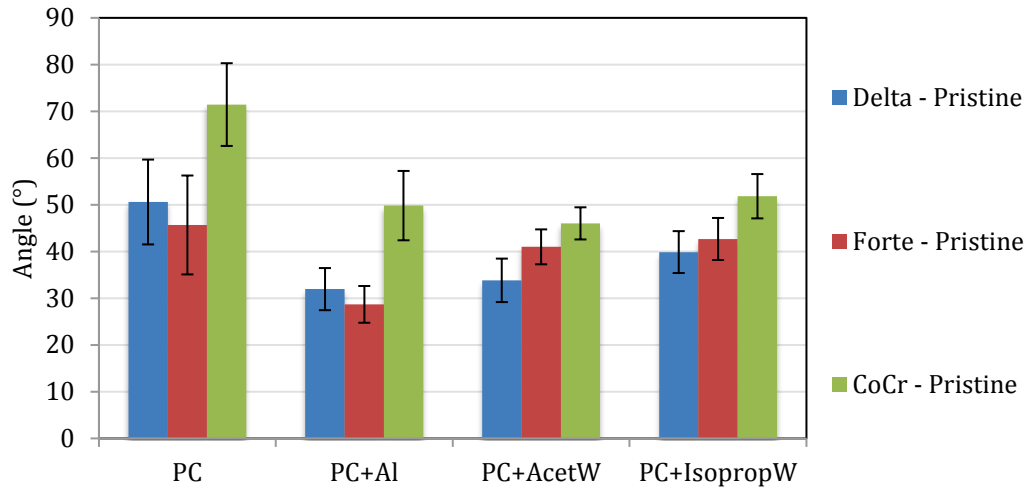
Figure 3.3. Comparison of quasistatic contact angle before and after gamma irradiation. Results obtained on ball heads

3.3.3 Organic solvents, NBCS exposure and incubation

Results of water contact angle for each condition are plotted in **Figure 3.4a, b** and **c**. The angles exhibited by the pristine ball heads appear similar to those found on flat surfaces. Results obtained after incubation with serum appear rather flat, and contrast to those obtained after incubation without serum, which maintains a higher similarity with pristine.

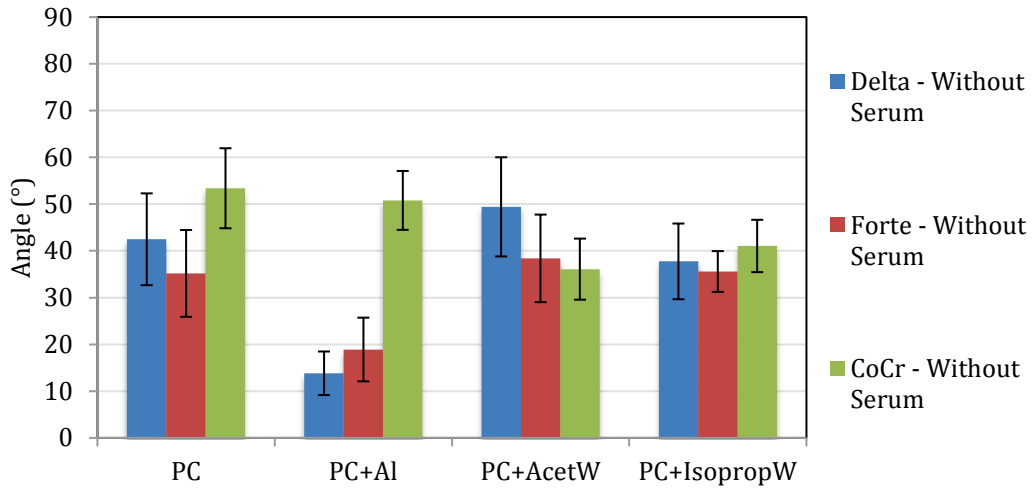
a

Pristine



b

Without serum



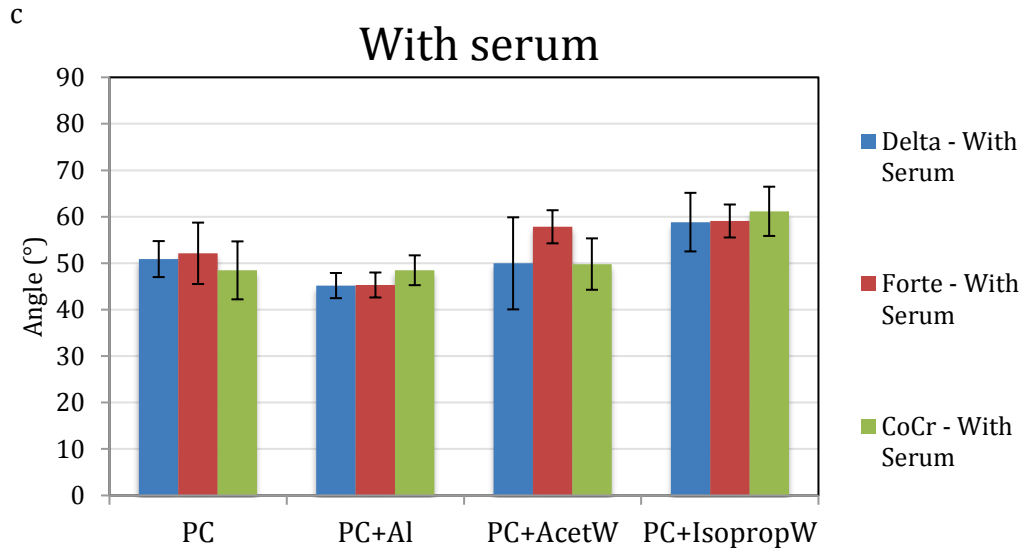


Figure 3.4. (a) Contact angles on surfaces right after cleaning. (b) Contact angles after incubation without serum. (c) Contact angle after incubation with serum. Results obtained on ball heads.

3.4 Discussion

3.4.1 Cleaning protocol

Results evidenced a strong influence of the cleaning protocol on the wettability of studied materials, ranging from 26° to 93°. For each material, the lowest hysteresis was found on PC+Al surfaces. Additionally, hysteresis in Forte presented no statistical difference between PC and PC+Al. In general terms, these results mean that PC+Al managed to eliminate the majority of heterogeneities from the surface.

The difference between PC and PC+Al can be related to the potential exposition to contamination while storage. While the aluminum foil protected PC+Al samples, PC surfaces were always in contact with the plastic bags and this interaction contaminated them in an uncontrolled way.

EthUS surfaces exhibited the highest quasistatic angles. They were even more hydrophobic than NoC samples and they presented very high values of hysteresis as well. Hence, the immersion of the surface in ethanol left traces of solvent, and this provided an imperfect cleaning.

An interesting effect was found after wiping with an ethanol soaked tissue: although it still tent to level the values of quasistatic angle as happened with ethanol in ultrasonic bath, rubbing the surfaces with an ethanol soaked tissue lowered their values. This was especially evident in the case of EthUS vs EthUS+W and it means wiping possibly removed an excess of adsorbed ethanol from the surface.

Finally, very similar wettability was found between PC+EthW and EthUS+W, especially on Forte (t-test, $p \gg 0.05$). This circumstance supports the idea that even if wiping removes remainings of ethanol in EthUS, it still left traces on PC+EthW. The effect on PC is observable by comparing PC and PC+EthW. The abrupt change experimented by Delta and Forte can be explained by solvent contamination from the wiping.

3.4.2 Effect of gamma irradiation

Gamma irradiation has enough energy to break chemical bonds and create free radicals [17–19]. Depending on the dosage, radiation can even affect the structure of polymeric materials [26], and this is why a detailed history of sterilization is kept for multi-use components. Assuming that the vast majority of contamination present in the surface is related to carbon derivatives, gamma irradiation could also remove part of it by creating reactive species that would oxidize the adsorbed organic molecules [27].

However, results did not seem to support this hypothesis: no dramatic decrease in angle was found after gamma irradiation. According to previous results, PC presented higher angles than PC+Al because PC lacked the “extra” protection provided by the aluminum foil against contamination from the package. The higher contact angle observed on GS can only be attributed to contamination from the package during a longer storage time (5 days).

To isolate the effect of gamma irradiation, we can compare PC+Al and GS+Al. Delta presented no statistical difference while Forte described a slight increase in angle ($p < 0.05$, t-test), and CoCr an undeniable decrease. Although the comparisons between Delta and Forte are statistically significant, the increase in Forte is minimum (4°) and could be put on the same level as Delta. Consequently, the protection of aluminum foil in PC+Al and GS+Al samples is the solely responsible for the lesser difference of Forte and Delta contact angles, in comparison with PC and GS.

In CoCr, the decrease in contact angle may point to a possible cleaning effect. Generally, CoCr exhibited the highest angles in all the series we evaluated. However it should theoretically present a similar wettability to Delta and Forte given the existence of a fine layer of chromium and molybdenum oxide on top [28]. One possible cause of the poorer wettability of CoCr could be a higher tendency to get contaminated. According to Takeda *et al.* [15], the higher OH density on the surface of a metal oxide, the higher its tendency to adsorb organic contamination from the atmosphere. In literature, we found different OH densities for CoCr: $2\text{-}5\text{ nm}^{-2}$ [21], and around 13 nm^{-2} [29], for alumina $14\text{-}19\text{ nm}^{-2}$ [30] and 15 nm^{-2} [29], and for zirconia $3\text{-}6\text{ nm}^{-2}$ [31]. These values are very similar to each other and they cannot justify the different behaviour observed in CoCr. Therefore, we conclude that these differences are most likely due to different requirements of CoCr in terms of cleaning. This would also explain why in **Figure 3.2**, PC+Al CoCr presents the lowest hysteresis and equivalent contact angle to Delta and Forte: when surface contamination is contained, CoCr presents a more similar wettability to Delta and Forte.

Moreover, the use of aluminum foil in a package system may in principle represent a barrier against gamma irradiation used for sterilization. However, having estimated the irradiation attenuation of a $25\text{ }\mu\text{m}$ thick layer, we conclude that the attenuation is inexistent ($>99.9\%$ is transmitted).

3.4.3 Organic solvents, NBCS exposure and incubation

When the surfaces were wiped with organic solvents after being cleaned as PC, we found a decrease of the contact angle in comparison with PC (**Figure 3.4a**). This decrease can be related to the removal of contamination from the plastic package. In comparison with PC+Al, Delta and Forte presented a slightly higher contact angle. If we assume that in PC+Al contamination levels are minimum, the loss of wettability after exposure to organic solvents would be the consequence of a possible contamination from the solvent itself.

Contrary to ceramics, both PC+AcetW and PC+IsopropW CoCr presented a statistically equivalent wettability to PC+Al (t-test, $p > 0.05$, in both cases). These results are consistent with the previous presented results and confirm the deficient performance of organic solvents as cleaning method.

More evidence of this is found in **Figure 3.4b**, where we plotted the results of contact angle taken after immersion of the surfaces in deionized water in the same conditions as the incubation with serum. While all samples were dried with a dry nitrogen gas stream before being tested, if affinity for water is high enough, some adsorbed molecules of water may remain at the surface [32,33]. In the plot, PC+Al Delta and Forte stand out from the rest of the columns exhibiting very low contact angles, evidencing a higher interaction of water with the surface of the ceramics. PC+Al provides the best cleaning state (the surfaces present the lowest hysteresis and hence the less amount of contamination), and the water molecules interact better with the surface, possibly forming H-bonds with the oxide, as schematically represented in **Figure 3.5**.

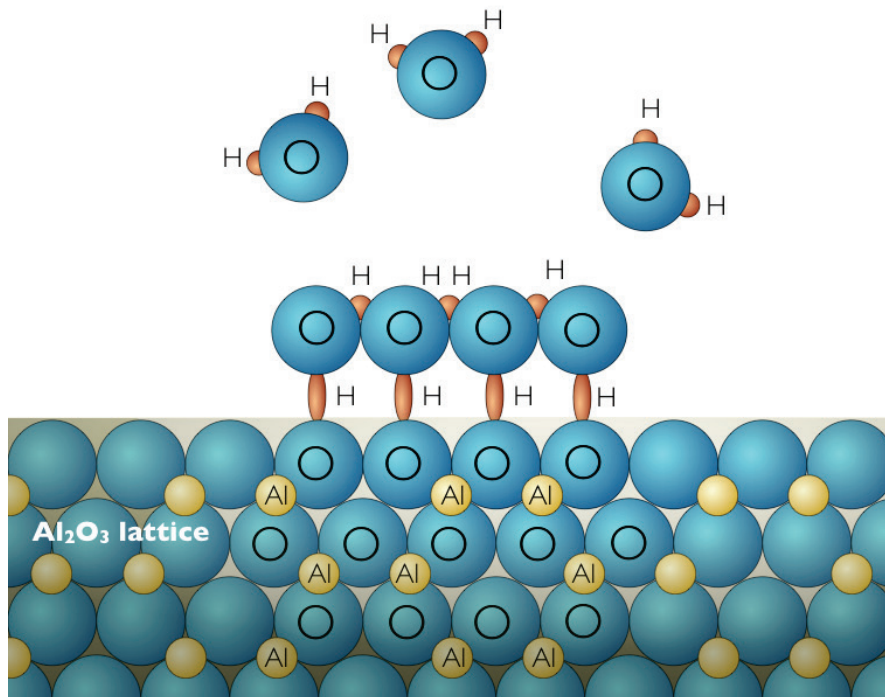


Figure 3.5. Representation of H-bonds on an aluminum oxide lattice

Figure 3.4c certifies that the exposition of the surface to protein-containing solutions has an effect on the surface wettability, detectable by contact angle measurements. In comparison with **Figure 3.4b**, all groups presented differences between incubation with and without serum, except PC and PC+Al CoCr, and PC+AcetW Delta, which presented no significant change (t-test, $p \gg 0.05$).

For each condition tested, all materials tended to level to the same angles after the incubation, blurring the pre-existing differences. However, each condition tested leveled to a different angle, even though all have been exposed to the

same kind of serum solution. On the one hand, PC+Al approached to 45°, and had the lowest standard deviation. Being serum an assortment of proteins, complex lipids, vitamins, minerals and other substances, this result may be indicative of a homogeneous distribution of adsorbents in the surface. On the other hand, PC+IsoporpW clearly approached to 60°, exhibiting a higher standard deviation. No statistical differences were found between the three materials after incubation in serum (ANOVA, $p>0.05$). The reason for the difference with PC+Al may be that the adsorbents from the serum are attaching differently (i.e. using different zones for the adhesion and hence exposing different zones to the exterior) due to solvent traces in the surface. This may also explain the higher standard deviation, given that the presence of solvent traces represents a source of heterogeneity.

PC and PC+AcetW exhibited angles somewhere in the range of 50°, although in the later the extreme variability complicated any analysis. The large standard deviation registered for PC+AcetW Delta was caused by the apparition of two groups of data: one that approached to 35° and another that approached to 58°, as shown in **Figure 3.6**. In the case of Forte and CoCr, this phenomenon was observed with less intensity and only after incubation without proteins. This may be related to the fact that surfaces cleaned with acetone have a less controlled amount of contamination in the surface.

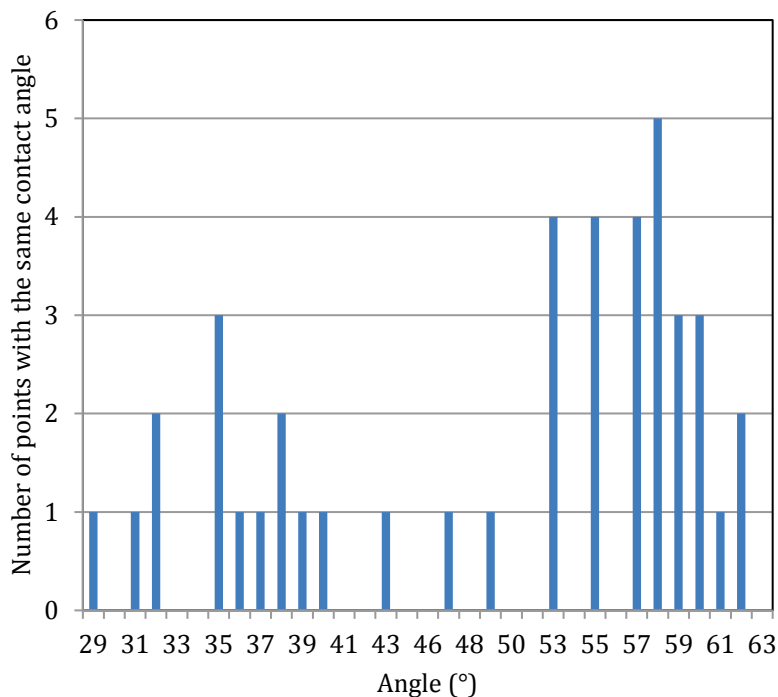


Figure 3.6. Results distribution of PC+AcetW Delta. Two groups can be observed among the population: one approaching to 35° and another to 58°.

3.5 Conclusions

In the present work, we have studied the influence on the water contact angle of different surface preparation procedures, typical packaging solutions and protein adsorption through incubation in diluted calf serum. The main conclusions can be summarized as follows:

1. The usage of organic solvents to prepare samples for wettability assessment is heavily discouraged in any form, neither in ultrasonic bath, nor wiping with clean tissue afterwards. We found higher angle hysteresis pointing to not-removed traces of solvent in the surface of the samples, resulting in higher and abnormal contact angles.
2. Even without organic solvent usage, surface wettability is constrained by the amount of adsorbed hydrocarbon contamination on it. The cleaning procedure for any surface study should put the focus on the removal of any contamination from the surface, including these adsorbed species. For this, XPS analysis can be used in a first instance to ensure no traces of solvents remain in the surface. Once the presence of other contaminants has been ruled out, contact angle measurements could be used to study qualitatively the amount of hydrocarbon contamination.
3. Storage conditions have a potential contaminating effect. It is recommended to keep the surfaces in a closed atmosphere-controlled environment and avoid direct contact of the surface to plastic bags and packages. As it was already proposed in literature [34,35], aluminum foil may be used to preserve pristine surfaces from contamination.
4. Gamma irradiation as sterilization procedure has a negligible impact on the wettability of the studied materials. The higher angles found after sterilization are explained by hydrocarbon contamination from the package.
5. Exposition to serum in diluted solutions has an impact on wettability. The adsorption of serum components follows the same mechanism as contamination, including proteins: the original pristine surface is masked by layers of different adsorbed substances, and this “new” surface would be the one to interact with the water drop during the wettability test.
6. Our results showed that the wettability of a surface exposed to serum is independent to the actual composition of the material among the samples studied, but it is somewhat dependent on the cleaning procedure they followed.
7. The set of experiments presented here had for main goal to ascertain the efficiency of cleaning procedure. The results should not be extended to wettability *in vivo* by synovial fluid, since the wettability by this fluid will not be the same as the wettability by water.

Bibliography

- [1] Myant C, Cann P. On the matter of synovial fluid lubrication: Implications for Metal-on-Metal hip tribology. *J Mech Behav Biomed Mater* 2014;34:338–48.
- [2] Liao YS, Benya PD, McKellop HA. Effect of protein lubrication on the wear properties of materials for prosthetic joints. *J Biomed Mater Res* 1999;48:465–73.
- [3] Scholes SC, Unsworth A. The effects of proteins on the friction and lubrication of artificial joints. *Proc Inst Mech Eng H* 2006;220:687–93.
- [4] Myant C, Underwood R, Fan J, Cann PM. Lubrication of metal-on-metal hip joints: The effect of protein content and load on film formation and wear. *J Mech Behav Biomed Mater* 2012;6:30–40.
- [5] Borruto A, Crivellone G, Marani F. Influence of surface wettability on friction and wear tests. *Wear* 1998;222:57–65.
- [6] Pawlak Z, Urbaniak W, Oloyede A. The relationship between friction and wettability in aqueous environment. *Wear* 2011;271:1745–9.
- [7] Wang K, Zhou C, Hong Y, Zhang X. A review of protein adsorption on bioceramics. *Interface Focus* 2012;2:259–77.
- [8] Jachimska B, Pajor A. Physico-chemical characterization of bovine serum albumin in solution and as deposited on surfaces. *Bioelectrochemistry* 2012;87:138–46.
- [9] Tanaka M, Motomura T, Kawada M, Anzai T, Kasori Y, Shiroya T, et al. Blood compatible aspects of poly(2-methoxyethylacrylate) (PMEA)—relationship between protein adsorption and platelet adhesion on {PMEA} surface. *Biomaterials* 2000;21:1471–81.
- [10] Blewis ME, Nugent-Derfus GE, Schmidt TA, Schumacher BL, Sah RL. A model of synovial fluid lubricant composition in normal and injured joints. *Eur Cell Mater* 2007;13:26–39.
- [11] Bishop NE, Hothan A, Morlock MM. High friction moments in large hard-on-hard hip replacement bearings in conditions of poor lubrication. *J Orthop Res* 2013;31:807–13.
- [12] Schrader ME. Wettability of clean metal surfaces. *J Colloid Interface Sci* 1984;100:372–80.
- [13] Joud J-C, Houmard M, Berthomé G. Surface charges of oxides and wettability: Application to TiO₂-SiO₂ composite films. *Appl Surf Sci* 2013;287:37–45.
- [14] Preston DJ, Miljkovic N, Sack J, Enright R, Queeney J, Wang EN. Effect of hydrocarbon adsorption on the wettability of rare earth oxide ceramics. *Appl Phys Lett* 2014;105.
- [15] Takeda S, Fukawa M, Hayashi Y, Matsumoto K. Surface OH group governing adsorption properties of metal oxide films. *Thin Solid Films* 1999;339:220–4.
- [16] Strohmeier BR. The effects of O₂ plasma treatments on the surface composition and wettability of cold-rolled aluminum foil. *J Vac Sci Technol A Vacuum, Surfaces, Film* 1989;7:3238.
- [17] Otsuka T, Takenori I, Kenji N, Naoki M, Kenichi H, Masayasu S, et al. On the wettability change of oxidized and gamma irradiated Zircaloy. *Proc 2005 Water React Fuel Perform Meet* 2005;37:1236.

- [18] LaVerne JA. OH radicals and oxidizing products in the gamma radiolysis of water. *Radiat Res* 2000;153:196–200.
- [19] Le Caër S. Water Radiolysis: Influence of Oxide Surfaces on H₂ Production under Ionizing Radiation. *Water* 2011;3:235–53.
- [20] Wusylko A, Freed R, Brandt J-M, Turgeon T, Kornev K, Harman M. Comparison Between Surface Roughness and Wettability on Retrieved Metal and Ceramic Femoral Heads. *Soc Biomater* 2014.
- [21] Puleo D. Biochemical surface modification of Co-Cr-Mo. *Biomaterials* 1996;17:217–22.
- [22] Roba M. Interaction of Synovial Fluid Components with Artificial Hip-Joint Materials. ETH Zurich, 2009.
- [23] Pan N, Gibson P, Lukas D, Zhong W, Rengsamy RS, Ghaddar N, et al. Thermal and Moisture Transport in Fibrous Materials. Cambridge, England: Woodhead Publishing Limited; 2006.
- [24] Neumann AW, David R, Zuo Y. Applied Surface Thermodynamics, Second Edition. CRC Press; 2010.
- [25] Extrand CW, Moon SI. Contact angles on spherical surfaces. *Langmuir* 2008;24:9470–3.
- [26] Aquino KA da S. Sterilization by Gamma Irradiation. *Gamma Radiat. Prof. Feri, InTech*; 2012, p. 171–206.
- [27] Paur H-R. Decomposition of volatile organic compounds and polycyclic aromatic hydrocarbons in industrial off gas by electron beam—a review. *Int Symp Radiat Technol Conserv Environ- Ment Zakopane, Poland, Sept 1997* 1997:1–17.
- [28] Hanawa T, Hiromoto S, Asami K. Characterization of the surface oxide film of a Co-Cr-Mo alloy after being located in quasi-biological environments using XPS. *Appl Surf Sci* 2001;183:68–75.
- [29] McCafferty E, Wightman JP. Determination of the concentration of surface hydroxyl groups on metal oxide films by a quantitative XPS method. *Surf Interface Anal* 1998;26:549–64.
- [30] Tsyganenko AA, Mardilovich PP. Structure of alumina surfaces. *J Chem Soc Faraday Trans* 1996;92:4843.
- [31] Redfern SE, Grimes RW, Rawlings RD. The hydroxylation of t-ZrO₂ surfaces. *J Mater Chem* 2001;11:449–55.
- [32] Grassian VH. Surface science of complex environmental interfaces: Oxide and carbonate surfaces in dynamic equilibrium with water vapor. *Surf Sci* 2008;602:2955–62.
- [33] Rubasinghe G, Grassian VH. Role(s) of adsorbed water in the surface chemistry of environmental interfaces. *Chem Commun (Camb)* 2013;49:3071–94.
- [34] Tadorelli M. Cleaning and surface properties. *Prep. Vac. Accel. Spec. Course Cern Accel. Sch.*, 2006, p. 321–40.
- [35] Scheuerlein C, Tadorelli M. The assessment of metal surface cleanliness by XPS. *Appl Surf Sci* 2006;252:4279–88.

4

EFFECT OF SURFACE CHEMISTRY

Direct silanization of zirconia for increased biointegration

Contents

4.1 Introduction.....	93
4.2 Materials and methods.....	96
4.2.1 Surface characterization.....	97
4.2.2 Mechanical testing	98
4.2.3 Aging kinetics	98
4.2.4 Cellular tests.....	98
4.2.5 Statistical tests.....	99
4.3 Results.....	100
4.3.1 Surface Characterization	100
4.3.2 Mechanical testing	105
4.3.3 Aging kinetics	106
4.3.4 Cellular tests.....	107
4.4 Discussion	109
4.4.1 Surface characterization.....	109
4.4.2 Mechanical testing	112
4.4.3 Aging kinetics	112
4.4.4 Cellular tests.....	112
4.5 Conclusions	115
Bibliography	116

4.1 Introduction

The global medical ceramics market is projected to be worth USD 16.3 Billion by 2020, registering an expected mean annual growth rate of 6.4% between 2015 and 2020 [1]. Among the medical materials, structural ceramics, such as zirconia, are projected to be the largest and fastest-growing type of medical ceramics between 2015 and 2020, as the demand in end-use applications is growing rapidly [1]. Typical applications of these materials are dental and orthopedic bone-substitution implants. In these cases, materials are required to withstand high loads and fatigue, as well as resisting any degradative or corrosive attack by physiological fluids. Furthermore the implant should not alter the composition of tissues or plasma during their life-time [2].

These materials are considered as 'biologically inert'. This means that when implanted, they do not initiate any negative reaction to surrounding biological tissue. However, this feature also hampers osseointegration: since bone cannot naturally grow on their surface [3], other means of fixation are necessary, such as cements or metallic shells. One typical strategy to improve a direct fixation of ceramic to bone is to add roughness to the surface at different scales [4–6]. This not only helps implant fixation through mechanical interlocking mechanisms, it also promotes bone ingrowth and a more natural way of osseointegration [7]. However, not all kinds of roughness have the same effect [4], and its true key parameters are still under debate [6]. Increasing the roughness of ceramic implants appears as promising and it is already developed at a clinical level, especially for dental implants [8,9]. However, even if it is overall positive, the main issue with roughening a surface is twofold: on the one hand it can decrease the mechanical properties of the implant [10–12] especially as far as ceramics are concerned, and on the other it can provide the perfect host substrate for bacterial adhesion and biofilm formation [13].

A way to avoid this is to control the chemical interaction of proteins and cells with the substrate. Since the conception of Self-Assembled Monolayer (SAM) in 1946 by Zisman [14], chemists have developed different techniques of surface modification based on the molecular adsorption and self-organization of molecules on the surface. These molecules typically present a "tail" that binds to substrate, a "body" that is usually hydrocarbonated, and a "head", which is pointing away from the substrate and left free to interact with the environment. The body can present variable length. Chemists wield a fine control of the chemistry of the new surface by carefully tailoring head, body and tail groups of the constituent SAM molecules to the specific needs. One of the techniques encompassed in surface modification through SAMs is silanization. It uses organofunctional alkoxy silanes as the adsorbing molecules and it requires the presence of hydroxyl groups (OH) on the substrate, which typically is silica. The formation of the bond is schematically described in **Figure 4.1**.

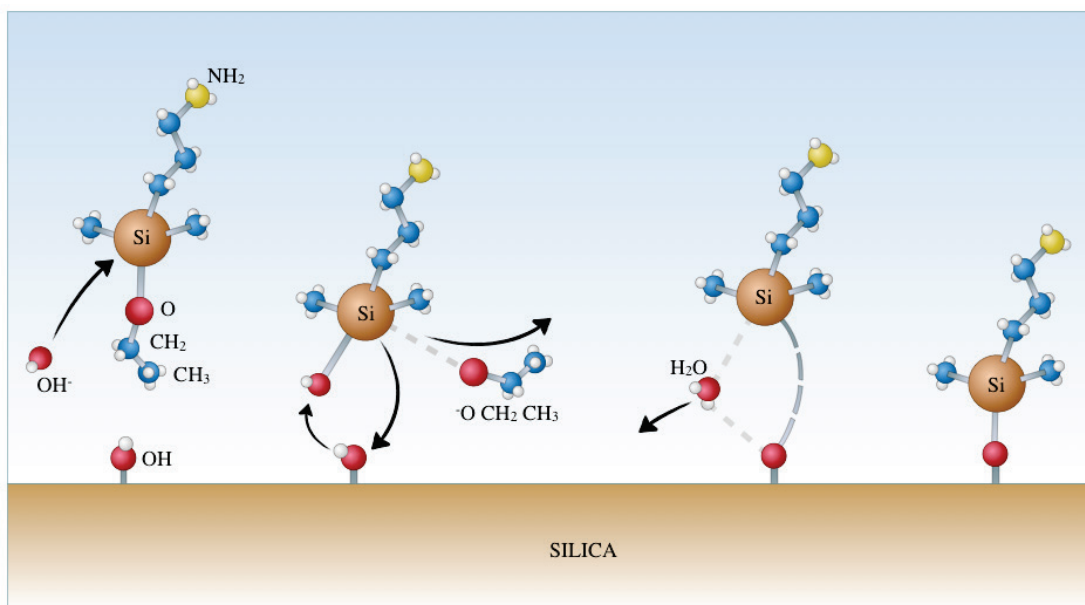


Figure 4.1. Schematic representation of silanization of silica.

The ability of silanization to modify the chemistry of the surface exhibits potential to be used in medical devices *in vivo*, as others have suggested [15–20]. The scale difference between molecules and cells implies that the biological environment is only concerned by the head group of the assembly. Thus the density should be high enough to ‘mask’ the substrate. By comparing carboxyl and methyl as head group, researchers observed high cell adhesion and growth on carboxyl-terminated SAM, while on those methyl-terminated cells exhibited rounded and clustered morphology, and in general poor adhesion capabilities [21–23]. Others have used amine-terminated SAMs on silica or gold as substrate, and compared them with carboxyl, methyl, hydroxyl and other groups (*e.g.* PEG or vinyl) [24–29]. They found that amine and carboxyl groups promote cell adhesion and spreading in contrast to methyl and hydroxyl, and regardless of the substrate (silica or gold) [24–29]. Additionally, researchers have investigated calcium phosphate nucleation and precipitation on these SAMs. They obtained dense and uniform precipitates after seven days, thereby supporting the possibility to be used as substrate for bone tissue [30]. The adduced precipitation mechanism consisted in an initial nucleation of the Ca²⁺ ions the surface, followed by the adsorption of the phosphate ions.

The use of silanes for oxide modifications is widely reported [31–33]. However on biological studies it is mostly limited to silica, although attempts have been made on other substrates such as titanium or alumina [26,34–37]. To our knowledge, there was only one study reporting the silanization on zirconia particles for chromatographic applications [38]. The main disadvantage of zirconia versus silica is the lower density of surface OH. In order to silanize a surface, silanes need to interact with the OH on the substrate and use them as anchor points. A possible strategy is the coating of zirconia by a silica layer similarly to the work of Schickle *et al.* [36,37]. They coated their initial alumina substrate with silica through Physical Vapor Deposition (PVD). While PVD allows thin depositions, in this case the stability of the SAM relies upon the ability of such coating to remain attached to the material. The use of SAMs on implants to

improve osseointegration necessitates a stable and permanent attachment. In this work, we were therefore willing to explore the direct silanization of zirconia with the use of O₂ plasma to promote hydroxylation of the surface both through ion implantation and through exposure to ambient moisture and water immersion.

Zirconia materials for biomedical applications are typically designed to exploit a natural toughening mechanism present within its structure, known as “transformation toughening”: metastable tetragonal grains retained after sintering can transform to the more stable monoclinic phase when mechanically solicited. The transformation is accompanied by a volume expansion due to the structural change, generating compressive stresses that hinder crack propagation. However, this becomes as well their main disadvantage because the same transformation can be triggered by the presence of water, through a nucleation and growth mechanism [39]. This process is referred to as “hydrothermal aging”, “Low Temperature Degradation (LTD)” or simply “aging”. Although LTD can be mitigated thanks to the advance development of new formulations to stabilize the structure, a modification such as the one presented in this paper could influence somehow its resistance to LTD, and this needed to be evaluated.

Therefore, in this work we aimed at developing a method to allow direct silanization on zirconia without the need of coatings. For this, we attempted silanization on polished and plasma-cleaned samples of zirconia. The samples were characterized, mechanically tested and their resistance to LTD was analyzed to check for changes related to the modification. Finally, functionalized zirconia was evaluated for osteoblast cell growth.

4.2 Materials and methods

Sintered discs of medical grade Ytria-stabilized Tetragonal Zirconia Polycrystal (Y-TZP) Nacera® Pearl were bought from DOCERAM (MOESCHTER Group, Dortmund, Germany) (**Table 4.1**) measuring $\varnothing 20$ mm and 1 mm thickness. The samples were obtained by conventional ceramic technology (cold isostatic pressing, followed by sintering at 1550°C for 2 hours, to achieve more than 99% of theoretical density). They were all polished in an automatic polishing machine up to 1 μm of diamond suspension prior to any treatment or test.

Table 4.1. Properties of zirconia samples as provided by the manufacturer

Composition (wt%)	ZrO ₂	92.5
	Y ₂ O ₃	5.5
	HfO ₂	1.9
	Other oxides	0.1
Bulk Density (g/cm ³)	6.05	
Color	White	
Fracture toughness, K_{Ic} (MPa·m ^{1/2})	8.0	
Young's Modulus (GPa)	205	
Vickers Hardness HV 0.5	1300	

Three types of samples were prepared, summarized in **Table 4.2**. After polishing, the samples for PC, PC H2O and PCS series were first ultrasonic-cleaned in isopropanol and afterwards subjected to plasma cleaning using O₂. Only the polished face of each sample was plasma-cleaned. We used a NGP 80 Reactive Ion Etching system (Oxford Instruments, UK) to generate the O₂ plasma of 100 W for 5 min, under 100 mTorr of vacuum pressure. The plasma power and chamber vacuum were selected to ensure the quality and stability of plasma during the cleaning. Regarding the duration of the treatment, De Ridder *et al.* [40] studied the cleaning effect of atomic oxygen and acknowledged that treatments longer than 5 min did not lead to a cleaner surface.

Since the hydroxylation of the surface would happen upon the exposure to ambient moisture, we hypothesized that we could increase the rate of hydroxylation by immersing the samples in deionized (DI) water, immediately after plasma cleaning. Thus, we took fresh PC samples and immersed them in DI water for 4 hours, and we labeled the group as "PC H2O".

Table 4.2. Type of samples studied

Series label	Description
NT	Polished
PC	Polished + Plasma Cleaned
PC H2O	Exactly as PC but kept in DI water for 4h.
PCS	Polished + Plasma Cleaned + Silanization

Prior to silanization, all glass and Teflon® equipment was washed with fresh Piranha solution (H₂SO₄/H₂O₂, 7:3, v/v) for 10 min, rinsed with DI water and dried at 110° C. To ensure absence of water in the environment, the plasma cleaned samples for PCS group were placed inside the reactor and left for 2h under a stream of dry N₂ at 147° C. The silanization was performed under controlled conditions in pentane, dried with molecular sieves. Amino propyl dimethyl ethoxysilane (APDMES) was added to pentane, to a final concentration between 0.06% and 0.6% (v/v) and allowed to react at room temperature under stirring for 1 h. Pentane was later evaporated, and the reaction was allowed to proceed under nitrogen stream at 150° C overnight. The silanized samples were then rinsed with pentane, tetrahydrofuran, and dichloromethane in an ultrasonic bath for 10 min each. Finally, the samples were stored in a desiccator at low vacuum for further use.

4.2.1 Surface characterization

We performed X-ray Photoelectron Spectroscopy (XPS) analysis on the three types of surfaces to study the effect of the plasma on PC series and the state of silanization on PCS series. The analysis was done in an AXIS Ultra DLD (Kratos Analytical, UK) using a monochromatic Al source (1486.6 eV) and operated using hybrid lens, slot aperture and a pass-energy of 20 eV for regional scans and 160 eV for the survey scan. Charge neutralization was used at default parameters. In all analysis, the angle of the beam was fixed at 90°. Additional analysis at 40° was performed on PCS samples to increase the sensitivity to the species on the surface. In all cases, the binding energies of all peaks were referenced to Zr3d5/2, fixed at 182.2 eV corresponding to a ZrO₂ [41]. The atomic percentages of each component were calculated and corrected using the XPS sensitivity factors provided by the manufacturer. Furthermore, since the surfaces of PC H2O were transported in DI water, they were dried under a stream of dry N₂ gas before placing them in the sample holder.

In parallel, we estimated the density of aminosilanes attached to the surface by means of the modified ADECA method (amino density estimation by colorimetric Assay)[42–44]. The principle of this method is based on three steps: staining, washing and detection. Three solutions were prepared: Two solutions (T1 and T3) and a staining solution (S2) containing Coomassie Brilliant Blue (CBB) colorimetric reagent. T1 contained 100 mL of methanol, 50 mL of acetic acid and 850 mL of DI water. S2 was prepared by dissolving 25 mg of CBB in 25 mL of acetic acid, 50 mL of methanol and DI water to a final volume of 500 mL. Finally, T3 contained 50 mL of 1M ammonia buffer and 50 mL of methanol.

First, the aminated surfaces were protonated in solution T1 for 10 min, and immediately immersed in S2 solution for 15 min. Each CBB molecule forms a complex with each N⁺, such as the one in each amine groups. Once the immobilized aminated layer was stained, the CBB was washed off the surface by immersion under stirring for three times in T1 during 10 min and then another 10 min in DI water. After drying under a stream of nitrogen gas, the samples

were transferred into solution T3 for 5 min under stirring, and this solution was collected and quantified by the Beer-Lambert law at 611 nm. For comparisons, we used a fresh PC sample as the negative control.

Static contact angle measurements were used as quality control on NT, PC and PCS, using DI water as the contact liquid. The samples of NT and PCS were cleaned using ethanol and DI water, and dried using a stream of nitrogen gas. The PC samples were tested right after plasma without further cleaning. The measurements were performed in a goniometer (Digidrop goniometer, GBX, France), and the images were analyzed using Windrop++ software. All measurements were performed the same day using 1 μL as the drop volume and within ten seconds after drop deposition.

4.2.2 Mechanical testing

To study the effect of the treatment on the mechanical performance, 15 treated and untreated discs were tested by 3-ball-on-3-ball biaxial bending on a universal testing machine. The used setup followed the guidelines presented by Fett *et al* [45]. Between the two possible configurations of the test, we selected the one where the loading and supporting spheres are in line. Hence, we used the following expression to calculate the maximum stress:

$$\sigma_{max} = \frac{F}{t^2} 0.656 \left(\frac{t}{R_1}\right)^{-0.196} + 0.274 \left(\frac{t}{R_1}\right)^{-0.448} \nu \quad (1)$$

where F is the load on failure, t represents the thickness of the sample, R_1 is the radius of the loading spheres location circle and ν is the Poisson's ratio.

4.2.3 Aging kinetics

LTD was studied through accelerated aging tests in autoclave at 134° C and under 2 bars steam pressure. Through X-Ray Diffraction (Rigaku D/Max-B, Cu $\text{KL}_{2,3}$ radiations), we evaluated the relative amount of monoclinic and tetragonal phase. Afterwards, we compared the areas of the corresponding peaks for the tetragonal (t_{101}) and monoclinic phase (m_{111} and -111) and calculated the relative volume content by making use of Garvie-Nicholson equation, modified by Toraya.

4.2.4 Cellular tests

We tested the proliferation rate and the adhesion response of osteoblasts (MG-63, American Type Culture Collection, USA) by culturing them over NT and PCS surfaces. The MG-63 cell line is composed of osteoblastic cells originally isolated

from a human osteosarcoma. The culture was done in the presence of RPMI 1640 medium (L-glutamine stable red phenol), with 10% of fetal bovine serum and 5% of antibiotics. The evaluation was carried out using the PrestoBlue® reagent: the blue non-fluorescent dye is rapidly taken up by cells, and reduced by the mitochondrial metabolic activity inside the cells. The by-product is a red-fluorescent dye. We then measured the fluorescence in a fluorimeter INFINITE PRO 200 (Tecan, Switzerland) to infer the cell proliferation.

The adhesion response was studied qualitatively through Scanning Electron Microscopy (SEM) by focusing on the cell morphology. For this, the cells were fixed with glutaraldehyde and progressively dehydrated by ethanol, followed by a gold/palladium plasma coating.

Three time-points were selected: 3, 6 and 10 days, and three samples per series were tested at each time-point. Blank reference consisted of 10%vol. PrestoBlue reagent in RPMI 1640 medium, and it was used to correct fluorescent values of the samples. Additionally, for each sample, a plastic control (cell culture-treated polystyrene) was included to verify the correct behavior of cells, and it was referred to as “Reference”.

4.2.5 Statistical tests

The data obtained in the mechanical tests was studied through Weibull statistics by fitting it to:

$$P(\sigma) = 1 - \exp\left(-\left(\frac{\sigma}{\sigma_0}\right)^m\right) \quad (2)$$

where P is the probability of failure, σ the applied stress, σ_0 the distribution central value and m the Weibull modulus. We adjusted the sample population to ten samples per condition and material. The probability of failure is evaluated by the ranking approach given by:

$$P = \frac{i-0.5}{N} \quad (3)$$

where N is the number of specimens, and i is the ranking from 1 to N . P is associated to the corresponding σ by ordering the failure data from the smallest to the largest. The distributions are linearized and plotted in logarithmic scales.

On both mechanical and cellular tests, we carried out statistical tests using t-test and a confidence interval of 5% ($\alpha=0.05$) to discuss the significance of results. Additionally, the error bars accompanying plots represent two times the standard deviation.

4.3 Results

4.3.1 Surface Characterization

The atomic percentages of each element are presented in **Table 4.3**.

Table 4.3. Atomic percentages of species on surface obtained by XPS analysis

Sample	Zr	O	Y	C	F	N	Si	Na	S
NT	17.6	47.1	1.2	33.8	-	-	-	0.4	-
PC	21.4	36.3	3.7	14.7	24.0	-	-	-	-
PC H ₂ O	16.4	38.2	1.1	38.2	3	-	-	0.3	1.8
PCS ($\theta=90^\circ$)	18.6	44.6	1.8	25.5	7.7	0.7	1.1	-	-
PCS ($\theta=40^\circ$)	16.6	40.1	1.7	32.4	6.9	0.9	1.3	-	-

Regional scans are presented in **Figure 4.2** through **Figure 4.8**.

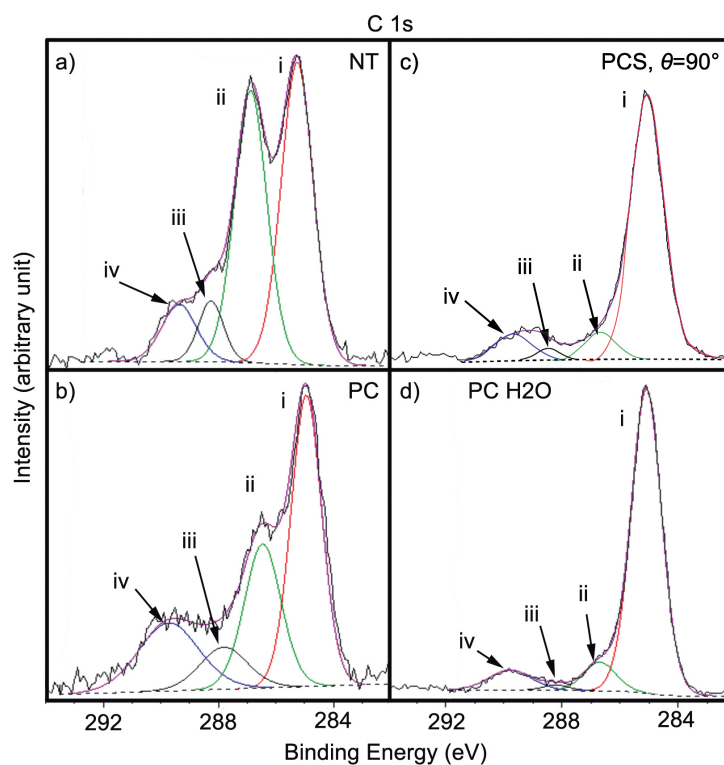


Figure 4.2. XPS spectra corresponding to the C 1s region of NT (a), PC (b), PCS $\theta=90^\circ$ (c), and PC H₂O (d). Deconvoluted peaks are: (i) C-C or C-H type, (ii) C-O type, (iii) O-C-O or C=O type, and (iv) CO₃ type.

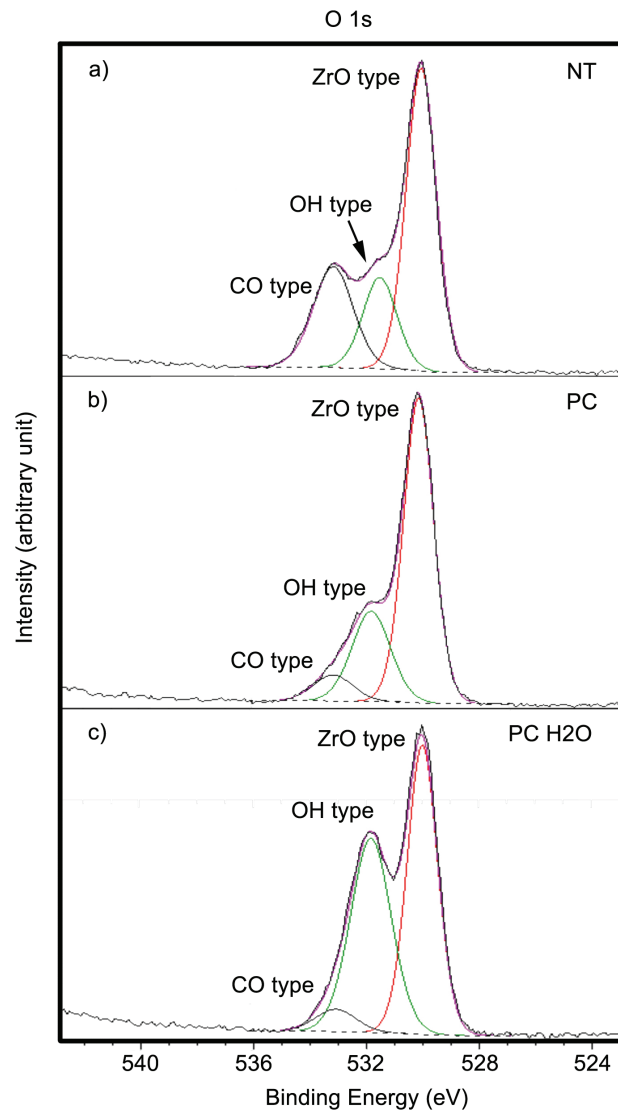


Figure 4.3. XPS spectra corresponding to the O 1s region of NT (a), PC (b) and PC H₂O (c).

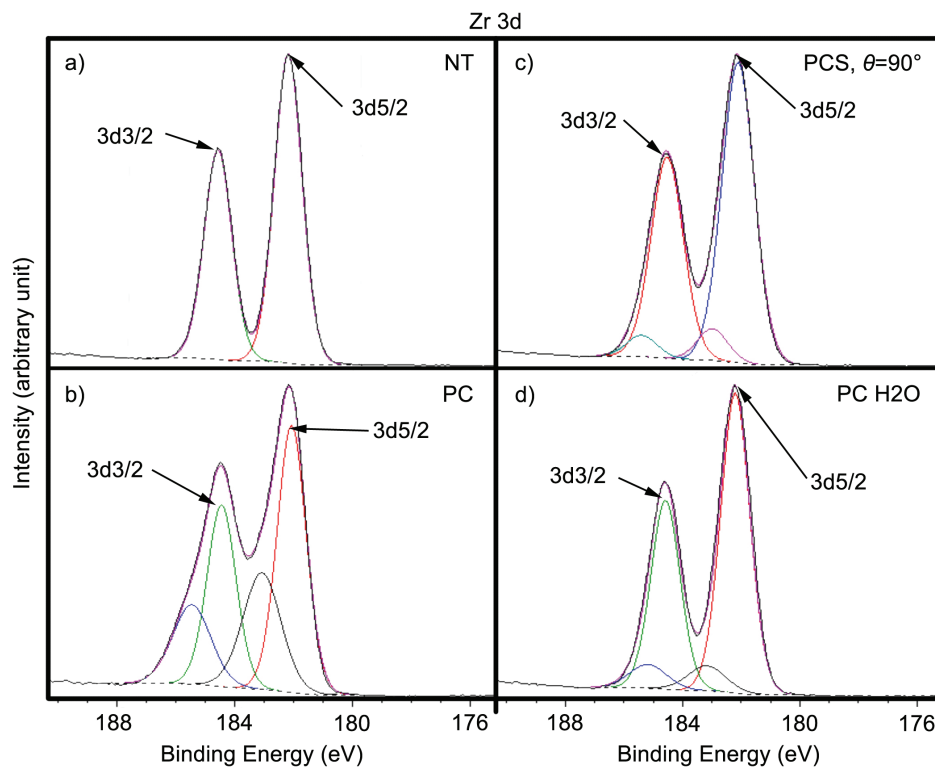


Figure 4.4. XPS spectra corresponding to the Zr 3d region of NT (a), PC (b), PCS $\theta=90^\circ$ (c), and PC H2O (d).

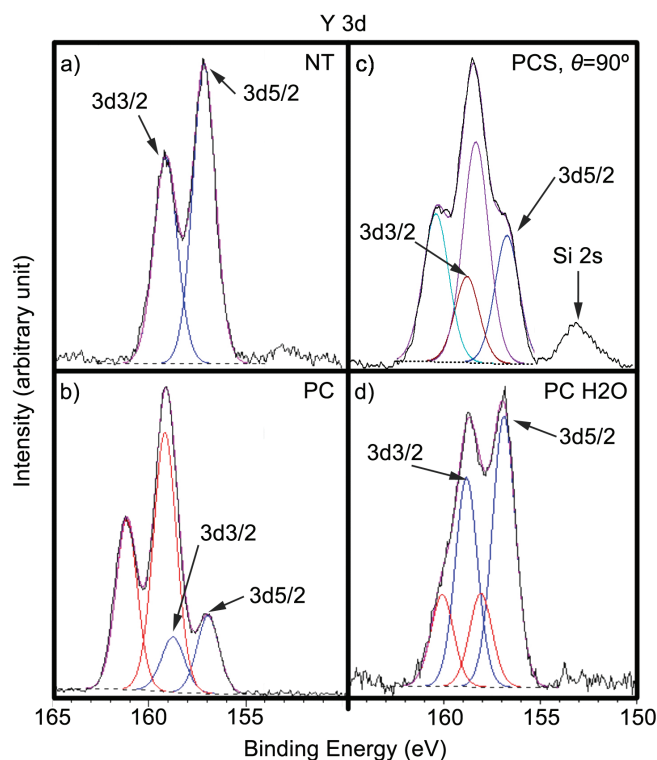


Figure 4.5. XPS spectra corresponding to the Y 3d region of NT (a), PC (b), PCS $\theta=90^\circ$ (c), and PC H2O (d). Additionally, in (c) the corresponding peak to Si 2s is comprised.

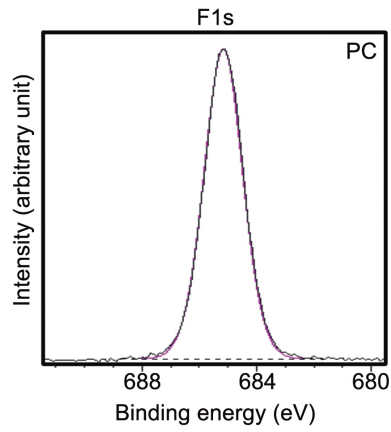


Figure 4.6. XPS spectrum corresponding to the F 1s region of PC.

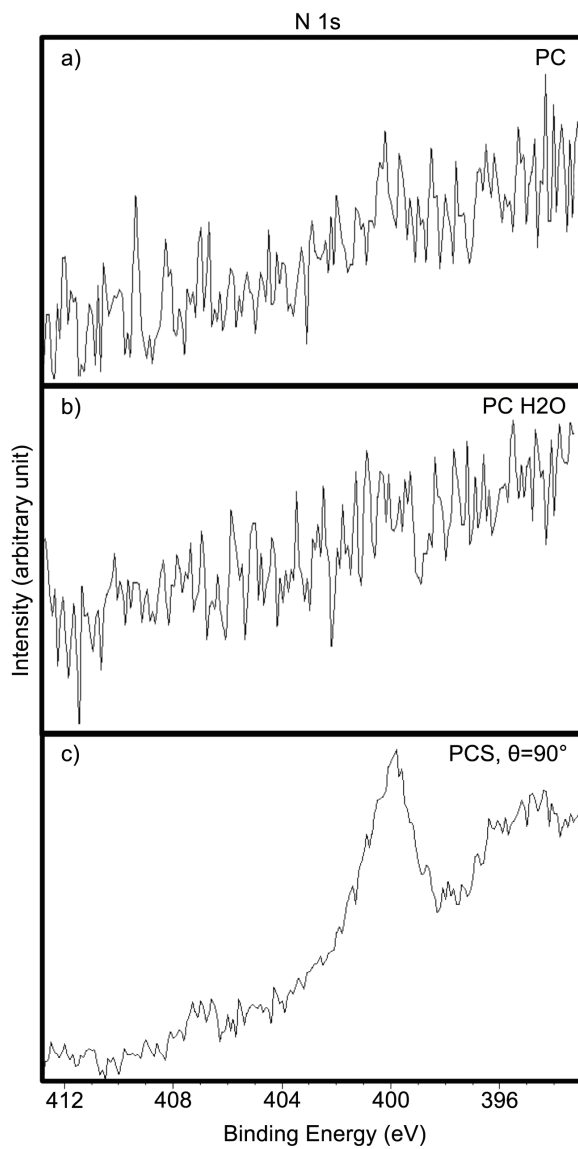


Figure 4.7. XPS spectra corresponding to the N 1s region of (a) PC, (b) PC H₂O and (c) PCS $\theta=90^\circ$.

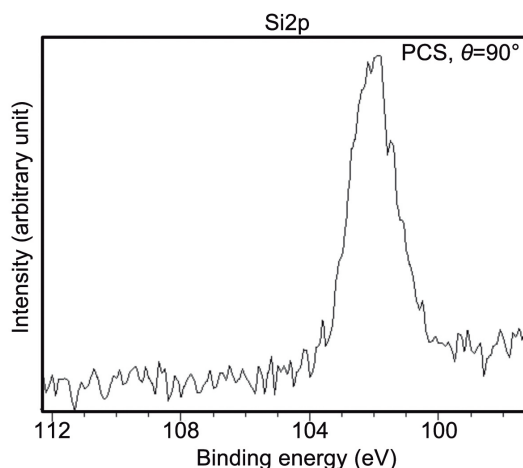


Figure 4.8. XPS spectra corresponding to the Si 2p region of PCS $\theta=90^\circ$.

Important Fluorine concentrations were found in PC, and were still present in PCS, while NT materials were free of it. The chemical shift was the same in all samples where F was detected. It confirmed its fluoride state and the binding energy matched the expected one for Zr-F and/or Y-F bonds [46–48]. The F 1s spectrum of PC is provided as an example in **Figure 4.6**. Its source can certainly be tracked down to the plasma reactor, given that the instrument is operated by multiple users using different gases including SF₆. However, the chamber is regularly cleaned after each operation using intense cleaning protocols (at least one hour long) using plasma of oxygen and nitrogen, and the presence of this element was neither wanted nor expected.

Analysis of PC material by XPS showed a decrease in the Carbon content after plasma and no increase of Oxygen related to OH in the surface. Four peaks were identified. Three of them (type i, ii, and iii) were respectively associated to C-C/C-H, C-O, O-C-O/C=O bonds. The fourth one (type iv) can either be interpreted as carbonate [49,50] or C-F bonds [51,52]. Since the F1s peak is located between 684 and 686 eV (**Figure 4.6**), these energies are incompatible with a C-F bond as they usually are presented at 689 eV and above [53,54]. Hence the “type iv” peak in **Figure 4.2** was interpreted as carbonate. Additionally, we found that after plasma, the two peaks corresponding to the Zirconium and Yttrium 3d orbitals (5/2 and 3/2) split into another two (**Figure 4.4** and **Figure 4.5**). This effect was also present in PCS samples, but the peaks showed a lower intensity.

After silanization, **Figure 4.7c** confirms the presence of N at energies compatible with amine-carbon binding [55,56]. XPS analysis also detected Si, and the peaks can be observed in **Figure 4.5c** for Si2s, and **Figure 4.8** for Si2p. The binding energies of both peaks were compatible with a organo-silicon involved in a siloxane bond [57,58], which would confirm a successful silanization of the surface. However, the N/Si ratio for S($\theta=90^\circ$) and S($\theta=40^\circ$) was of 0.63 and 0.69 respectively, and away from the theoretical 1 that would come from the 1:1 proportion of N and Si in the APDMES molecule. The estimation of density using the modified ADECA method yielded 8.55×10^{13} amino groups/cm² on a PCS sample after comparison with a freshly PC surface. This amount is slightly lower than APDMES on silica, which can yield up to 1.3×10^{14} amino groups/cm² [44].

Contact angle measurements are summarized in **Figure 4.9**. The contrast between series is evident, being NT the least wettable. PC exhibited a very low contact angle, but it increased after immersion in water for four hours. PCS samples presented a consistent contact angle value, in between NT and PC.

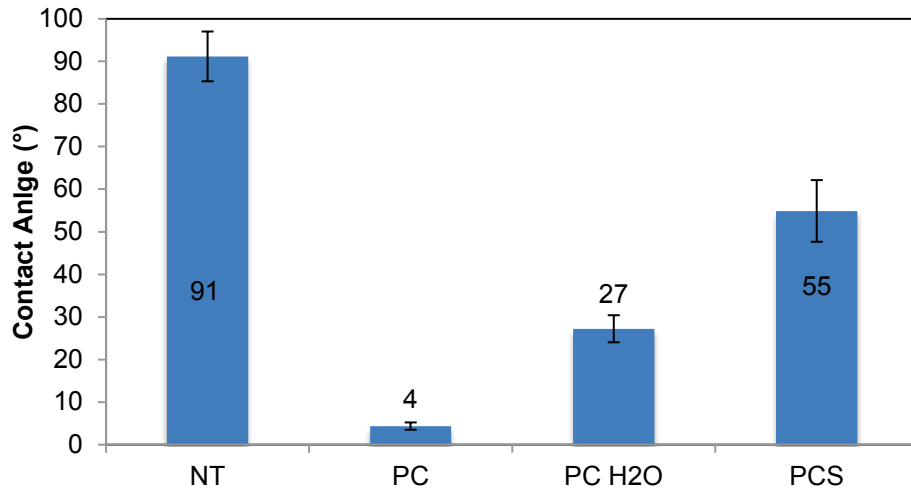


Figure 4.9. Contact angle measurements

4.3.2 Mechanical testing

Bending results are presented in **Figure 4.10** and **Table 4.4**. No apparent difference was found neither between the Weibull moduli, nor between the central values of distributions.

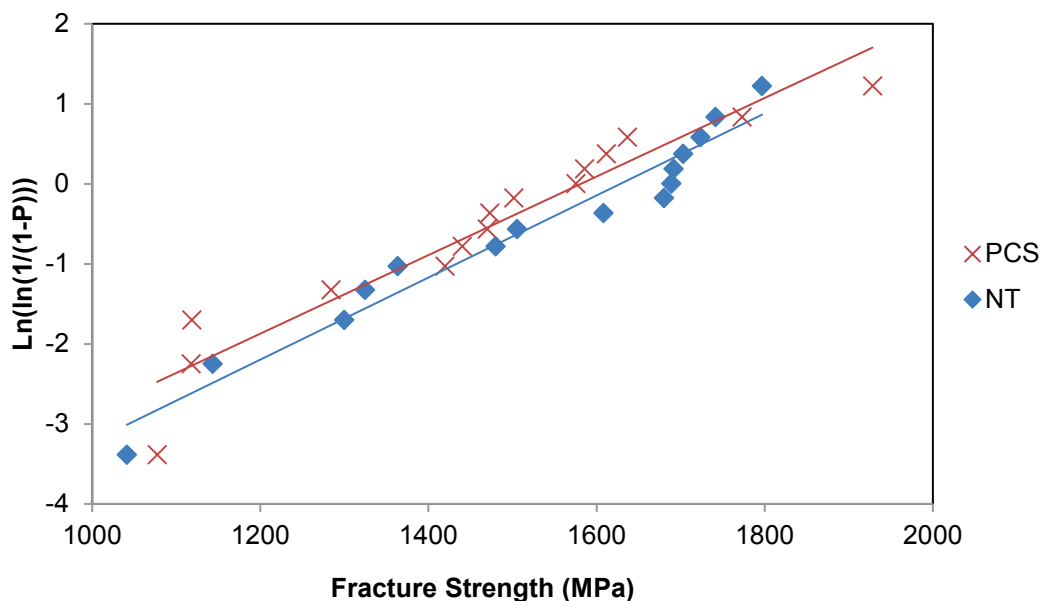


Figure 4.10. Mechanical tests: Biaxial bending test results presented in a Weibull plot.

Table 4.4. Summary of Weibull parameters obtained for each tested series.

Series	Central Value (MPa)	Weibull modulus
NT	1620	7.2
PCS	1568	7.0

4.3.3 Aging kinetics

Figure 4.11 shows monoclinic content versus accelerated aging time for each material. Initially only NT and PCS were studied. After analyzing the results, we decided to perform another test on PC samples, to investigate the causes of difference in behaviour between NT and PCS, and discern whether the effect was caused by the silanization or the plasma. Because the process is very time-consuming, we decided to focus on the interval 2 – 50 h. Results show two different behaviours: NT presents a faster increase in monoclinic content than PC or PCS, which display a very slight increase on the first 10 h of aging, a moderate one between 10 and 50 h and a large one from 50 h and up to saturation.

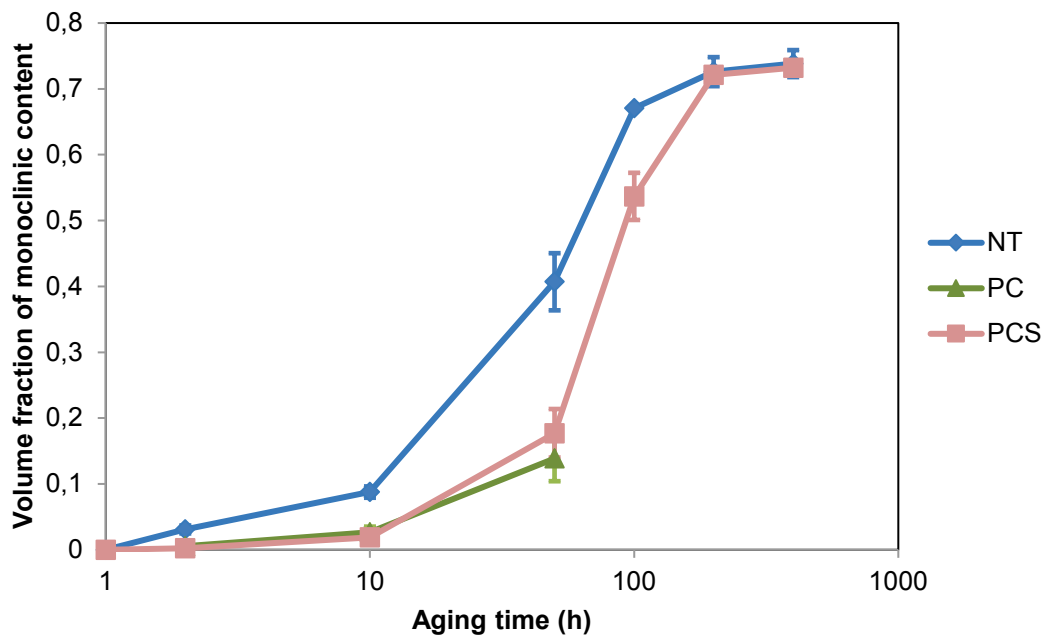


Figure 4.11. Aging kinetics: Evolution of monoclinic phase versus time in autoclave, after accelerated aging.

4.3.4 Cellular tests

Results of cell proliferation are summarized in **Figure 4.12**. Cell growth is visible on the two materials and along the experiments, proving that the chemical process did not modify in any way the proliferation of the studied cells and it had no toxic or adverse effect. No significant differences were found in the amount of cells at day 3 and 10 (t-test, $p > 0.05$ both), but at day 6, significantly higher number of cells (t-test, $p < 0.05$) was detected on PCS surface.

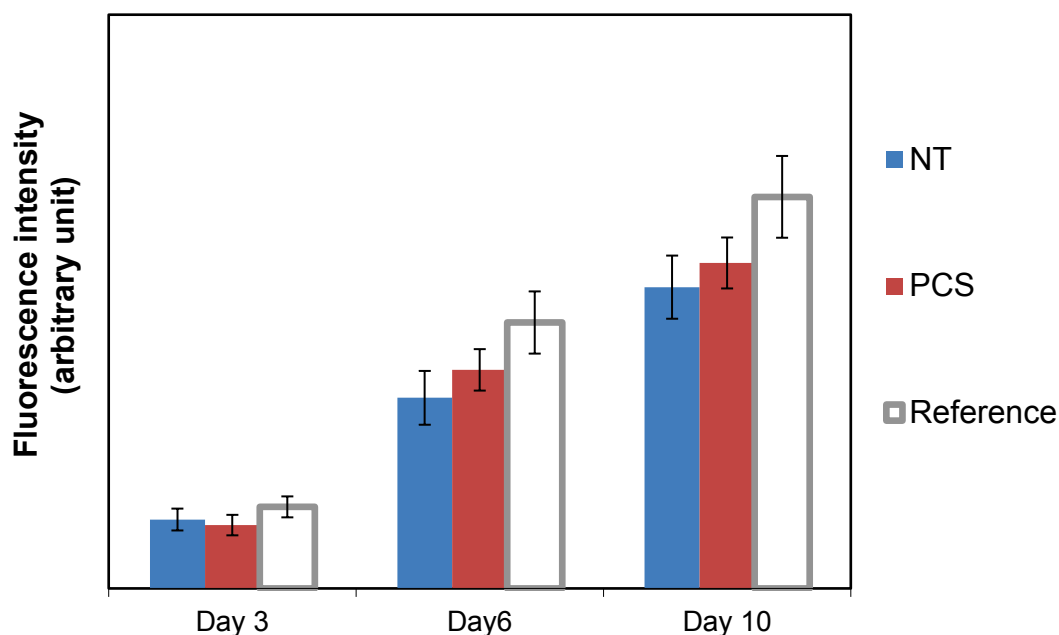


Figure 4.12. MG-63 proliferation averaged results of three series on NT and PCS samples and the reference (cell culture treated polystyrene).

Cell attachment, studied qualitatively through the SEM pictures, revealed an apparent higher affinity for the silanized surface after three days of culture (**Figure 4.13a** and **b**). Cells appeared highly spread in PCS, while in NT they presented a rounded form signifying a poorer cellular interaction with the surface. After six and ten days, both surfaces displayed well-spread attached cells, but density appeared higher on PCS. **Figure 4.13g** and **h** show details of the numerous inter-cell connections found at day 10.

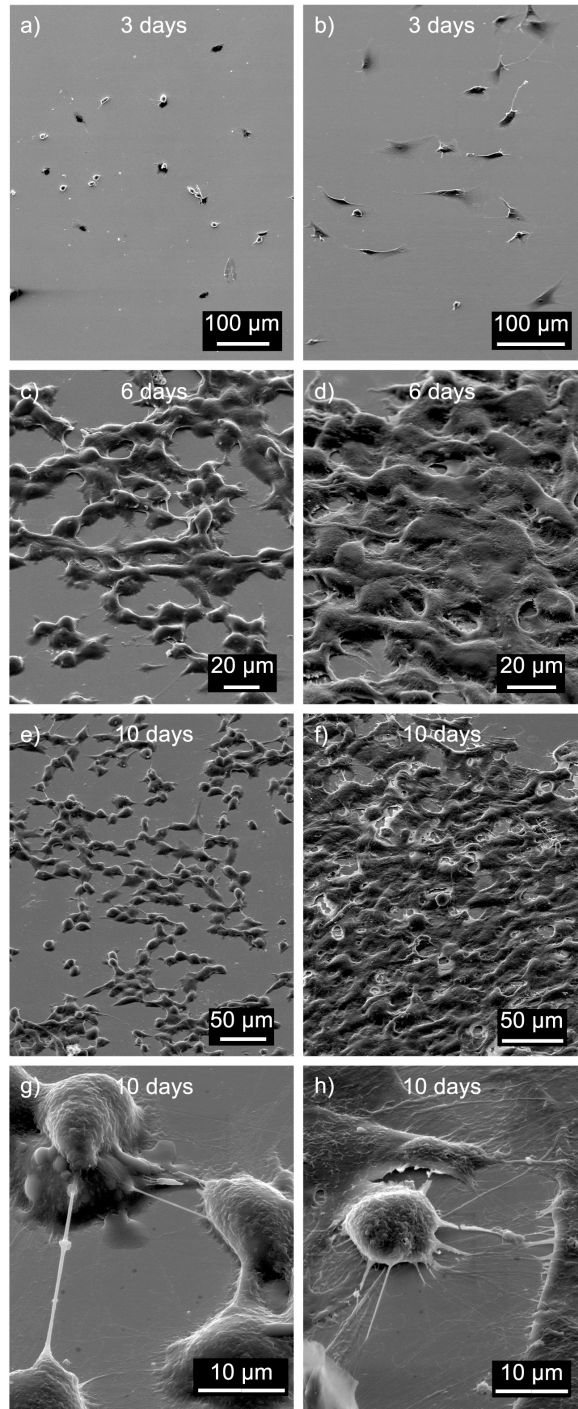


Figure 4.13. SEM images of NT (a, c, e, g) and PCS (b, d, f, h) on time-points 3, 6 and 10 days.

4.4 Discussion

4.4.1 Surface characterization

Plasma cleaning removed from the surface adsorbed species, mainly hydrocarbons, as observed in the levels of C in NT in respect to PC. **Figure 4.2a** and **b** show however a decrease mainly on the C-O type (labeled as “ii” in the plot) as well as a softer decrease on the C-C/C-H type (“i” in the plot). Immersing the PC samples in water (PC H₂O) resulted in an increase of C as well as the apparition of Na and S species. The origin of such contamination is uncertain to us, but it is reasonable to think that it may come as impurities in the immersion water. After silanization, C levels also rose, but this is linked to the fact that each APDMES molecule contains five atoms of C. The two methyl groups were expected to show a new peak below 285 eV, but no new peaks were found at PCS. Regarding the presence of Na and S species, it is clear that the immersion exposes the surface to uncontrolled contamination. Although we used DI water, the purity level was not enough and the surfaces adsorbed some of the present impurities and possibly the glassware contained residual pollution.

Figure 4.3b shows that oxygen content in PC samples is only reduced in the C-O type. No increase of O-H type was detected. However, keeping the plasma-cleaned samples in water for 4 hours did seem to increase the degree of hydroxylation of the surface, as shown by **Figure 4.3c**, which may be indicative of a chemisorbed monolayer of water in the form of OH groups coating the surface. All the same, even if the surfaces were dried under a stream of pure nitrogen gas, this increase in the O-H peak could still be caused by multilayers of physisorbed water that remained attached. Unfortunately, it would be very complicated to attempt to separate both signals, physisorbed and chemisorbed water, from the main peak. Alternatively, we can proceed by deduction: since XPS analysis was performed at 3×10^{-9} Torr of chamber pressure, there is little chances for a physisorbed layer of water to remain stable on the surface, given that the vapor pressure of water at 20° C is about 17.5 Torr. Redfern *et al.* [59] used theoretical simulations to study the hydroxylation of (100), (101) and (110) surfaces of tetragonal zirconia. According to them, the simulations predict the formation of a 50% covered monolayer on (100) and (110), while in the case of (101) no layer will form. The increment of OH presence between PC and PC H₂O could then be possibly explained by having different degrees of coverage on the favorable orientations.

Another noticeable change is the splitting of 3d_{3/2} and 3d_{5/2} peaks of Zr. This splitting is mostly evident after the plasma step. However, it fades away with the exposure of the surface to 4h immersion in water or to the silanization process. In Y peaks, a similar effect was observed with even higher intensity than in Zr. The same phenomenon was observed by Piascik *et al.* [60], where the authors attempted plasma of SF₆ as a way of promoting hydroxylation of Yttria-stabilized Zirconia. According to the authors, the peak splitting on the 3d orbital peak of Zr

is caused by the substitution of the Zr-O bonds with Zr-F bonds, in a competitive fluorination. The result is a glassy fluorozirconate phase of 2-3 nm and distributed non-uniformly across the surface. The formation of new 3d peaks are related to the difference in electronegativity between O and F, which shifts slightly the peak towards higher energy in the case of Zr-F. Those results are in line with what we observed in our materials, and the new peaks on Y and Zr spectra exhibited binding energies compatible with Y-F [48,61] and Zr-F bonds [46,47,62,63].

More intense peak splitting was observed on PC samples, where the F happened to be at maximum intensity. Interestingly, upon exposure to solvents, either water or the ones involved in the silanization process, both the levels of F and peak splitting were reduced to a minimum. A possible explanation to this was found in an old publication by Pantano and Brow [64], where the authors demonstrated the high solubility of fluorozirconates in aqueous environments. The dissolution of the glassy layer of fluorozirconate during the immersion in solvents would explain the disappearance of both F and the observed peak splitting phenomenon on Zr and Y.

The use of the modified ADECA method confirmed the presence of amino groups on PCS and provided an estimation of the molecule density (8.55×10^{13} per cm^2). Redfern *et al.* [59] estimated the OH density coverage of zirconia for the (100) and (110) family of planes at 6×10^{14} and 3×10^{14} OH-/ cm^2 respectively, assuming a 50% coverage, while their calculations gave no stable coverage on (101). If we assume that each APDMES is bonded to an OH group on the surface, the estimated APDMES density was about 25% the theoretical values of OH density provided by Redfern *et al.* assuming a randomly oriented grain distribution on the surface. However, given the speculative nature of these estimations, the main conclusion to be drawn is that APDMES density in PCS was lower than theoretically possible but still in the range.

Finally, contact angle measurements represent the result of the interaction between the environment, the liquid and the surface. Since the interaction takes place at the molecular scale, anything on top of the surface will modify the energy of the surface, including adsorbed carbon derivatives from the atmosphere [65–69]. In literature, all scientific evidence reviewed [67,70–73] pointed to the superhydrophilicity of metal oxides, such as zirconia. In their article, Preston *et al.* provided an interesting comparison of experimental data obtained from published results of contact angle as a function of surface atomic percent carbon. The plot is reproduced in **Figure 4.14**, and we included the points corresponding to NT, PC and PC H₂O to further illustrate the idea.

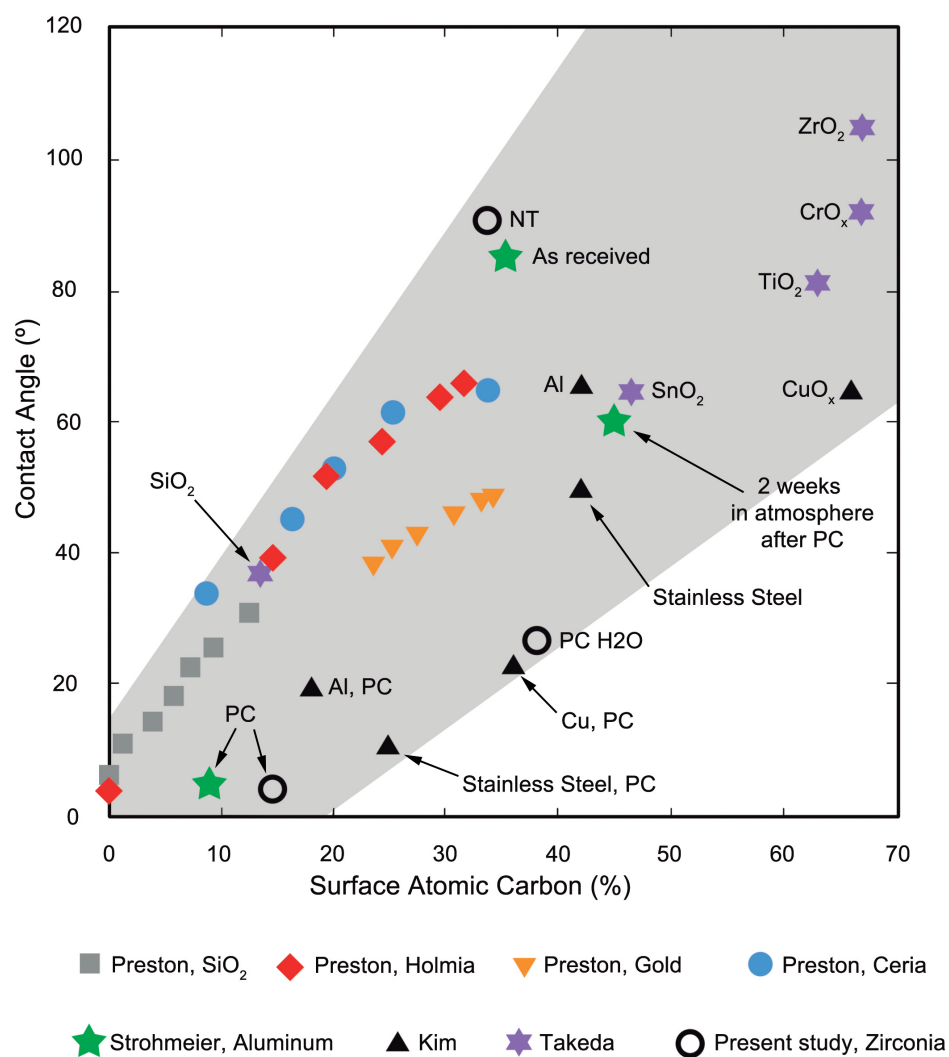


Figure 4.14. Comparison of experimental data from the present work to previously published results for equilibrium contact angle as a function of surface atomic carbon (Source: Preston et al., 2014; References: [67,70–72]).

High angles were expected on NT surfaces, given their exposure to organic solvents and atmospheric contamination. The low contact angle obtained for PC is representative of the clean state of the zirconia surface. Strohmeier [70] obtained very similar results for aluminum foil cleaned by oxygen plasma. However, comparisons of surface atomic carbon on surface should be done with care because these data points were taken by different research groups, at different moments in time, using different equipment, studying different materials (hence different penetration coefficients in XPS) and in different environmental conditions (which are known to affect wettability). PC H₂O exhibited a higher contact angle, and this can be correlated to the higher amount of C measured by XPS. Regarding PCS, the value was not represented in the plot of **Figure 4.14** because APDMES contains carbon atoms that shall not be considered as contamination. The contact angle for PCS averaged 55°, which is in the range of what other authors have reported for amine-terminated SAMs [26–

29,74,75]. Hence, these results of contact angle confirmed once again the presence of APDMES on PCS.

4.4.2 Mechanical testing

Biaxial bending tests appear clear: there is no significant difference between both distributions (t-test, $p > 0.05$). This proves that the chemical treatment, including the plasma-cleaning step, has no impact, neither on the population of defects, nor on the crack resistance of the ceramic.

4.4.3 Aging kinetics

Results of **Figure 4.11** show a clear effect of plasma cleaning on the aging kinetics of LTD on tested samples. However, little evidence was found in literature that could explain this phenomenon. Dos Santos *et al.* [76] attempted to study the aging performance of plasma cleaned zirconia. Although the procedure they used was very different to the one presented here, they used oxygen plasma as the last step, which would provide an equivalent state to PC. Still in their case, plasma cleaning had no obvious effect on ageing kinetics.

Rohnke *et al.* [77] suggested the possibility of oxygen reduction and emission under oxygen plasma on zirconia. If that is the case, a higher stability of tetragonal zirconia should be expected due to the creation of oxygen vacancies [78–80]. Alternatively, as seen in section 4.3.1 the plasma treatment introduced F in the surface. The formation of a non-uniformed layer of fluorozirconate [60] possibly protected the inner layers from the degradation, shielding the material against the nucleation and propagation of LTD until it is dissolved [64]. There is not enough evidence to support either of these hypotheses in our case, and so we can only leave it to speculation. In any case there is an undeniable positive shielding-effect of plasma that retarded degradation without affecting the bulk's mechanical properties.

4.4.4 Cellular tests

Although we do not have quantitative data on the cell affinity to each surface, cells appeared much spread on PCS after the first three days, which could be attributed to the amino groups on the surface. We suspect the amines could have allowed a higher adsorption of proteins or a more favorable configuration of them that helped cell attachment (such as fibronectin or vitronectin). As expressed previously [21,23,29,35,81] the surface has a chemical effect on protein adsorption, and that will also influence cell adhesion [21–23,29]. There are however, many aspects of protein adsorption that contribute to their affinity to a surface and their effect on cells [21,81]. If there are chemical differences

between zirconia and aminosilanized surfaces, they could be responsible for the different initial cell adhesion response through a different interaction with the medium proteins. According to Wang *et al.* [81], the electrostatic interactions between ceramics and proteins may take the dominant role. To qualitatively compare the net charge, we can make use of ζ -potential. The isoelectric point is defined as the pH at which the ζ -potential becomes zero. For both zirconia and aminosilanized surfaces, the isoelectric point was found to be higher than 7: close to pH 9 for zirconia [82–84], and closer to pH 10 for aminosilanized surfaces [85–88]. On top of that, both types of surface present a positive charge at pH 7. As reported by Wang *et al.*, a protein oppositely charged to the surface adsorbs much higher amounts than an equally charged surface. Given that both present electrical charges of the same sign, this means that if any, the differences between the two should come from the actual value of the charge.

Wang *et al.* described several other parameters as possible influences: surface roughness, surface reactivity or hydrophobicity. The initial samples were the same and they presented the same roughness; no surface reactivity is expected either in the way it is expected from bioactive glasses. Hence, among all of them, we can only consider hydrophobicity. The measurements of contact angle in **Figure 4.9** revealed the higher hydrophobicity of NT. Tidwell *et al.* [21] obtained high cell densities on functionalized surfaces of gold using a carboxylic group as the terminal group and after three days, the cells appeared well spread in contrast to what they obtained of methyl or acetyl terminated chains. They contended that the carboxyl-terminated surfaces presented a higher affinity to fibronectin, which helps cell adhesion, and a lower affinity to albumin. Although cell growth cannot be correlated with one single aspect of protein adsorption, their results point to the idea that higher affinity to albumin hinders cell adhesion. Arima *et al.* [28] observed a better adhesion of cells to amine and carboxyl-terminated SAMs than to methyl or hydroxyl-terminated ones, even on albumin-preadsorbed surfaces. They concluded that fibronectin and vitronectin were displacing the adsorbed albumin, following the mechanism described as “Vroman effect” [89].

Given the chemical similarities of both substrates, except hydrophobicity, one possible explanation to the difference after three days of culture could be a slightly higher affinity of fibronectin and vitronectin to amine-terminated surfaces than to zirconia (NT). While in both surfaces displacement of albumin is expected, on PCS it happened at a faster rate, allowing a richer interaction with cells than on NT. This should explain the density difference observed in **Figure 4.13** between left (NT) and right (PCS) columns. However, the evolution of cells on the NT surface shifts to resemble the one of PCS after 10 days. This could mean that the displacement of adhesion-blocking proteins eventually happens on NT, but later than PCS.

Alternatively, multiple works demonstrated the higher preference of albumin for hydrophobic surfaces [35,81,90,91]. This means that the higher hydrophobicity of NT would recruit more albumin to its surface. If we accept that the Vroman effect is governing the protein adsorption in this case, then NT surfaces would

have more albumin to displace, and hence it would take longer to present a friendlier surface for cell adhesion.

4.5 Conclusions

In the present work, we have proven the feasibility of directly silanizing the surface of zirconia using plasma cleaning as pretreatment. Our results open the window of a new generation of surface modification techniques that rely on the subtlety of the chemical interactions between the material and the biological agents, allowing increasing levels of complexity and higher control of the surface properties for tailoring them to the specific application needs. The main conclusions can be summarized as follows:

1. The silanization was a success, but it yielded slightly lower densities of APDMES on the modified surfaces of zirconia than on typical silica substrates.
2. Oxygen plasma as pre-treatment did not increase the amount of OH on the surface, but it helped cleaning it without physical damage. Hydroxylation of the surface through immersion in water seems feasible and displays potential to allow higher silane density. However risk of uncontrolled contamination limited our use of it. In future works, this strategy could be explored again, but putting special care on controlling the exposure to contamination.
3. We have discovered an important, initially unexpected, increase in the aging resistance of zirconia after plasma cleaning. Further research will have to be conducted to determine the real cause of such enhancement. The fortuitous involvement of unwanted fluorine from the plasma-cleaning step remains a question.
4. No adverse effect of silanization was found on the mechanical response of the treated samples. The modification techniques only took part on the surface, without creating critical surface defects or damaging anyhow the structure.
5. Cell tests showed that, despite the lower density of silanes compared to silanization on typical silica surfaces, it was sufficient to improve adhesion. The reason of this improvement was associated to a higher ability of the silanized surfaces to recruit proteins that help cell adhesion. On NT surface, the recruitment eventually happens, but at a slower speed than on PCS, providing a more favourable onset for the silanized surface.

Bibliography

- [1] Marketsandmarkets.com, Medical Ceramics Market by Material, by Application, and by Region - Global Forecast to 2020, 2016.
- [2] A. Ravaglioli, A. Krajewski, Bioceramics, Chapman & Hall, London, 1991.
- [3] M. Dehestani, L. Ilver, E. Adolfsson, Enhancing the bioactivity of zirconia and zirconia composites by surface modification., *J. Biomed. Mater. Res. B. Appl. Biomater.* 100 (2012) 832–40.
- [4] M. Gahlert, T. Gudehus, S. Eichhorn, E. Steinhauser, H. Kniha, W. Erhardt, Biomechanical and histomorphometric comparison between zirconia implants with varying surface textures and a titanium implant in the maxilla of miniature pigs., *Clin. Oral Implants Res.* 18 (2007) 662–8.
- [5] A. Wennerberg, The importance of surface roughness for implant incorporation, *Int. J. Mach. Tools Manuf.* 38 (1998) 657–662.
- [6] A. Wennerberg, T. Albrektsson, Suggested guidelines for the topographic evaluation of implant surfaces., *Int. J. Oral Maxillofac. Implants.* 15 (2000) 331–344.
- [7] F. Marco, F. Milena, G. Gianluca, O. Vittoria, Peri-implant osteogenesis in health and osteoporosis, *Micron.* 36 (2005) 630–644.
- [8] X. Oliva, J. Oliva, J.D. Oliva, H.S. Prasad, M.D. Rohrer, Osseointegration of Zirconia (Y-TZP) Dental Implants: A Histologic, Histomorphometric and Removal Torque Study in the Hip of Sheep, *Int. J. Oral Implantol. Clin. Res.* 4 (2013) 55.
- [9] R. Depprich, H. Zipprich, M. Ommerborn, C. Naujoks, H.-P. Wiesmann, S. Kiattavorncharoen, et al., Osseointegration of zirconia implants compared with titanium: an in vivo study., *Head Face Med.* 4 (2008) 30.
- [10] T. Kosmač, C. Oblak, P. Jevnikar, N. Funduk, L. Marion, The effect of surface grinding and sandblasting on flexural strength and reliability of Y-TZP zirconia ceramic, *Dent. Mater.* 15 (1999) 426–433.
- [11] T. Kosmač, C. Oblak, P. Jevnikar, N. Funduk, L. Marion, Strength and reliability of surface treated Y-TZP dental ceramics., *J. Biomed. Mater. Res.* 53 (2000) 304–313.
- [12] M. Guazzato, M. Albakry, L. Quach, M. V Swain, Influence of surface and heat treatments on the flexural strength of a glass-infiltrated alumina/zirconia-reinforced dental ceramic., *Dent. Mater.* 21 (2005) 454–463.
- [13] M. Gharechahi, H. Moosavi, M. Forghani, Effect of Surface Roughness and Materials Composition, *J. Biomater. Nanobiotechnol.* 03 (2012) 541–546.
- [14] A. Ulman, Formation and Structure of Self-Assembled Monolayers, *Chem. Rev.* 96 (1996) 1533–1554.
- [15] A. Mahapatro, Bio-Functional Nano-Coatings on Metallic Biomaterials, *Mater. Sci. Eng. C.* 55 (2015) 227–251.
- [16] F. Böke, K. Schickle, H. Fischer, Biological Activation of Inert Ceramics: Recent Advances Using Tailored Self-Assembled Monolayers on Implant Ceramic Surfaces, *Materials (Basel).* 7 (2014) 4473–4492.
- [17] Y. Arima, K. Kato, Y. Teramura, H. Iwata, Design of biointerfaces for regenerative medicine, in: S. Kunugi, T. Yamaoka (Eds.), *Polym. Nanomedicine*, Springer Berlin Heidelberg, Berlin, Heidelberg, 2012: pp. 167–200.
- [18] P. Colpo, A. Ruiz, L. Ceriotti, F. Rossi, Whole Cell Sensing Systems I: Reporter Cells and Devices, in: S. Belkin, B.M. Gu (Eds.), *Whole Cell Sens. Syst. I*, Springer Berlin Heidelberg, Berlin, Heidelberg, 2010: pp. 109–130.

- [19] K. Anselme, L. Ploux, A. Ponche, Cell/Material Interfaces: Influence of Surface Chemistry and Surface Topography on Cell Adhesion, *J. Adhes. Sci. Technol.* 24 (2010) 831–852.
- [20] T. Groth, Z.-M. Liu, M. Niepel, D. Peschel, K. Kirchhof, G. Altankov, et al., Chemical and Physical Modifications of Biomaterial Surfaces to Control Adhesion of Cells, in: P.V. Shastri, G. Altankov, A. Lendlein (Eds.), *Adv. Regen. Med. Role Nanotechnology, Eng. Princ. Role Nanotechnology, Eng. Princ.*, Springer Netherlands, Dordrecht, 2010: pp. 253–284.
- [21] C.D. Tidwell, S.I. Ertel, B.D. Ratner, B.J. Tarasevich, S. Atre, D.L. Allara, Endothelial Cell Growth and Protein Adsorption on Terminally Functionalized, Self-Assembled Monolayers of Alkanethiolates on Gold, *Langmuir.* 13 (1997) 3404–3413.
- [22] C.A. Scotchford, E. Cooper, G.J. Leggett, S. Downes, Growth of human osteoblast-like cells on alkanethiol on gold self-assembled monolayers: The effect of surface chemistry, *J. Biomed. Mater. Res.* 41 (1998) 431–442.
- [23] K.B. McClary, T. Ugarova, D.W. Grainger, Modulating fibroblast adhesion, spreading, and proliferation using self-assembled monolayer films of alkylthiolates on gold., *J. Biomed. Mater. Res.* 50 (2000) 428–39.
- [24] J. Li, T. Guan, C. Hao, L. Li, Y. Zhang, Effects of Self-Assembled Monolayers with Different Chemical Groups on Ovarian Cancer Cell Line Behavior In Vitro, *J. Chem.* 2015 (2015) 1–10.
- [25] Y. Arima, H. Iwata, Preferential adsorption of cell adhesive proteins from complex media on self-assembled monolayers and its effect on subsequent cell adhesion., *Acta Biomater.* 26 (2015) 72–81. doi:10.1016/j.actbio.2015.08.033.
- [26] A. Oliveros, C.L. Frewin, S.J. Schoell, M. Hoeb, M. Stutzmann, I.D. Sharp, et al., Assessment of cell proliferation on 6H-SiC biofunctionalized with self-assembled monolayers, *J. Mater. Res.* 28 (2012) 78–86.
- [27] H. Schweikl, R. Müller, C. Englert, K.-A. Hiller, R. Kujat, M. Nerlich, et al., Proliferation of osteoblasts and fibroblasts on model surfaces of varying roughness and surface chemistry., *J. Mater. Sci. Mater. Med.* 18 (2007) 1895–905.
- [28] Y. Arima, H. Iwata, Effects of surface functional groups on protein adsorption and subsequent cell adhesion using self-assembled monolayers, *J. Mater. Chem.* 17 (2007) 4079.
- [29] N. Faucheux, R. Schweiss, K. Lützow, C. Werner, T. Groth, Self-assembled monolayers with different terminating groups as model substrates for cell adhesion studies., *Biomaterials.* 25 (2004) 2721–30.
- [30] G.K. Toworfe, R.J. Composto, I.M. Shapiro, P. Ducheyne, Nucleation and growth of calcium phosphate on amine-, carboxyl- and hydroxyl-silane self-assembled monolayers, *Biomaterials.* 27 (2006) 631–642.
- [31] J.A. Schwarz, C.I. Contescu, *Surfaces of Nanoparticles and Porous Materials*, CRC Press, 1999.
- [32] U.A.T. Brinkman, A.E. Bruno, A.L. Burlingame, *TRAC: Trends in Analytical Chemistry*, Elsevier Science, 2013.
- [33] C.F. Poole, *The Essence of Chromatography*, Elsevier, 2003.
- [34] L. Tack, K. Schickle, F. Böke, H. Fischer, Immobilization of specific proteins to titanium surface using self-assembled monolayer technique., *Dent. Mater.* 31 (2015) 1169–79.
- [35] F. Meder, T. Daberkow, L. Treccani, M. Wilhelm, M. Schowalter, A. Rosenauer, et al., Protein adsorption on colloidal alumina particles

functionalized with amino, carboxyl, sulfonate and phosphate groups., *Acta Biomater.* 8 (2012) 1221–9.

[36] K. Schickle, R. Kaufmann, D.F. Duarte Campos, M. Weber, H. Fischer, Towards osseointegration of bioinert ceramics: Introducing functional groups to alumina surface by tailored self assembled monolayer technique, *J. Eur. Ceram. Soc.* 32 (2012) 3063–3071.

[37] K. Schickle, A. Korsten, M. Weber, C. Bergmann, S. Neuss, H. Fischer, Towards osseointegration of bioinert ceramics: Can biological agents be immobilized on alumina substrates using self-assembled monolayer technique?, *J. Eur. Ceram. Soc.* 33 (2013) 2705–2713.

[38] J. Yu, Z. El Rassi, Preparation of amino-zirconia bonded phases and their evaluation in hydrophilic interaction chromatography of carbohydrates with pulsed amperometric detection, *J. High Resolut. Chromatogr.* 17 (1994) 773–778.

[39] S. Deville, L. Gremillard, J. Chevalier, G. Fantozzi, A critical comparison of methods for the determination of the aging sensitivity in biomedical grade yttria-stabilized zirconia., *J. Biomed. Mater. Res. B. Appl. Biomater.* 72 (2005) 239–245.

[40] M. de Ridder, R.G. van Welzenis, H.H. Brongersma, Surface cleaning and characterization of yttria-stabilized zirconia, *Surf. Interface Anal.* 33 (2002) 309–317.

[41] V.I. Nefedov, D. Gati, B.F. Dzhurinskii, N.P. Sergushin, Y. V. Salyn, An X-ray photoelectron spectroscopic study of certain oxides, *Russ. J. Inorg. Chem.* 20 (1975) 1279–1283.

[42] G. Coussot, C. Perrin, T. Moreau, M. Dobrijevic, A. Le Postollec, O. Vandennebeele-Trambouze, A rapid and reversible colorimetric assay for the characterization of aminated solid surfaces., *Anal. Bioanal. Chem.* 399 (2011) 1061–9.

[43] G. Coussot, C. Faye, A. Ibrahim, M. Ramonda, M. Dobrijevic, A. Le Postollec, et al., Aminated dendritic surfaces characterization: a rapid and versatile colorimetric assay for estimating the amine density and coating stability., *Anal. Bioanal. Chem.* 399 (2011) 2295–302.

[44] Z. Yang, Y. Chevolot, T. Géhin, V. Dugas, N. Xanthopoulos, V. Laporte, et al., Characterization of three amino-functionalized surfaces and evaluation of antibody immobilization for the multiplex detection of tumor markers involved in colorectal cancer., *Langmuir.* 29 (2013) 1498–509.

[45] T. Fett, G. Rizzi, E. Ernst, R. Müller, R. Oberacker, A 3-balls-on-3-balls strength test for ceramic disks, *J. Eur. Ceram. Soc.* 27 (2007) 1–12.

[46] V.I. Nefedov, Y. V. Kokunov, Y.A. Buslaev, M.A. Poraj-Koshits, M.P. Gustyakova, E.G. Il'in, X-ray electron study of internal levels of fluorides, *Zhurnal Neorg. Khimii.* 18 (1973) 931–934.

[47] C. Sleight, A.P. Pijpers, A. Jaspers, B. Coussens, R.J. Meier, On the determination of atomic charge via ESCA including application to organometallics, *J. Electron Spectros. Relat. Phenomena.* 77 (1996) 41–57.

[48] M.V. Ryzhkov, V.A. Gubanov, M.P. Butzman, A.L. Hagström, E.Z. Kurmaev, Electronic structure and experimental spectra of some rare-earth oxyfluorides, *J. Electron Spectros. Relat. Phenomena.* 21 (1980) 193–204.

[49] S.L. Stipp, M.F. Hochella, Structure and bonding environments at the calcite surface as observed with X-ray photoelectron spectroscopy (XPS) and low

energy electron diffraction (LEED), *Geochim. Cosmochim. Acta.* 55 (1991) 1723–1736.

[50] U. Gelius, P. Hedén, J. Hedman, B. Lindberg, R. Manne, R. Nordberg, et al., *Molecular Spectroscopy by Means of ESCA III. Carbon compounds*, *Phys. Scr.* 2 (1970) 70.

[51] D.T. Clark, D. Kilcast, D.B. Adams, W.K.R. Musgrave, *An ESCA study of the molecular core binding energies of the chlorobenzenes*, *J. Electron Spectros. Relat. Phenomena.* 6 (1975) 117–134.

[52] S.C. Yoon, B.D. Ratner, *Surface structure of segmented poly(ether urethanes) and poly(ether urethane ureas) with various perfluoro chain extenders. An x-ray photoelectron spectroscopic investigation*, *Macromolecules.* 19 (1986) 1068–1079.

[53] G. Beamson, D. Briggs, *High Resolution XPS of Organic Polymers: The Scienta ESCA300 Database*, Wiley, 1992.

[54] D. Briggs, *Handbook of x-ray and ultraviolet photoelectron spectroscopy*, Heyden, 1977.

[55] T. Yoshida, K. Yamasaki, S. Sawada, *An X-Ray Photoelectron Spectroscopic Study of 2-Mercaptobenzothiazole Metal Complexes*, *Bull. Chem. Soc. Jpn.* 52 (1979) 2908–2912.

[56] T.S. Jones, M.R. Ashton, N. V Richardson, R.G. Mack, W.N. Unertl, *The interaction of the polyimide precursors PMDA (1,2,4,5-benzenetetracarboxylic anhydride) and m-PDA (1,3-phenylenediamine) with Ni(110)*, *J. Vac. Sci. Technol. A.* 8 (1990).

[57] T.G. Vargo, J.A. Gardella, *Development of Ti K α x radiation for electron spectroscopy for chemical analysis of polymer surfaces*, *J. Vac. Sci. Technol. A.* 7 (1989).

[58] H. Matsuyama, M. Teramoto, K. Hirai, *Effect of plasma treatment on {CO₂} permeability and selectivity of poly(dimethylsiloxane) membrane*, *J. Memb. Sci.* 99 (1995) 139–147.

[59] S.E. Redfern, R.W. Grimes, R.D. Rawlings, *The hydroxylation of t-ZrO₂ surfaces*, *J. Mater. Chem.* 11 (2001) 449–455.

[60] J.R. Piascik, S.D. Wolter, B.R. Stoner, *Development of a novel surface modification for improved bonding to zirconia*, *Dent. Mater.* 27 (2011) e99–e105.

[61] Y. Uwamino, A. Tsuge, T. Ishizuka, H. Yamatera, *X-Ray Photoelectron Spectroscopy of Rare Earth Halides*, *Bull. Chem. Soc. Jpn.* 59 (1986) 2263–2267.

[62] T.H. Büyüklımanlı, J.H. Simmons, *XPS studies of polyhedral linkages in binary fluoride films*, *J. Non. Cryst. Solids.* 120 (1990) 262–266.

[63] H.J.M. Bosman, A.P. Pijpers, A.W.M.A. Jaspers, *An X-Ray Photoelectron Spectroscopy Study of the Acidity of SiO₂-ZrO₂Mixed Oxides*, *J. Catal.* 161 (1996) 551–559.

[64] C.G. Pantano, R.K. Brow, *Hydrolysis Reactions at the Surface of Fluorozirconate Glass*, *J. Am. Ceram. Soc.* 71 (1988) 577–581.

[65] N.A. Kelly, *The Contamination of Fluorocarbon-Film Bags by Hydrocarbons and Nitrogen Oxides*, *J. Air Pollut. Control Assoc.* 33 (1983) 120–125.

[66] W. Birch, A. Carré, K.L. Mittal, *13 - Wettability Techniques to Monitor the Cleanliness of Surfaces*, in: R. Kohli, K.L. Mittal (Eds.), *Dev. Surf. Contam. Clean.*

Fundam. Appl. Asp., William Andrew Publishing, Norwich, NY, 2008: pp. 693–723.

[67] D.J. Preston, N. Miljkovic, J. Sack, R. Enright, J. Queeney, E.N. Wang, Effect of hydrocarbon adsorption on the wettability of rare earth oxide ceramics, *Appl. Phys. Lett.* 105 (2014).

[68] M. Tadorelli, Cleaning and surface properties, in: *Prep. Vac. Accel. Spec. Course Cern Accel. Sch.*, 2006: pp. 321–340.

[69] C. Scheuerlein, M. Tadorelli, The assessment of metal surface cleanliness by XPS, *Appl. Surf. Sci.* 252 (2006) 4279–4288.

[70] B.R. Strohmeier, The effects of O₂ plasma treatments on the surface composition and wettability of cold-rolled aluminum foil, *J. Vac. Sci. Technol. A Vacuum, Surfaces, Film.* 7 (1989) 3238.

[71] M.C. Kim, S.H. Yang, J.-H. Boo, J.G. Han, Surface treatment of metals using an atmospheric pressure plasma jet and their surface characteristics, *Surf. Coatings Technol.* 174-175 (2003) 839–844.

[72] S. Takeda, M. Fukawa, Y. Hayashi, K. Matsumoto, Surface OH group governing adsorption properties of metal oxide films, *Thin Solid Films.* 339 (1999) 220–224.

[73] T. Otsuka, I. Takenori, N. Kenji, M. Naoki, H. Kenichi, S. Masayasu, et al., On the wettability change of oxidized and gamma irradiated Zircaloy, *Proc. 2005 Water React. Fuel Perform. Meet.* 37 (2005) 1236.

[74] X. Zeng, G. Xu, Y. Gao, Y. An, Surface wettability of (3-aminopropyl)triethoxysilane self-assembled monolayers., *J. Phys. Chem. B.* 115 (2011) 450–4.

[75] F. Zhang, K. Sautter, A.M. Larsen, D.A. Findley, R.C. Davis, H. Samha, et al., Chemical vapor deposition of three aminosilanes on silicon dioxide: surface characterization, stability, effects of silane concentration, and cyanine dye adsorption., *Langmuir.* 26 (2010) 14648–54.

[76] D.M. dos Santos, A.J. Vechiato-Filho, E.V.F. da Silva, M.C. Goiato, P.F. Cesar, E.C. Rangel, et al., Aging Effect of Atmospheric Air on Zirconia Surfaces Treated by Nonthermal Plasma, *J. Adhes. Dent.* 17 (2015) 413–419.

[77] M. Rohnke, J. Janek, J.A. Kilner, R.J. Chater, Surface oxygen exchange between yttria-stabilised zirconia and a low-temperature oxygen rf-plasma, *Solid State Ionics.* 166 (2004) 89–102.

[78] X. Guo, Low temperature degradation mechanism of tetragonal zirconia ceramics in water: role of oxygen vacancies, *Solid State Ionics.* 112 (1998) 113–116.

[79] X. Guo, On the degradation of zirconia ceramics during low-temperature annealing in water or water vapor, *J. Phys. Chem. Solids.* 60 (1999) 539–546.

[80] X. Guo, Hydrothermal degradation mechanism of tetragonal Zirconia, *J. Mater. Sci.* 36 (2001) 3737–3744.

[81] K. Wang, C. Zhou, Y. Hong, X. Zhang, A review of protein adsorption on bioceramics, *Interface Focus.* 2 (2012) 259–277.

[82] L. Zych, R. Lach, K. Haberko, P. Rutkowski, B. Trybalska, J. Piekarczyk, The effect of nanometric zirconia particle additives on microstructure and mechanical properties of dense alumina, *Process. Appl. Ceram.* 3 (2009) 131–135.

- [83] M.-L. Rami, M. Meireles, B. Cabane, C. Guizard, Colloidal Stability for Concentrated Zirconia Aqueous Suspensions, *J. Am. Ceram. Soc.* 92 (2009) S50–S56.
- [84] D. Gutknecht, J. Chevalier, V. Garnier, G. Fantozzi, Key role of processing to avoid low temperature ageing in alumina zirconia composites for orthopaedic application, *J. Eur. Ceram. Soc.* 27 (2007) 1547–1552.
- [85] R.A. Bini, R.F.C. Marques, F.J. Santos, J.A. Chaker, M. Jafelicci, Synthesis and functionalization of magnetite nanoparticles with different amino-functional alkoxy silanes, *J. Magn. Magn. Mater.* 324 (2012) 534–539.
- [86] I.J. Bruce, T. Sen, Surface modification of magnetic nanoparticles with alkoxy silanes and their application in magnetic bioseparations., *Langmuir.* 21 (2005) 7029–35.
- [87] Z. Xu, Q. Liu, J.A. Finch, Silanation and stability of 3-aminopropyl triethoxy silane on nanosized superparamagnetic particles: I. Direct silanation, *Appl. Surf. Sci.* 120 (1997) 269–278.
- [88] S. Čampelj, D. Makovec, M. Drogenik, Functionalization of magnetic nanoparticles with 3-aminopropyl silane, *J. Magn. Magn. Mater.* 321 (2009) 1346–1350.
- [89] L. Vroman, A.L. Adams, G.C. Fischer, P.C. Munoz, Interaction of high molecular weight kininogen, factor XII, and fibrinogen in plasma at interfaces., *Blood.* 55 (1980) 156–9.
- [90] M. Tanaka, T. Motomura, M. Kawada, T. Anzai, Y. Kasori, T. Shiroya, et al., Blood compatible aspects of poly(2-methoxyethylacrylate) (PMEA)—relationship between protein adsorption and platelet adhesion on {PMEA} surface, *Biomaterials.* 21 (2000) 1471–1481.
- [91] Y.L. Jeyachandran, J.A. Mielczarski, E. Mielczarski, B. Rai, Efficiency of blocking of non-specific interaction of different proteins by {BSA} adsorbed on hydrophobic and hydrophilic surfaces, *J. Colloid Interface Sci.* 341 (2010) 136–142.

RESUME

Ce travail de thèse est structuré en trois parties séparées ayant chacune des objectifs différents, mais étant toutes trois axés autour de l'étude de la surface de matériaux pour applications biomédicales. Chaque chapitre a été élaboré séparément sous la forme d'article scientifique correspondant aux publications des résultats de la présente thèse.

La surface des céramiques bio-inertes (zircone, alumine), utilisés dans des dispositifs médicaux pour l'orthopédie et l'odontologie, est souvent traitée pour augmenter sa rugosité, de façon à améliorer sa fixation à l'os ou à des matériaux antagonistes à l'aide de ciments et résines. Il s'agit d'une pratique habituelle héritée des implants en métal. L'alumine et la zircone présentent des avantages par rapport aux métaux comme par exemple une meilleure résistance à l'usure, une excellente biocompatibilité et, pour les pièces dentaires, une meilleure esthétique. Malheureusement, elles présentent aussi des désavantages : les céramiques sont en effet plus fragiles que les métaux, et donc plus exposées aux risques d'endommagement par rupture. La zircone dispose d'un mécanisme de résistance accrue à la propagation de fissures appelé « renforcement par transformation de phase » (*Phase Transformation Toughening* en anglais), qui est fondé sur la transformation sous contraintes de grains quadratiques en grains monocliniques. Cette transformation s'accompagne d'une augmentation de volume, ce qui aide à fermer la fissure et arrêter sa propagation et qui, *in fine*, augmente la ténacité de la zircone. Malheureusement, cette transformation peut aussi être activée en présence d'eau, ce qui pose des problèmes de contraintes résiduelles et de microfissurations en surface qui peuvent faire augmenter la fragilité de la pièce et provoquer sa défaillance prématurément. La dégradation de la zircone par transformation de la phase quadratique en présence d'eau est connue sous le nom de « vieillissement » (ou *Low Temperature Degradation, LTD*).

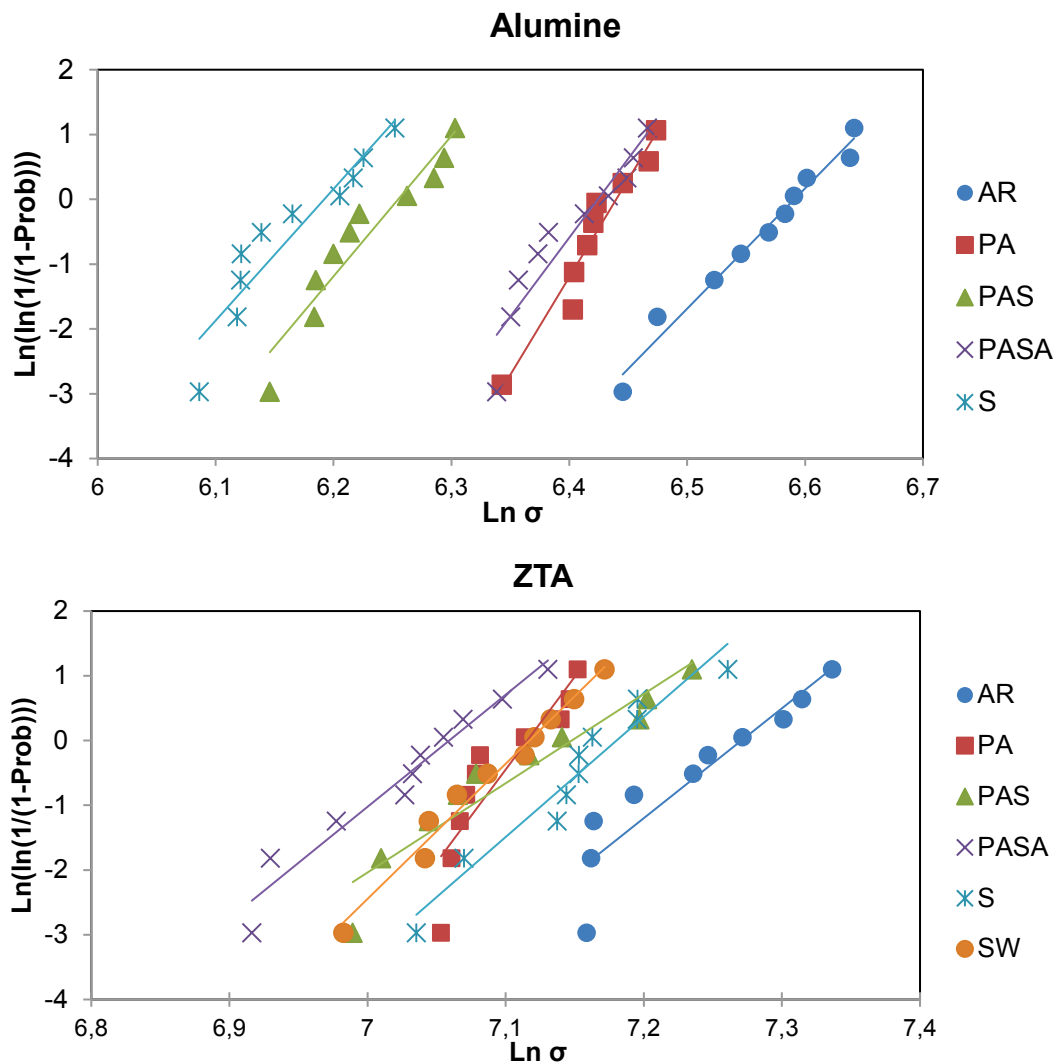
La première partie de cette thèse se focalise sur l'évaluation de l'impact d'un même traitement de rugosité par sablage réalisé après frittage sur une alumine, une zircone (3mol.%Y-TZP) et un composite alumine-zircone (ZTA), trois céramiques fréquemment utilisées dans des dispositifs médicaux commerciaux. Le traitement de sablage consiste en une projection de grains abrasifs à grande vitesse. Ce traitement crée de la rugosité, mais en même temps des défauts en surface (sous la forme de petites fissures) et une certaine distribution de contraintes résiduelles en fonction de l'épaisseur. Dans cette étude comparative, nous avons analysé comment chacun de ces éléments modifie le comportement mécanique des matériaux, et dans le cas de la zircone et le composite ZTA, comment le traitement modifie leur sensibilité au vieillissement.

Nous avons reçu de la part de la société CeramTec GmbH (Plochingen, Allemagne) des barrettes d'alumine, zircone et ZTA (de dimensions : $3 \times 4 \times 60$ mm³) de qualité biomédicale, que nous avons séparées en groupes et traitées comme indiqué dans le **Tableau R. 1**.

Tableau R. 1. Nom de groupes, et traitements suivis pour chacun.

Groupe	Traitement
AR	Sans traitement. Comme reçu
PA	Poli + Recuit
PAS	Poli + Recuit + Sablé
PASA	Poli + Recuit + Sablé + Recuit
S	Sablé
SW	Sablé + 50h immergé dans l'eau à 134° C

Les barrettes ont été testées en flexion quatre-points. Les résultats ont été traités et analysés suivant une statistique de Weibull. Les graphiques résultants sont présentés en **Figure R. 1**.



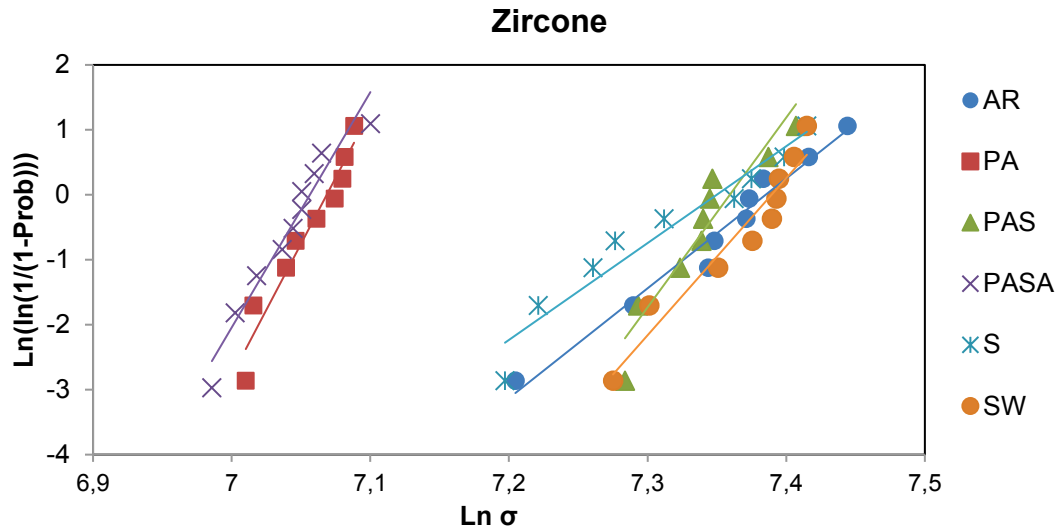


Figure R. 1. Distribution de Weibull des résultats de flexion 4-point

Ces résultats montrent un impact très différent entre chacun des matériaux traités. La plus haute fragilité de l'alumine conduit à une réduction importante de la résistance à la rupture après sablage. En plus, les résultats montrent que les contraintes résiduelles ont un rôle prédominant par rapport aux défauts de surface. Dans l'alumine, les contraintes résiduelles associées au sablage affaiblissent le matériau alors que dans la zircone et la ZTA elles les renforcent.

L'impact des différents traitements sur le comportement de vieillissement de la zircone a été étudié par vieillissement accéléré en autoclave à 134° C et sous pression de vapeur d'eau de 2 bars. Les courbes de vieillissement de la ZTA et de la zircone sont présentées en **Figure R. 2**.

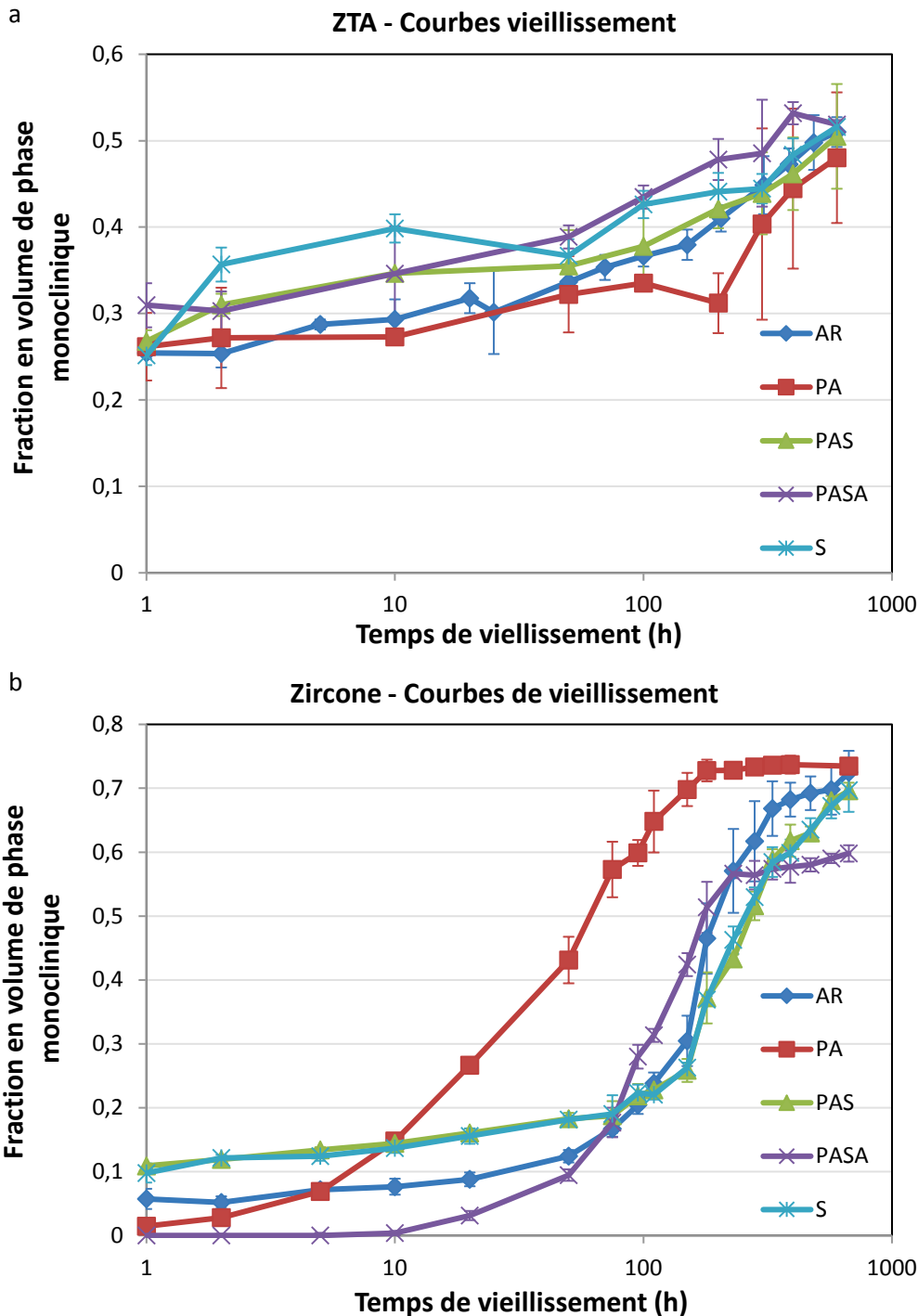


Figure R. 2. Evolution de la fraction volumique de phase monoclinique sous vieillissement accéléré en autoclave de ZTA (a) et zircone (b).

Le composite ZTA présente une meilleure résistance au vieillissement que la zircone monolithique (variation du taux de phase monoclinique plus faible), comme observé dans la **Figure R. 2a**. Toutes les courbes sont statistiquement équivalentes. Cette stabilité est due au fait que la phase majoritaire est l'alumine, qui limite la propagation de la transformation. Dans le cas de la zircone, on observe des différences significatives entre les traitements. Dans le cas du PA, l'absence de contraintes résiduelles favorise la transformation de phase. Par

contre dans le cas du PASA, qui devrait présenter *a priori* un comportement similaire à celui du PA, on observe la transformation qu'à partir de 10h en autoclave. Cette résistance exceptionnelle trouve son origine dans la formation d'une couche de grains de zircone quadratique de taille nanométrique après le recuit. Nous avons réussi à observer ce changement en nano-tomographie par *Focussed Ion Beam* (FIB) (images présentées dans la **Figure R. 3**). La formation de cette couche s'explique par une recristallisation pendant le recuit des grains monocliniques et maclés en surface, qui se sont transformés pendant le sablage, en grains plus petits et quadratique. Finalement, l'épaisseur de la zone recristallisée a été estimée en 150 nm. Cette zone recristallisée est analogue à celle qui peut se former dans les matériaux métalliques écrouis en surface puis recuits : l'énergie plastique emmagasinée lors du sablage entraîne un mécanisme de recristallisation, dont l'étendue doit dépendre de la déformation plastique engendrée en surface.

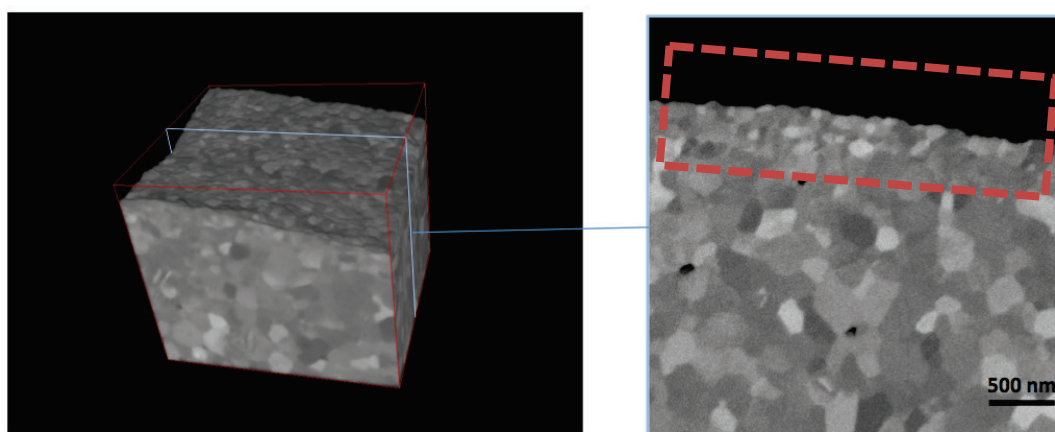


Figure R. 3. À gauche, le volume analysé ($3.2 \times 3.1 \times 2.9 \mu\text{m}$). À droite, la section transversale montrant le profil d'épaisseur. La zone recristallisée a été marquée en rouge.

La surface des implants n'est pas uniquement destinée à leur fixation. Par exemple dans les couples de frottement des implants orthopédiques, les surfaces sont utilisées de façon à substituer la fonction des articulations (hanche, épaule, genou, *etc.*). Dans ces cas, la lubrification joue un rôle fondamental, minimisant l'usure et donc augmentant la vie moyenne des implants. Cependant, les mécanismes expliquant la lubrification et les comportements tribologiques de ces couples *in vivo* sont très peu compris. Différents travaux montrent l'importance de la présence des protéines, surtout celles ayant de très hautes masses moléculaires. Il est généralement accepté que la mouillabilité est un facteur important, car plus une surface est hydrophile, plus elle va attirer de lubrifiant entre les deux surfaces. Cependant, les valeurs reportées de mouillabilité par les différents fabricants et chercheurs ne sont pas cohérentes entre elles, et présentent des problèmes de contamination organique dans leurs protocoles de mesure. De plus, l'adsorption de protéines change les propriétés chimiques de surface, la mouillabilité incluse. Enfin, quelques auteurs

soutiennent que la mouillabilité d'une surface affecte les mécanismes d'adsorption de protéines.

Dans le deuxième chapitre, nous avons donc étudié l'effet de la contamination, et des différentes techniques de nettoyage permettant de la réduire, sur la mouillabilité des surfaces par l'eau. Nous avons étudié des matériaux typiquement utilisés dans la tête des implants de hanche : alumine (« Forte »), composite alumine-zircone (« Delta »), cobalt-chrome-molybdène (« CoCr »). Ensuite, nous avons sélectionné parmi ces techniques de nettoyage celles le plus pertinentes et nous avons étudié leur impact sur l'adsorption des protéines en utilisant des mesures de mouillabilité. L'ensemble des traitements étudiés est explicité dans le **Tableau R. 1**.

Tableau R. 1. Description des différents traitements de nettoyage étudiés et ses abréviatures

Abréviature	Description
NoC	« No cleaning » – Les échantillons ont été testés après polissage et sans nettoyage spécifique.
EthUS	« Ethanol in Ultrasonic bath » – Les échantillons ont été immergés dans de l'éthanol dans un bain à ultrason pendant 5 min, puis séchés avec un courant d'azote pure.
EthUS+W	« Ethanol in Ultrasonic bath and Wipers » – Les échantillons ont été nettoyés comme EthUS et avec un tissu de salle blanche trempé dans de l'éthanol.
PC	« Production Cleaning » – Les échantillons ont été nettoyés par CeramTec GmbH utilisant un procédé propriétaire consistant à les immerger dans différents bains à ultrason à différents pH puis dans de l'eau désionisée comme rinçage neutralisant. Enfin, les échantillons sont séchés avec un courant d'air chaud et emballés dans des sachets en plastique sous vide.
PC+Al	« Production Cleaning Al Foil » Les échantillons ont été nettoyés comme PC, et emballés cette fois dans une feuille d'aluminium avant mettre l'ensemble dans sachets en plastique sous vide.
PC+EthW	Production Cleaning and Ethanol Wipers – Les échantillons ont été nettoyés comme PC, puis juste avant les mesures nettoyés avec un tissu de salle blanche trempé dans de l'éthanol.
PC+AcetW	Production Cleaning and Acetone Wipers – Les échantillons ont été nettoyés comme PC, puis juste avant les mesures nettoyés avec un tissu de salle blanche trempé dans de l'acétone.
PC+IsopropW	Production Cleaning and Isopropanol Wipers – Les échantillons ont été nettoyés comme PC, puis à nouveau avec un tissu de salle blanche trempé dans de l'isopropanol.

L'efficacité des traitements de nettoyage pour éliminer la contamination a été mesurée à travers de tests dynamiques de mouillabilité en mesurant l'angle de contact au début en ajoutant de l'eau (angle d'avancée), et après en la soustrayant (angle de reculée). Pour cela, nous avons utilisé des disques plats et polis. La différence entre ces deux mesures d'angle est connue comme étant une « hystérèse », et elle est liée à l'hétérogénéité d'une surface. Si tous les échantillons présentent une surface polie avec une rugosité très faible, la source principale de l'hystérèse sera la contamination en surface. Les résultats de l'hystérèse sont présentés en **Figure R. 4**.

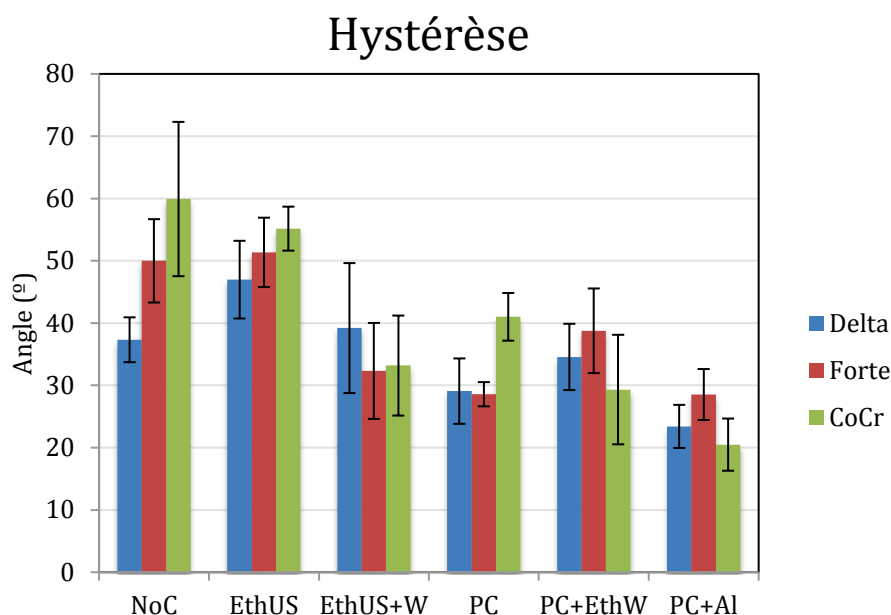


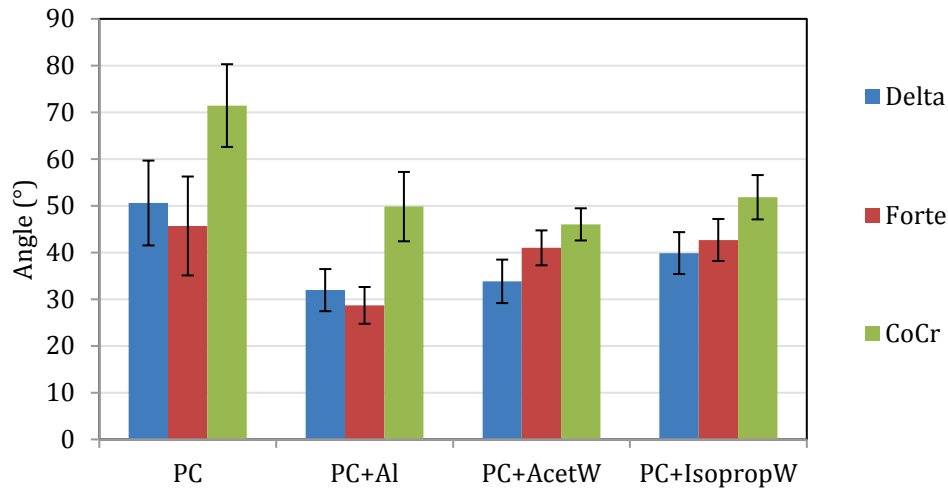
Figure R. 4. Résultats de hystérésis mesurée sur surface plates.

Les résultats montrent une très forte influence du traitement de nettoyage dans la mesure des hystérèses enregistrée. Pour tous les matériaux, PC+Al a été le traitement avec l'hystérèse le plus faible, signifiant que ce traitement est capable d'éliminer la majorité des hétérogénéités de la surface.

De façon similaire, nous avons mesuré l'angle de contact de l'eau sur des têtes fémorales. La particularité dans ce cas est que la surface présente une courbure, ce qui complique les mesures dynamiques. Ainsi dans cette partie, nous avons utilisé des mesures en mode quasi-statique (nous ne faisons pas varier le volume de la goutte, mais elle est toujours soumise à l'évaporation). Il est à noter que ces résultats ne sont pas comparables directement avec ceux présentés dans la **Figure R. 4**. Les échantillons ont été testés juste après le traitement de nettoyage, et après incubation dans une solution diluée contenant sérum de veau, à 36° C pendant 30 min. Les résultats sont présentés sur la **Figure R. 5**.

a

Avant sérum



b

Après sérum

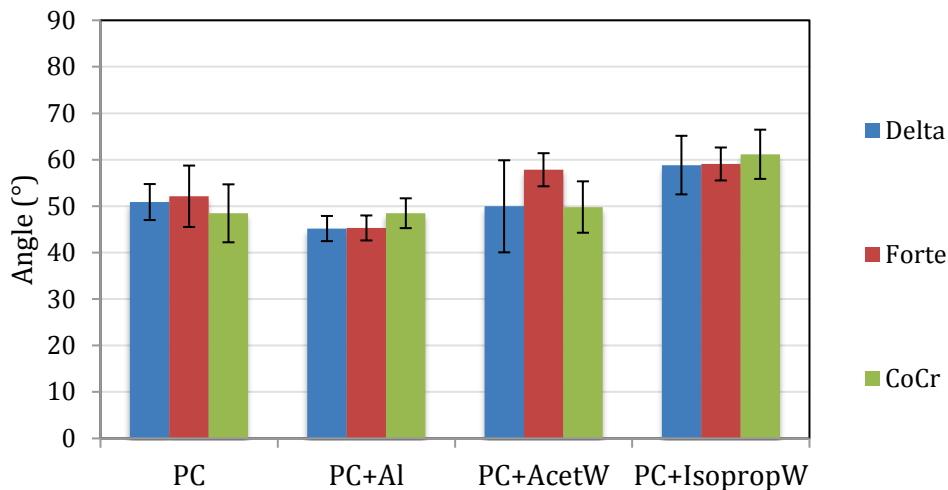


Figure R. 5. Résultats d'angle de contact sur les têtes fémorales avant immersion dans le sérum et après.

Quand les échantillons ont été testés directement après nettoyage, on observe beaucoup de contraste entre chaque condition, et l'on peut distinguer des différences entre chaque matériau. Par contre, l'exposition au sérum déclenche l'adsorption des protéines, qui vont masquer la surface. A ce point, on observe peu de différences entre les matériaux, mais on les détecte entre traitements de nettoyage. Cet effet peut être causé par une distribution différente de protéines (ou de leur orientation) sur chacune des surfaces, motivée par une distribution différente des hétérogénéités (*i.e.* contamination).

La chimie de surface a en fait un très grand effet sur l'adsorption de protéines. Elles sont très importantes aussi dans les interactions cellule-prothèse. En ce qui concerne l'intégration des prothèses dans le corps humain, les cellules utilisent

des protéines en surface comme points de fixation et d'identification. Les implants avec une surface capable de recruter plus de protéines qui aident à l'adhésion des cellules auront plus des chances d'être intégrés que des implants avec protéines qui empêchent l'adhésion cellulaire. Il existe déjà des implants céramiques ayant des compositions très proches de la partie inorganique de l'os, comme ceux basés sur la hydroxyapatite, mais malheureusement, ces implants ne sont pas mécaniquement performants et présentent des taux de dissolution incompatible avec un soutien à long terme.

Ainsi, pour ces applications où il est nécessaire d'avoir une solution de longue durée (comme des implants orthopédiques ou odontologiques), il serait intéressant d'avoir un implant inert avec une surface active et chimiquement similaire à l'os. Dans le troisième et dernière chapitre de cette thèse, nous avons exploré un nouveau concept de modification de surface de la zircone consistant en un greffage des organo-silanes directement aux groupes hydroxyle (-OH) présents à la surface de la zircone sans utiliser de couche intermédiaire. Le processus est connu en chimie sous le nom de « silanisation ». Ce type de modification est très efficace sur la surface de la silice (SiO₂), qui peut facilement être hydroxylée quand elle est immaculée et exposée à l'humidité ambiante. Malheureusement, la surface de la zircone présente moins de groupement OH que la silice. Pour favoriser son hydroxylation, nous avons exploré une voie de nettoyage par plasma d'oxygène avec pour l'objectif d'éliminer la contamination organique et d'augmenter le nombre de groupement OH en surface par implantation des ions. Le but final de cette partie du projet est d'adapter la technique de la silanisation à la zircone de manière à prouver son potentiel pour l'amélioration de l'osseointegration de prothèse sans endommager leur performance mécanique.

Nous avons établi trois types d'échantillons, décrits dans le **Tableau R. 2**. Pour l'organosilane, nous avons choisi le 3-aminopropylethoxysilane (APDMES). Il s'agit d'un silane avec un groupe amine (-NH₂) comme groupe fonctionnel, dont des travaux antérieurs ont montré qu'il interagit bien avec les cellules.

Nous avons caractérisé les échantillons par XPS (X-ray Photoelectron Spectroscopy), puis étudié les effets du plasma et de la silanization sur leur comportement mécanique, résistance au vieillissement, et sur l'adhésion cellulaire. Les résultats sont présentés sur les **Figure R. 6**, **Figure R. 7** et **Figure R. 8**.

Tableau R. 2. Description des types d'échantillons

Abréviature	Description
NT	Poli
PC	Poli + Nettoyé par plasma
PCS	Poli + Nettoyé par plasma + Silanisé

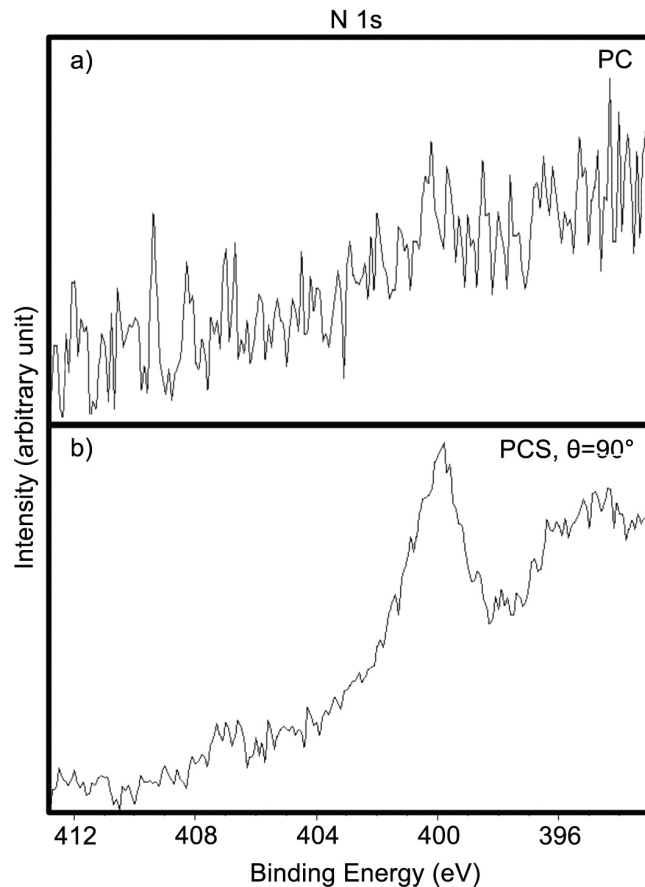


Figure R. 6. Région du spectre XPS correspondant à N 1s pour PC et PCS.

Sur la **Figure R. 6**, on observe le pic d'azote correspondant au groupe amine du APDMES, signifiant que la silanisation a été réussite. Nous avons aussi observé un pic de silicium compatible avec la présence de silane. Le plasma d'oxygène réduit le taux de contamination, mesuré en fonction du pourcentage de carbone. Contrairement à ce que nous espérions, il ne semble pas d'augmenter la quantité d'oxygène sous la forme des OH. Finalement, on observe un pic important de fluor après plasma. L'énergie de ce pic n'est pas compatible avec du fluor organique.

Aucun effet dans le comportement mécanique n'a pas été détecté entre NT et PCS. Cela signifie que l'ensemble des modifications n'a pas aucun impact : ni sur la population de défauts, ni sur la résistance à la propagation de fissures.

Par contre, nous avons trouvé un effet très positif dans la résistance au vieillissement des échantillons traités par plasma, comme le montre la **Figure R. 7**. Une recherche plus ample serait nécessaire dans le futur, car l'implication fortuite du fluor provenant du plasma nettoyage reste toujours en question.

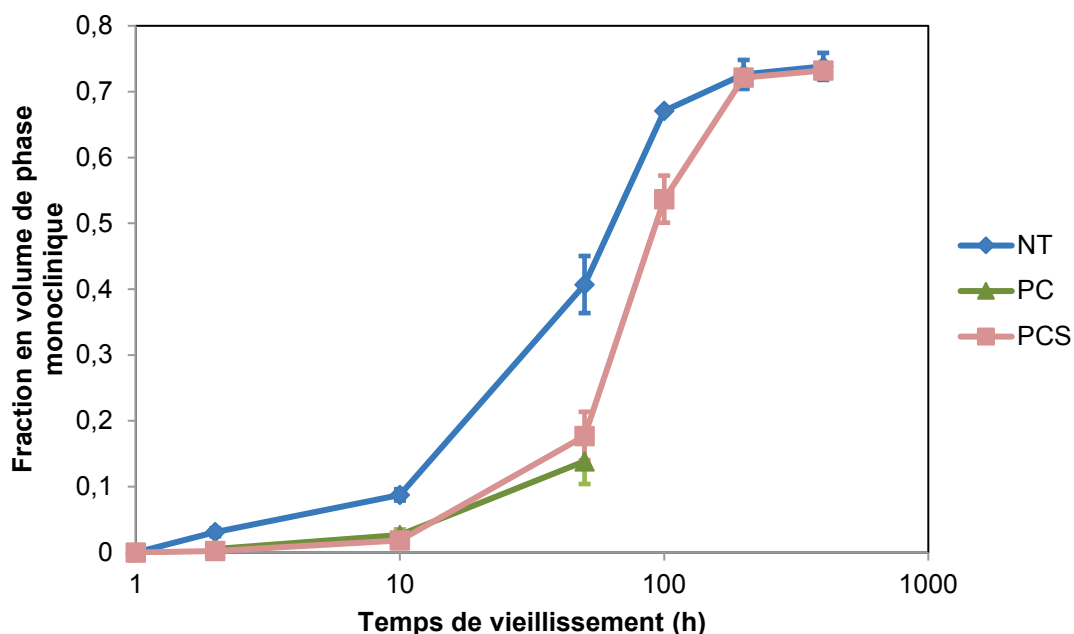


Figure R. 7. Evolution de la fraction en volume de phase monoclinique en fonction du temps en autoclave à 134°C.

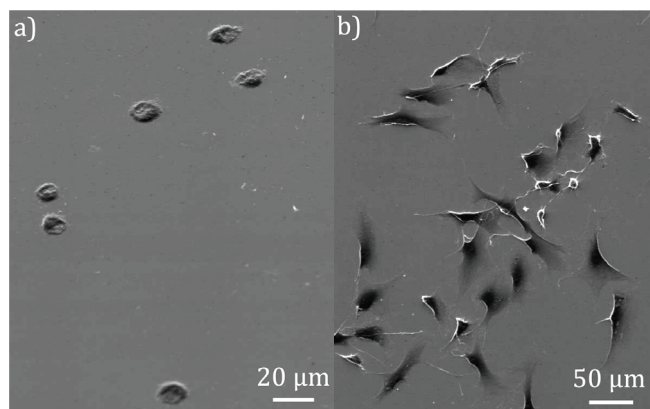


Figure R. 8. Images à microscope électronique de balayage des cultures cellulaires après 3 jours de a) la surface de NT, et b) la surface de PCS.

La **Figure R. 8** montre que les cellules en PCS présentait une morphologie plus étalée, signifiant que la modification de surface apportée par la silanisation semble capable d'augmenter l'interaction entre les cellules et la surface. En comparaison, les cellules sur NT présentait une morphologie plus ronde, manifestant une interaction plus pauvre. En même temps nous avons réalisé une étude de la prolifération cellulaire ; les résultats montrent une prolifération majeure dans le PCS après 10 jours. Ces résultats s'expliquent par une adhésion plus rapide qui permet une prolifération plus tôt.

En conclusion, nous avons prouvé que la silanisation sur la zircone est faisable et conduit à une adhésion cellulaire meilleure et plus rapide. Nos résultats ouvrent la possibilité à de nouveaux moyens de modification des implants, fondées sur

les interactions chimiques entre le matériau et les agents biologiques, permettant l'augmentation des niveaux de complexité et un contrôle plus élevé des propriétés de surface pour les adapter aux besoins spécifiques de l'application.

Index of Figures

Figure 1.1. Crystallographic structure of α -alumina.....	12
Figure 1.2. Crystallographic structure of the allotropes of zirconia.....	12
Figure 1.3. Crack deflection on strontium aluminate platelet. (Source: CeramTec GmbH www.ceramtec.com).....	15
Figure 1.4. Body parts susceptible of being replaced by permanent bioinert implants nowadays.....	17
Figure 1.5. Parts on a dental implant.....	18
Figure 1.6. Evolution in implant dentistry. (Source: CeraRoot, Oral Iceberg S.L. www.ceraroot.com).....	19
Figure 1.7. Titanium implant (left) and zirconium implant (right). (Source: Miles of Smiles, www.milesofsmilesdental.net).....	20
Figure 1.8. Parts on a total hip replacement.....	21
Figure 1.9. Ceramic-on-Polymer joint. The ceramic ball head wore the liner and even continued through the metallic shell. (Source: Dr. med. Karl-Heinz Günther, www.doccheck.com).....	23
Figure 1.10. Third body wear resistance in CoC. (Source: CeramTec GmbH www.ceramtec.com).....	24
Figure 1.11. X-ray on hip joint showing dislocation of head (Source: Singh et al. [36]).....	25
Figure 1.12. Different of ranges of motion (ROM) as a function of the ball head size. (Source: CeramTec GmbH www.ceramtec.com).....	25
Figure 1.13. Birmingham Hip Resurfacing implant. (Source: The McMinn Centre www.mcminncentre.co.uk).....	26
Figure 1.14. Difference between traditional THA and BHR. The coloured zone represents the amount of bone removed. (Source: The McMinn Centre www.mcminncentre.co.uk).....	26
Figure 1.15. Detail of screw hole access on a temporary screw-retained restoration (Source: loveperio.com).....	28
Figure 1.16. Example of dental implant with roughness at different scales. (Source: dentis-implant.com).....	29
Figure 1.17. Zirconia dental implants in vivo. The images on top correspond to a sandblasted surface, while the images at the bottom correspond to a machined surface. (a) Implant, (b) bone, (c) tissue at the neck of the implant, (d) peaked threads. (Source: Gahlert et al. [48])	30
Figure 1.18. Four different profiles with the same average height parameter (R_a).....	31
Figure 2.1 Representation of a macro indentation and its effect on the crack lengths of the smaller indentation through the residual stress field.....	49
Figure 2.2. Residual stresses around the macro indentation on each material.....	53
Figure 2.3. Indentations on the surface of ZTA. (a) Annealed at 900° C, and (b) completely annealed at 1200° C.....	53
Figure 2.4. On the left the analyzed volume (3.2 x 3.1 x 2.9 μm) and on the right, the cross-section showing the profile in depth. The recrystallized zone is highlighted by the dashed red rectangle.	55
Figure 2.5. Evolution of monoclinic zirconia content after accelerated aging in autoclave in ZTA (a) and Zirconia (b).....	56
Figure 2.6. Weibull distributions of 4-point bending test results.....	57
Figure 2.7. Graphical representation of the hypothesized residual-stress distribution for each material.....	64
Figure 3.1. Comparison of experimental data from Preston[14] to previously results for equilibrium contact angle as a function of surface atomic percent carbon (Source: Preston et al., 2014).....	75
Figure 3.2. (a) Results of quasistatic contact angle, and (b) hysteresis after dynamic measurements. All these results were obtained on flat surfaces.....	79
Figure 3.3. Comparison of quasistatic contact angle before and after gamma irradiation. Results obtained on ball heads.....	80
Figure 3.4. (a) Contact angles on surfaces right after cleaning. (b) Contact angles after incubation without serum. (c) Contact angle after incubation with serum. Results obtained on ball heads.	82
Figure 3.5. Representation of H-bonds on an aluminum oxide lattice.....	85

Figure 3.6. Results distribution of PC+AcetW Delta. Two groups can be observed among the population: one approaching to 35° and another to 58°.....	86
Figure 4.1. Schematic representation of silanization of silica.....	94
Figure 4.2. XPS spectra corresponding to the C 1s region of NT (a), PC (b), PCS $\theta=90^\circ$ (c), and PC H2O (d). Deconvoluted peaks are: (i) C-C or C-H type, (ii) C-O type, (iii) O-C-O or C=O type, and (iv) CO3 type.....	100
Figure 4.3. XPS spectra corresponding to the O 1s region of NT (a), PC (b) and PC H2O (c).	101
Figure 4.4. XPS spectra corresponding to the Zr 3d region of NT (a), PC (b), PCS $\theta=90^\circ$ (c), and PC H2O (d).....	102
Figure 4.5. XPS spectra corresponding to the Y 3d region of NT (a), PC (b), PCS $\theta=90^\circ$ (c), and PC H2O (d). Additionally, in (c) the corresponding peak to Si 2s is comprised.....	102
Figure 4.6. XPS spectrum corresponding to the F 1s region of PC.	103
Figure 4.7. XPS spectra corresponding to the N 1s region of (a) PC, (b) PC H2O and (c) PCS $\theta=90^\circ$	103
Figure 4.8. XPS spectra corresponding to the Si 2p region of PCS $\theta=90^\circ$	104
Figure 4.9. Contact angle measurements	105
Figure 4.10. Mechanical tests: Biaxial bending test results presented in a Weibull plot.	105
Figure 4.11. Aging kinetics: Evolution of monoclinic phase versus time in autoclave, after accelerated aging.....	106
Figure 4.12. MG-63 proliferation averaged results of three series on NT and PCS samples and the reference (cell culture treated polystyrene).	107
Figure 4.13. SEM images of NT (a, c, e, g) and PCS (b, d, f, h) on time-points 3, 6 and 10 days.	108
Figure 4.14. Comparison of experimental data from the present work to previously published results for equilibrium contact angle as a function of surface atomic carbon (Source: Preston et al., 2014; References: [67,70–72]).	111

Index of Tables

Table 2.1. Properties of studied materials.....	47
Table 2.2. Group names, treatments followed and expected presence of SD and RS. Single plus (+) represents low, double plus (++) high, and null () absence.	47
Table 2.3. Statistical parameters studied and their definitions.....	50
Table 2.4. Results of surface roughness for each material and series, obtained through OI..	54
Table 2.5. Central value of Weibull distributions corresponding to a probability of failure of 63,2% (MPa) (left) and Weibull modulus (right).....	58
Table 2.6. Surface roughness of commercial dental implants (Source: Svanborg et al. [40] (Titanium); Zinelis et al. [46] (Zit-Z and WhiteSky)).....	59
Table 2.7. Summary of results obtained for each series and material of estimated RS and defect types responsible of failure. Positive RS (>0) mean tensile, and negative (<0) compressive. Defects are either intrinsic (i.e. already present in the material, and related to fabrication) or extrinsic (i.e. created during surface modification). A question mark (?) expresses uncertainty due to lack of explicit evidence.	63
Table 3.1. Description of the cleaning procedures.	76
Table 4.1. Properties of zirconia samples as provided by the manufacturer	96
Table 4.2. Type of samples studied.....	96
Table 4.3. Atomic percentages of species on surface obtained by XPS analysis.....	100
Table 4.4. Summary of Weibull parameters obtained for each tested series.	106



INSA

FOLIO ADMINISTRATIF

THESE DE L'UNIVERSITE DE LYON OPEREE AU SEIN DE L'INSA LYON

NOM : CARAVACA

DATE de SOUTENANCE : 16 septembre 2016

Prénoms : Carlos

TITRE : Modified functional surfaces for increased biointegration : surface chemistry, mechanical integrity and long-term stability of zirconia and alumina based ceramics.

NATURE : Doctorat

Numéro d'ordre : 2016LYSEI080

Ecole doctorale : Matériaux de Lyon

Spécialité : Science des Matériaux

RESUME :

Ce travail de thèse est axé autour de l'étude de la surface des matériaux pour applications biomédicales, et il a été structuré en trois parties indépendantes. La surface des céramiques bioinertes (zircone, alumine), utilisées dans des dispositifs médicaux pour l'orthopédie et l'odontologie, est souvent traitée pour augmenter sa rugosité, de façon à améliorer la fixation à l'os ou aux ciments et résines. Malheureusement, ces modifications peuvent endommager les matériaux et affecter leur intégrité à long terme. La première partie de cette thèse se focalise sur l'évaluation de l'impact d'un même traitement de rugosité par sablage réalisé après frittage sur une alumine, une zircone (3mol.%Y-TZP) et un composite alumine-zircone (ZTA), en se focalisant sur les défauts en surface et la distribution des contraintes résiduelles. Des différences très marquées ont été observées entre chaque matériau : dans l'alumine la distribution des contraintes résiduelles affecte de manière négative la contrainte à la rupture, alors que dans la zircone on observe un renforcement.

La surface des implants n'est pas uniquement destinée à leur fixation. Elle peut également posséder une fonction très spécifique, comme par exemple celle de substituer l'articulation (hanche, épaule, genou, etc.) avec des couples de frottement orthopédiques. La lubrification joue un rôle fondamental, minimisant l'usure et donc augmentant la vie moyenne des implants. Il est généralement admis que la mouillabilité est un facteur important dans la lubrification. Cependant la lubrification est aussi liée à la présence de protéines, et leur adsorption notamment change les propriétés chimiques des surfaces, la mouillabilité incluse. De plus, la mouillabilité d'une surface affecte les mécanismes d'adsorption de protéines. Dans le deuxième chapitre, nous avons étudié les effets de la contamination, et de différentes techniques de nettoyage permettant de la réduire, sur la mouillabilité vis-à-vis de l'eau. Nous avons étudié des matériaux typiquement utilisés pour réaliser des têtes de prothèses totales de hanche : alumine, composite alumine-zircone et alliage cobalt-chrome-molybdène. Puis nous avons sélectionné les plus pertinentes parmi ces techniques de nettoyage et nous avons étudié leur impact sur l'adsorption des protéines en utilisant des mesures de mouillabilité.

Au-delà de la simple lubrification, les protéines jouent aussi un rôle dans l'interface implant - tissu vivant. En effet, les cellules utilisent les protéines en surface comme points de fixation et identification. Les implants présentant une surface capable de recruter plus de protéines aidant à l'adhésion des cellules auront plus des chances d'être intégrés que des implants recrutant des protéines qui empêchent l'adhésion. Dans le troisième et dernière chapitre, on a exploré un nouveau concept de modification de surface de la zircone consistant en un greffage d'organosilanes directement sur les groupements hydroxyle (-OH) présents à la surface de la zircone sans utiliser de couche intermédiaire. Pour favoriser l'hydroxylation de la surface, nous avons exploré la voie du nettoyage par plasma d'oxygène afin d'éliminer la contamination organique et d'augmenter la densité de groupements hydroxyles en surface. Le but final de cette partie du projet est d'adapter la technique de la silanisation à la zircone de manière à prouver son potentiel pour l'amélioration de l'ostéointégration de prothèse sans endommager leur performance mécanique.

MOTS-CLÉS : surface, silanisation, zircone, alumine, propriétés mécaniques, vieillissement, mouillabilité

Laboratoire (s) de recherche :

Université de Lyon
MATEIS – UMR CNRS 5510 – INSA de Lyon
7, Avenue Jean Capelle, 69621 Villeurbanne Cedex, France

Directeur de thèse: Jérôme CHEVALIER

Co-directeur de thèse : Laurent GREMILLARD

Président de jury : A. Leriche

Composition du jury : M. Anglada (rapporteur), A. Leriche (rapporteur), A.A. Porporati (examinateur), P. Miranda (examinateur), E. Laurenceau (examinateur), Y. Chevolut (invité)